

IZMIR KATIP CELEBI UNIVERSITY ★ GRADUATE SCHOOL OF SCIENCE
ENGINEERING AND TECHNOLOGY

**SYNTHESIS, CHARACTERIZATION AND APPLICATION OF NEW
ORGANIC ELECTROACTIVE MOLECULES FOR PHOTOVOLTAIC
DEVICES**



Ph.D. THESIS

Mesude Zeliha ARKAN

Department of Materials Science and Engineering

Thesis Advisor: Assoc.Prof. Dr. Şerafettin DEMİÇ

MARCH 2017

IZMIR KATIP CELEBI UNIVERSITY ★ GRADUATE SCHOOL OF SCIENCE
ENGINEERING AND TECHNOLOGY

**SYNTHESIS, CHARACTERIZATION AND APPLICATION OF NEW
ORGANIC ELECTROACTIVE MOLECULES FOR PHOTOVOLTAIC
DEVICES**



Ph.D. THESIS

**Mesude Zeliha ARKAN
(D130111008)**

Department of Materials Science and Engineering

Thesis Advisor: Assoc.Prof. Dr. Şerafettin DEMİÇ

MARCH 2017

İZMİR KÂTİP ÇELEBİ ÜNİVERSİTESİ ★ FEN BİLİMLERİ ENSTİTÜSÜ

**FOTOVOLTAİK CİHAZLAR İÇİN YENİ ORGANİK ELEKTROAKTİF
MOLEKÜLLERİN SENTEZİ, KARAKTERİZASYONU VE UYGULAMALARI**

DOKTORA TEZİ

**Mesude Zeliha ARKAN
(D130111008)**

Malzeme Bilimi ve Mühendisliği Anabilim Dalı

Tez Danışmanı: Doç. Dr. Şerafettin DEMİÇ

MART 2017

Mesude Zeliha ARKAN, a Ph.D. student of iKCU Graduate School of Science Engineering and Technology student ID 130111008, successfully defended the thesis entitled “**SYNTHESIS, CHARACTERIZATION AND APPLICATION OF NEW ORGANIC ELECTROACTIVE MOLECULES FOR PHOTOVOLTAIC DEVICES**”.

which she prepared after fulfilling the requirements specified in the associated

Thesis Advisor : **Assoc. Prof. Dr. Şerafettin DEMİÇ**
İzmir Katip Çelebi University

Jury Members : **Assoc.Prof. Dr. Sermet KOYUNCU**
Çanakkale Onsekiz Mart University

Assoc. Prof. Dr. Cem TOZLU
Karamanoğlu Mehmet Bey University

Assoc.Prof. Dr. Mustafa CAN
İzmir Katip Çelebi University

Asst. Prof. Dr. Fethullah GÜNEŞ
İzmir Katip Çelebi University

Date of Submission : 20 February 2017

Date of Defense : 10 March 2017





To my family,



ACKNOWLEDGEMENT

I would especially like to thank my advisor, Assoc.Prof.Dr. Şerafettin Demić, for his healthy degree of optimisms when experiments disappointed and all seemed lost. I would also like to thank him for the warm and friendly atmosphere he garnered in his group; it encouraged sharing of ideas, insightful discussions and a productive work environment.

Next, I would like to thank Assoc.Prof.Dr.Mustafa Can and Assoc.Prof.Dr.Cem Tozlu for their helps on my thesis.

Additionally, I would like to thank Assoc.Prof.Dr. Hüseyin Ertik, Res.Asst.Abdullah Bayram, Res.Asst.Eyyüp Yalçın and Cebrail Özbek for their kindly helps.

I want to thank my parents. It is with their help for all my life that I became who I am today. Thanks for always being there for me, believing in me, and motivating me to set out on my own path.

My special thanks go to my husband, Emre Arkan, for his helps and moral support.

Finally, I want to thank TUBITAK for the 113M978 project support.

February 2017

Mesude Zeliha ARKAN

TABLE OF CONTENTS

| | <u>Page</u> |
|--|--------------|
| ACKNOWLEDGEMENT | ix |
| ABBREVIATIONS | xiii |
| SYMBOLS | xvi |
| LIST OF TABLES | xvii |
| LIST OF FIGURES | xix |
| SUMMARY | xxiii |
| ÖZET | xxv |
| 1. INTRODUCTION | 25 |
| 1.1 Photovoltaic Cells..... | 29 |
| 1.1.1. Organic photovoltaics..... | 31 |
| 1.1.1.1. Bilayer organic solar cell | 30 |
| 1.1.1.2. Bulk heterojunction solar cell | 31 |
| Metal oxides..... | 35 |
| Self-assembled monolayers..... | 36 |
| 1.1.2. Dye-synthesized solar cell..... | 35 |
| 1.1.2.1. Dyes..... | 38 |
| Metallic dyes..... | 38 |
| Metal free organic dyes..... | 38 |
| 1.1.2.2. Electrolyte..... | 39 |
| DSSCs with solid electrolytes (ssDSSC)..... | 39 |
| DSSCs with ionic liquids as electrolytes..... | 39 |
| 1.2 Characterization of Solar Cells..... | 40 |
| 1.2.1. Short circuit current (I _{sc})..... | 40 |
| 1.2.2. Open circuit voltage (V _{oc})..... | 41 |
| 1.2.3. Maximum power (P _{max}), current at P _{max} (I _{mp}), voltage at P _{max} (V _{mp})..... | 41 |
| 1.2.4. Fill factor (FF)..... | 42 |
| 2. MATERIALS AND METHODE | 43 |
| 2.1. Synthesis of Molecules | 43 |
| 2.2. UV-Visible Absorption and Cyclic Voltammetry..... | 44 |
| 2.3. Kelvin Probe and Efficiency Analyses..... | 44 |
| 3. RESULTS AND DISCUSSION | 45 |
| 3.1. Synthesis and Structural Analyses..... | 45 |
| 3.1.1. SAM molecules..... | 45 |
| 3.1.1.1. Synthesis of methyl 4-(5'-bromo[2,2'-bithien]-5-yl) benzoate..... | 45 |
| 3.1.1.2. Synthesis of methyl 4-(5'-phenyl[2,2'-bithiophen]-5-yl) benzoate (ZE-Ph)..... | 46 |
| 3.1.1.3. Synthesis of 4-[5'-(4-methoxyphenyl)-2,2'-bithiophen-5-yl] benzoic acid (ZE-1MeO)..... | 46 |
| 3.1.1.4. Synthesis of 4-[5'-(3,5-dimethoxyphenyl)-2,2'-bithiophen-5-yl] benzoic acid (ZE-2MeO)..... | 47 |

| | |
|---|------------|
| 3.1.1.5. Synthesis of 4-[5'-(3,4,5-trimethoxyphenyl)-2,2'-bithiophen-5-yl] benzoic acid (ZE-3MeO)..... | 47 |
| 3.1.2. Dye molecules..... | 52 |
| 3.1.1.6 Synthesis of 1-(hexyloxy)-4-iodophenol (1)..... | 52 |
| 3.1.1.7 Synthesis of (4-bromophenyl)bis[4-(hexyloxy)phenyl]amine(2)..... | 53 |
| 3.1.1.8 Synthesis of (4-{bis[4-(hexyloxy)phenyl]amino}phenyl) boronic acid (3)..... | 53 |
| 3.1.1.9 Synthesis of 6-(4-{bis[4-(hexyloxy)phenyl]amino}phenyl)-1H,3H-benzo[de]isochromene-1,3-dione (4)..... | 54 |
| 3.1.1.10 Synthesis of 4-(4-{bis[4-(hexyloxy)phenyl]amino}phenyl)-7-oxo-7H-benzimidazo[2,1-a]benzo[de]isoquinoline-11-carboxylic acid (5)..... | 54 |
| 3.1.1.11 Synthesis of methyl 4-bromo-7-oxo-7H-benzimidazo[2,1-a]benzo[de]isoquinoline-11-carboxylate(6)..... | 55 |
| 3.1.1.12 Synthesis of methyl 4-[4-(diphenylamino)phenyl]-7-oxo-7Hbenzimidazo[2,1-a]benzo[de]isoquinoline-11-carboxylate (7)..... | 55 |
| 3.1.1.13 Synthesis of 4-[4-(diphenylamino)phenyl]-7-oxo-7Hbenzimidazo[2,1-a]benzo[de]isoquinoline-11-carboxylic acid (8)..... | 56 |
| 3.2 UV-Visible Absorption Spectrums of SAM Molecules..... | 57 |
| 3.2.1. SAM molecules..... | 57 |
| 3.2.2. Dye molecules..... | 58 |
| 3.3 Cyclic Voltammetry Results of SAM Molecules..... | 60 |
| 3.3.1. SAM molecules..... | 60 |
| 3.3.2. Cyclic voltammetry results of SAM molecules on ITO surface..... | 62 |
| 3.3.3. Dye molecules..... | 64 |
| 3.4 ITO/SAM Kelvin Probe Microscope Analyses..... | 65 |
| 3.5 Contact Angle Results..... | 67 |
| 3.6 Investigation of Electrical Characterization of Solar Cells..... | 70 |
| 3.6.1 SAM molecules..... | 70 |
| 3.6.2 Dye molecules..... | 83 |
| 3.7. Incident Photon to Current Efficiency (IPCE) of SAM Molecules..... | 82 |
| 4. CONCLUSION..... | 85 |
| REFERENCES..... | 88 |
| APPENDIX..... | 96 |
| CURRICULUM VITAE..... | 117 |

ABBREVIATIONS

| | |
|----------------------|---|
| PV | photovoltaic |
| OPV | organic photovoltaic |
| CIGS | copper indium gallium diselenide Cu(In,Ga)Se_2 |
| PCE | power conversion efficiency |
| UV | ultra viole |
| Vis | visible |
| BHJ | bulk heterojunction |
| PC61BM | PC61BM ([6,6]-phenyl-C61-butyric acid methyl ester) |
| PC71BM | PC61BM ([6,6]-phenyl-C71-butyric acid methyl ester) |
| MEH-PPV vinylene) | poly[2-methoxy,5- (20-ethyl-hexyloxy)-p-phenylene |
| MDMO-PPV | poly[2-methoxy-5-(30,70-dimethyloctyloxy)-1,4- phenylene vinylene] |
| P3HT | poly-3-hexylthiophene |
| HOMO | Highest Occupied Molecular Orbital |
| LUMO | Lowest Unoccupied Molecular Orbital |
| ITO | Indium tin oxide |
| HIL | hole injection layer |
| PEDOT:PSS | Poly (3,4-ethylenedioxythiophene) : poly(styrenesulfonate) |
| OSC | organic solar cell |
| SAM | self-assembled monolayer |
| HTM | hole transport material |
| DSSC | dye sensitized solar cell |
| ssDSSC | solid state dye sensitized solar cell |
| IL | ionic liquid |
| FF | fill factor |
| Pt | theoretical power |
| DME | 1,2-dimethoxyethane |
| THF | tetrahydrofuran |
| NMR | nuclear magnetic resonance |
| FT-IR | foruer transform infra-red |
| TLC | thin layer chromatography |
| DMSO | dimethylsuphoxide |
| DMF | N,N-dimethylformamide |



SYMBOLS

| | |
|-----------------|--------------------------------|
| λ | wavelength |
| η | efficiency |
| I_{\max} | current of maximum power point |
| V_{\max} | voltage of maximum power point |
| P_{in} | light power from source |
| P_{\max} | maximum power |
| I_{mp} | current at maximum power |
| V_{mp} | voltage at maximum power |
| I_{sc} | short circuit current |
| V_{oc} | open circuit voltage |



LIST OF TABLES

| | <u>Page</u> |
|--|-------------|
| Table 3.1 : Photophysical parameters of MZ-341 and MZ-235 dyes. The molar extinction coefficients in $M^{-1} cm^{-1}$ are shown in parentheses. | 59 |
| Table 3.2 : HOMO and LUMO energy levels of SAM molecules | 60 |
| Table 3.3 : Oxidation potentials and HOMO energy levels of ITOs with SAM molecules | 64 |
| Table 3.4 : Contact potential difference between conductive tip Pt and substrate | 66 |
| Table 3.5 : Contact angle values of MoO_3 and SAM coated MoO_3 | 69 |
| Table 3.6 : Electrical parameters obtained from solar cells using different SAM materials. MoO_3 coated films were left in SAM for 24 hours..... | 70 |
| Table 3.7 : Electrical parameters obtained from solar cells using different ZE-3MeO SAM molecule. MoO_3 coated films were left in SAM for 9 and 15 hours. | 72 |
| Table 3.8 : Electrical parameters obtained from solar cells using different SAM materials. MoO_3 coated films were left in SAM for 9 hours..... | 73 |
| Table 3.9 : Electrical parameters obtained from solar cells using different SAM materials. MoO_3 coated films were left in SAM for 24 hours..... | 74 |
| Table 3.10 : Electrical parameters obtained from solar cells using different SAM materials. MoO_3 coated films were left in SAM for 12 hours..... | 75 |
| Table 3.11 : Electrical parameters obtained from solar cells using different SAM materials. MoO_3 coated films were left in SAM for 9 hours..... | 76 |
| Table 3.12 : Electrical parameters obtained from solar cells using different SAM materials. ITO substrats were left in SAM for 20 hours..... | 78 |
| Table 3.13: Average electrical parameters of cells with ITO/SAM/ MoO_3 anode electrode configuration..... | 80 |
| Table 3.14: The highest electrical parameters of cells with ITO/SAM/ MoO_3 anode electrode configuration..... | 80 |
| Table 3.15 : Solar cell parameters for DSSC with MZ dyes..... | 84 |



LIST OF FIGURES

| | <u>Page</u> |
|---|-------------|
| Figure 1.1 : A bilayer OPV, ideal bulk heterojunction and real bulk heterojunction solar cells | 31 |
| Figure 1.2 : A schematic diagram showing the different parts of the SAM molecule | 37 |
| Figure 1.3 : DSSC's schematic diagram | 38 |
| Figure 1.4 : Maximum Power for an I-V Sweep..... | 43 |
| Figure 1.5 : Getting the Fill Factor From the I-V Sweep..... | 44 |
| Figure 3.1: Molecule structures of SAM molecules | 47 |
| Figure 3.2: NMR spectrum of 4-[5'-(3,4,5-trimethoxyphenyl)-2,2'-bithiophen-5-yl] benzoic acid (ZE-3MeO)..... | 50 |
| Figure 3.3: FT-IR spectrum of 4-[5'-(3,4,5-trimethoxyphenyl)-2,2'-bitien-5-yl]benzoic acid..... | 51 |
| Figure 3.4: Synthesis procedure of SAM molecules..... | 51 |
| Figure 3.5: Structures of dye molecules..... | 52 |
| Figure 3.6: Synthesis procedure of MZ dyes..... | 57 |
| Figure 3.7: Absorption spectrum of SAM molecules..... | 58 |
| Figure 3.8: Absorption and Fluorescence spectrums of MZ dyes a)MZ-341 b)MZ-235..... | 59 |
| Figure 3.9: Cyclic voltammogram of ZE-Ph..... | 61 |
| Figure 3.10: Cyclic voltammogram of ZE-1MeO..... | 61 |
| Figure 3.11: Cyclic voltammogram of ZE-2MeO..... | 62 |
| Figure 3.12: Cyclic voltammogram of ZE-3MeO..... | 62 |
| Figure 3.13: Cyclic voltammogram of ITO/ZE-1MeO..... | 63 |
| Figure 3.14: Cyclic voltammogram of ITO/ZE-2MeO..... | 63 |
| Figure 3.15: Cyclic voltammogram of ITO/ZE-3MeO..... | 63 |
| Figure 3.16: Cyclic voltammogram of ITO/ZE-Ph..... | 64 |
| Figure 3.17: Cyclic voltammograms of MZ dyes a) MZ-235 b) MZ-341..... | 65 |
| Figure 3.18: CPD results of ITO substrat and SAM coated ITOs..... | 66 |
| Figure 3.19: Illustration of contact angles formed by sessile liquid drops on a smooth homogeneous solid surface..... | 67 |
| Figure 3.20: Contact angle measuring photo of MoO ₃ and SAM molecules..... | 69 |
| Figure 3.21: J-V graphs of solar cells prepared using different SAM materials..... | 71 |
| Figure 3.22: J-V graphs of solar cells prepared using ZE-3MeO SAM molecule..... | 72 |
| Figure 3.23: J-V graphs of solar cells prepared using different SAM materials..... | 73 |
| Figure 3.24: J-V graphs of solar cells prepared using different SAM materials..... | 74 |

| | |
|---|----|
| Figure 3.25: J-V graphs of solar cells prepared using different SAM materials..... | 76 |
| Figure 3.26: J-V graphs of solar cells prepared using different SAM materials..... | 77 |
| Figure 3.27: J-V graphics of ITO/SAM/MoO ₃ cells..... | 79 |
| Figure 3.28: J-V graphics of solar cells with ITO/SAM/MoO ₃ electrode configuration under illumination and dark..... | 81 |
| Figure 3.29: J-V curves of MZ dyes a) under light illumination (1.5 A.M 1000 W/m ²) b) in dark..... | 82 |
| Figure 3.30: IPCE curves of solar cells with/without SAM molecules..... | 84 |







SYNTHESIS, CHARACTERIZATION AND APPLICATION OF NEW ORGANIC ELECTROACTIVE MOLECULES FOR PHOTOVOLTAIC DEVICES

SUMMARY

PEDOT:PSS is with its acidic property solves the indium atoms from ITO and indium atoms diffuses in active layer in an organic solar cell. This event causes an decreasing in solar cell efficiency. In the same strategy, SAM molecules can be used as hole injection layer. On the other hand MoO_3 can be used as anode buffer layer. In this thesis it is wanted to make SAM molecules have to not absorb visible range of solar spectrum for the efficient harvesting of solar energy by donor molecule. Otherwise the HOMO level of SAM molecule have to be between work function of ITO and HOMO level of donor molecule. In this way SAM molecules which don't absorb the visible range of solar spectrum and with the suitable HOMO levels were designed, and applied on organic solar cell. On the other hand, while the series resistance in the solar cells to be formed with the synthesized molecules decreases according to the standard, parallel resistance increase is aimed.

DSSCs were proposed instead of silicon solar cells with their easy production and low cost fabrication. The photosensitizer which is liable for the visible and near-infrared utilization of the solar light, is one of the basic components of the DSSCs. Metal free organic dyes can be thought as an alternative for the solar energy to electricity conversion in DSSCs. One of the important parameter for the dye is harvesting solar energy efficiently. If the dye absorbs all solar spectrum more energy could be harvested. Furthermore, the energy levels of dye has to be suitable with TiO_2 and hole transport material. On the basis of this we designed two metal free organic dyes for DSSC, absorbing uv-visible range of solar spectrum and having proper HOMO-LUMO levels, were designed, and applied on dye sensitized solar cell.



**FOTOVOLTAİK CİHAZLAR İÇİN YENİ ORGANİK ELEKTROAKTİF
MOLEKÜLLERİN SENTEZİ, KARAKTERİZASYONU VE
UYGULAMALARI
ÖZET**

PEDOT: PSS asidik özelliğiyle ITO'nun indiyum atomlarını çözer ve indiyum atomları bir organik güneş pilinde aktif katmanda dağılır. Bu olay, güneş pil veriminde azalmaya neden olur. Aynı şekilde SAM (kendiliğinden organize tek katman) molekülleri boşluk transfer katmanı olarak kullanılabilir. Bu tezde, SAM moleküllerinin donör tabakanın absorpsiyonunu engellemek için görünür bölgede absorpsiyon yapmaması istenmiştir. Ayrıca, SAM moleküllerinin HOMO enerji seviyesi aktif tabakanın HOMO enerji seviyesi ile ITO'nun iş fonksiyonu arasında olmalıdır. Buradan yola çıkarak bu tezde görünür bölgede absorpsiyon yapmayan, uygun HOMO enerji seviyeli SAM molekülleri sentezlendi. Diğer yandan, sentezlenen moleküller ile oluşturulacak güneş hücrelerinde seri direnç standarda göre azalırken paralel direncin artması hedeflenmektedir.

Boya duyarlı güneş hücreleri kolay ve düşük maliyetli üretimleri ile silikon güneş hücrelerine alternatif olmaktadır. Güneş ışığını absorblamakla görevli boya, boya duyarlı güneş hücresinin en önemli parametrelerinden biridir. Metal içermeyen organik boyalar, boya duyarlı güneş hücrelerinde güneş enerjisini elektrığe döndürmede kullanılan çevre duyarlı yapılardır. Boya için en önemli parametrelerden biri güneş enerjisini verimli bir şekilde soğurmaktır. Boya tüm güneş spektrumunu absorblarsa daha fazla enerji hasat edilir. Ayrıca boyanın enerji seviyeleri de boşluk iletim malzemesi ve TiO_2 ile uyumlu olmalıdır. Bu bağlamda bu tez çalışmasında güneş spektrumunda UV-görünür bölgeyi absorplayan ve uygun HOMO-LUMO seviyelerine uygun boyalar sentezlenip uygulamaları yapıldı.



1. INTRODUCTION

In the new global economy, energy and environment have become two of the most central issues in the 21st century [1]. Civilization of mankind has resulted in great success in industrial development and given rise to predicted extinction of non-renewable energy sources and irreversible weather condition change. The population of Earth is almost 7.5 billion and people utilize energy in everyday to make life better, more productive and convenient. Over the decades, the energy consumption in the world have increased dramatically and ultimately reached a striking record of 8919 MTOE (million tonnes of oil equivalent) in the year of 2011 [2]. Vital part of energy that mankind uses is based on fossil fuels including petroleum, natural gas and coal that comprise big part of energy consumption in recent years [3]. The statistics have indicated that although global consumption in fossil based energy has accounted up to 80%, depletion of reserves is indispensable by the end of this century due to the continuous exploitation of human being [4]. Moreover, this consumption has resulted in excessive emission of greenhouse gases such as CO₂, which has caused global warming. Based on the report of Intergovernmental Panel on Climate Change's (IPCC), the overall average temperature of Earth has augmented by 0.5~0.8 oC since 1850 [5]. In the long term, three main alternatives can be proposed to decrease the CO₂ emission, without any decrease in global energy consumption [6]:

- Nuclear power; today there are around 440 nuclear power reactor operable around the world. They provide over %11 global energy demand.

- Carbon sequestration; this concept enable us to use reserves of fossil fuels provided that we have to take care of emissions and storage of them in available cavities in the earth.

- Sustainable energy; all required energy can be generated with these technologies by putting outstanding effort in developing existing and new techniques for sustainable energy production.

The initial option is not favorable and time limited solution due to the potential risk and finite amount of uranium reserve. The second alternative is neither sustainable solution nor tested method in large scale and therefore it is not for certain that it will work. Sustainable energy sources can be considered as the most promising alternatives and long term solution to be utilized [6].

From the perspective of energy level consumption, the values are not equally increasing all around the world [7]. For instance, consumption levels are relatively stable in Europe and these quantities will remain similar in the next 20 years according to predictions by the U.S. Energy Information Administration (EIA) [8]. Together with the European Union (EU), the individual governments have proposed goals associated with energy consumption and production. The following requirements have to be fulfilled until 2020 [9].

- I. Emission of chemicals (i.e. CO₂, NO_x, CH₄ etc.) that cause greenhouse have to be decreased by 20%
- II. 20% of energy demand should be supplied by renewable energy sources.
- III. Energy efficiency should be improved by 20% within the EU

In addition to aforementioned expectation, the EU has further long-term aims; until 2050, energy consumption should be decreased by 30% and greenhouse emission should be reduced by 80%. The administrations of five Nordic countries have declared even advanced goals for their own countries by intending reduction of greenhouse emission by 85% [10,11].

The desire for sources to produce more sustainable energy has appeared as an urgent problem. In this respect, the word of “sustainable” has more than one meaning. These energy sources should be both renewable and CO₂ neutral. This group of preferred energy sources embraces: hydroelectric energy, wind energy, wave energy, geothermal energy, biomass-based energy and sun energy. Even though some of these energy sources including biomass-based, wind power and hydroelectric power are well-developed in a few EU states, fossil based fuels are still vital for energy supply in Finland, Denmark, and remaining part of the world [11]. Therefore, research into renewable energy technologies has been introduced as the key point for the sustainable future.

In general, within the concept of renewable energy, solar energy is described as the only inexhaustible source with large potential [12, 13]. It is generated as a result of continuous fusion reaction inside the Sun and the produced power is about 3.8×10^{23} kW. The Earth's upper atmosphere approximately can receive 1.7×10^{17} kW of radiated power. In spite of all reflection from atmosphere and absorption in clouds, arriving solar energy receiving to oceans and landmasses of the Earth can reach to 8.0×10^{16} kW that is a tremendous energy source [14]. According to the International Energy Agency (IEA), the solar energy falling on earth in one hour was bigger than world annual energy usage in 2012. It is because of this, solar cells have demonstrated remarkable potential with considerably rapid growth [15]. More specifically, 139 GW total capacities had been installed all around the world until the beginning of 2014 [12,13]. With solar cell technology, this radiation, without any material consumption, can directly be converted into the most useful form of energy, electricity.

1.1 Photovoltaic Cells

The use of photovoltaic devices (PVs) is the simplest way of the direct alteration of solar energy into the electric power. The first practical PVs, developed by Daryl Chapin et al. at Bell Laboratory in 1954, was fabricated as p-n junction and reached power conversion efficiency (PCE) of 6%, which was also known as first-generation solar cell [16]. The mechanism of solar cell is rather simple. When a solar cell is subjected to illumination, the front and back sides are charged differently, and solar cell becomes a battery. The reason of this effect can be explained by two basic mechanisms. Incoming light is absorbed by electrons in solar cell and thereby promoted to higher energy level. While the electrons are elevated to a higher energy level, an oppositely charged hole remains behind them. An electric field formed in solar cell discrete these inversely charged particles by pushing them in different directions and lead to the oppositely charged front and backside of solar cell. Electric current flows after the connecting of back and front contacts with a load as long as solar cell is kept under illumination. This current enables electrons to come back to the solar cell at the lower energy level and the process can become repeatable [6].

Today's market, crystalline or polycrystalline silicon (Si) dominate over 90% of solar cell modules. There are many reasons having led to great achievement of

silicon based solar cell. The most important factors would be appropriate long-term stability and high PCE. Huge amount of silicon reserve (around 20%) on Earth crust is another advantage of this technology. However, production of high purity semiconductor materials is the first obstacle for all types of inorganic solar cell to reach ideal efficiency. Therefore, compare to conventional technology, this type of solar cells lead to ten times higher cost to generate same amount of electricity. Also, wafer technology is required for the fabrication of solar cell module that entail production Si wafers and soldering them together [6]. This results in further manufacture cost and complexity in production process.

Thin film solar cells are other types of photovoltaic system and called as second generation solar cell. It comprises several thin films with the thicknesses of $10\mu\text{m}$ or less that is deposited on low cost substrate. The advantage of this technology is that large scale and complete solar cell module can be produced in one piece via monolithic integration, which significantly lower the production cost compare to crystalline Si solar cells. So far, there are three thin film technologies, which are amorphous silicon (a-silicon), cadmium telluride (CdTe) and copper indium gallium diselenide Cu(In,Ga)Se_2 (CIGS), candidate for large-scale production [6]. Despite industrial activity was relatively high, particularly for CdTe-based thin film solar cells, until 2002, industrial activity was closed during that year due to the lack of market acceptance corresponding to high amount of toxic element Cd used in this device [17].

Organic photovoltaic cell or Organic Photovoltaics (OPVs) are categorized as third generation solar cell. They are, basically, excitonic solar cell [18]; nevertheless, their physical properties are different from those of inorganic counterparts. Through researches conducted in this area, deeper knowledge has been gained by scientists and significant increase in PCE is obtained. Specifically, after the development of solution process for small molecules and polymer materials, this technology has become more exciting and has been subjected to great academic and industrial interest due to their easy adaptation to commonly used industrial techniques such as the wet coating and printing lines [19]. This progress resulted in fabrication of thin, low-cost and flexible plastic based OPVs. More recently, transparent electrodes and semi-transparent solar cells with broad absorption covering to UV region has been developed and used as building materials [20,21].

1.1.1 Organic photovoltaics

In 1959, Kallman and Pope first used anthracene molecules to make solar cell that is also accepted as the beginning of OPVs [22]. The field gained special interest and advanced further in 1970's when conducting polymer were discovered and used for doping to achieve conductivities [23] . This discovery became famous and was awarded with Nobel Prize in Chemistry in first year of millenium gained by Heeger, MacDiarmid and Shirakawa [24]. Another important turning point was achieved by Tang in 1986, which was the utilization of the joining of two distinct molecules. One of the molecules is electron-donor and the other is electron-acceptor [25]. The introduction of C60 ([60] Fullerene) as a new acceptor group in 1992, by Sariciftci et.al and improvement of different device structure are other featured milestones of OPVs. Further developments have been focused on types of device structure, engineering of materials and processing conditions [26].

Organic Photovoltaic cells can be mainly classified as “Bilayer Organic Solar cell, Bulk heterojunction Solar Cell and Dye-Sensitized Solar Cell”.

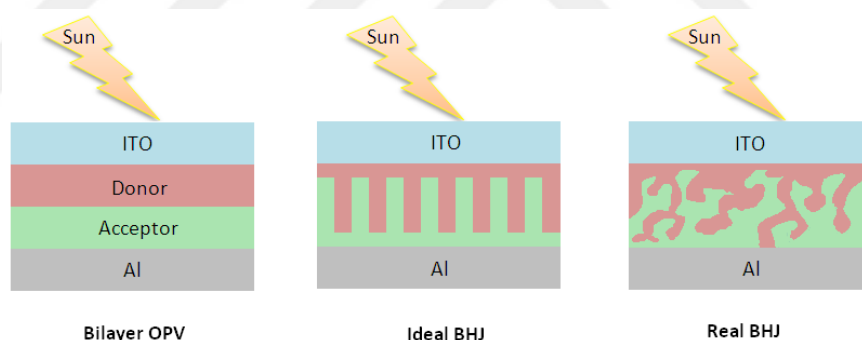


Figure 1.1 : A bilayer OPV, ideal bulk heterojunction and real bulk heterojunction solar cells

1.1.1.1 Bilayer organic solar cell

In bilayer solar cell, donor (p-type) and acceptor (n-type) materials are coated layer by layer. For the ideal device structure, 10-20 nm distances at donor-acceptor interface are theoretically required for electron-hole pair to reach the interface of layers. The higher distance brings about the quenching of the photon, low quantum yield and formation of minimum photocurrent[27].

In the early scientific researches, metal phthalocyanine has preferred as donor material together with acceptor C60 molecule in bilayer organic solar cell and

obtained PCE was reported around 3,6%. However, it was found that the obtained results were not repeatable [28]. Therefore, in this configuration (C60/MPc, M=Zn,Cu) the most reliable PCE was around 2,0-2,5% [29].

To further increase power conversion efficiency in bilayer organic solar cell, device fabrications were conducted by using several p-type organic materials. Particularly, tin phthaloyanine was introduced as an extra layer into the C60/CuPc system to change the absorption into the infra-red part of solar spectrum. But, reported PCE remained at around 1% [30]. In another study, boron- subphthalocyanine used as a donor material instead of Cu/Pc to increase open circuit voltage (Voc) [31]. Indeed, obtained Voc in this system was twice larger than that of found in C60/CuPc arrangement. However, the achieved PCE was only 2.1% owing to a decrease in short-circuit current density. A subsequent, more careful optimization of this combination provided PCE of about 3% [32].

Another strategy to make the performance of the bilayer solar cell better is based on utilizing different n-type materials. Pyrrolidinofullerenes bearing chelating pyridyl groups, which is derivatives of fullerene C60, have been used instead of nonmodified fullerene C60. Since this substance is highly soluble in organic solvents, it enables to fabricate films from solution by spin coating that is more efficient and economic process than vapor deposition. The main advantage of this compound is pyridyl groups on molecular structure because it can form complexes with zinc phthalocyanine at the border between donor and acceptor layers and increases the efficiency of charge separation in the donor and acceptor interface [33]. On another side, main disadvantage of this compound is organic moieties on the structure that remarkably impair electron transport ability of fullerenes. As a consequence, maximal PCE obtained for pyrrolidinofullerene/ZnPc cells is 1.6% [34-35].

It is probably that replacement of metal phthalocyanine with other organic donor is the most promising strategy for increasing performance of bilayer cells. It was indicated that combination of oligothiophene electron-donor material with fullerene acceptor provides PCE up to 3.4% that seems to be record value for bilayer solar cells.

1.1.1.2 Bulk heterojunction solar cell

Different from bilayer solar cell, in a bulk heterojunction (BHJ) solar cell donor and acceptor substances exist as a mixture in active layer. The practical reason of this is due to the solubility and applicability of organic substances in organic solvent. Therefore, it is possible to decrease the fabrication cost of device by depositing from solvent via modern printing technology. The main advantage of BHJ solar cell over bilayer organic solar cell is its superior PCE that is the consequence of high interface area between donor and acceptor materials. Therefore, efficient separation of excited charge can provide at around % 100 quantum yields in BHJ solar cell [36].

A short time ago, considerable progress has been taken place in BHJ solar cell by exceeding the barrier of %10 PCE [37]. Although a clear relationship between material properties and device performance has yet to be established, it is possible to tailor some electronic features such as absorption and energy levels during the synthesis. Considering the natural photosynthetic system, it is observed that highly ordered and conjugated self-organized nanostructures regulate the process of light absorption and charge separation [38]. Hence, arrangement of molecular packaging for advanced applications with organic materials is one of the most vital issues in the solar cells fabrication [39,40]. In the view of these researches, it is borne out that in addition to electronic structure, several parameters covering morphology of the materials has direct effect on device performance.

A p-type (donor) and an n-type (acceptor) semiconductor are the two components which can form interpenetrating networks through depositing simultaneously from solution, and therefore enable transport of charger carries to their relevant electrodes in BHJ solar cells. Most regularly preferred n-type materials are fullerene derivatives, such as PC61BM ([6,6]-phenyl-C61-butyric acid methyl ester) and PC71BM, in consequence of their low lying energy levels, reversible electrochemical reductions and solubility in organic solvents [41]. Moreover, fullerenes have special π -conjugated systems and π -electron functionality in addition to their exceptionally high stability. In organic photoelectric conversion, fullerenes play a role that is difficult for other π -electron systems to fill and therefore still have the potential to bring about a revolution in solar cells [42].

The early OPV researches were mostly using poly[2-methoxy,5-(20-ethyl-hexyloxy)-p-phenylene vinylene] (MEH-PPV)/C60 composites that were then replaced by the better processable blend of poly[2-methoxy-5-(30,70-dimethyloctyloxy)-1,4-phenylene vinylene] (MDMO-PPV)/1-(3-methoxycarbonyl)propyl-1-phenyl[6,6]C61 (PCBM) [43-45]. However, since efficiencies of this combination remained at 3% at best [46-48] due to the low mobility and rather large band gap of the PPV-type polymers, general interest in this group of substance is faded. An important step in the progress of OPV cells is the usage of P3HT as a donor material. The prominent advantage of the P3HT is the formation of laminar structure when subjected to elevated temperature. Compare to MDMO-PPV system, P3HT provides high current density through improved charge transfer characteristic. Even though this characteristic makes P3HT the most general and popular donor material for many fundamental and conceptual studies, it has insufficient absorption in visible region and thus its maximum PCE remains at around %5. Since the structure of P3HT does not allow the structural modification to overcome this limitation, researchers have been looking for alternative organic moieties including co-polymers and small molecules.

Over the time, donor components have subjected to significant diversification and embrace polymer systems [41,49,50] and discrete molecules [51]. Most of sunlight-induced photoexcitations (excitons) take place in p-type (donor) materials because fullerene has limited absorption. Diffusion of electrons occurs until they reach a donor/acceptor border, where electron flows to acceptor material. [52] Electrons migrate through the acceptor and holes migrate through the donor phase to the respective electrodes. The related ideal donor materials should meet with some following requirements:

- (1) wide-range and intense absorption in the solar spectrum's low energy region to ensure effective light harvesting;
- (2) deep (Highest Occupied Molecular Orbital) HOMO energy level to alter high Voc of OSCs[53];
- (3) good solubility for solution-processing.

A combination of several parameters embracing structural insight, morphology control, polymer design and instrument engineering has given rise to PCEs

approaching 6-8.3% range for fullerene-conjugated polymer blends [54-61] and later this value has reached to 10.5% [62]. To fabricate efficient polymer based solar cells, the majority of reported papers use narrow bandgap conjugated polymers (as donor materials) together with a fullerene derivative (as acceptor materials). Nevertheless, the random nature of polymerization reactions bring about wide range in characteristics of molecular weight and finally in instrument performance.

It is well known fact that indium tin oxide (ITO) is frequently utilized electrode material for device fabrication from the point of view of large conductivity and high transparency. However, since substantial energetic mismatch exist at the interface of ITO and organic semiconductor, a direct hole-injection (extraction) from ITO to organic transport material is insufficient. This energetic mismatch entails high operation voltages to exceed the injection barrier that lead to decreased efficiency. Hence, different anode interfacial layers (or hole-injection layer (HIL)) can be inserted as hole-selective layer between the electrode and active layer to minimize hole- extraction barriers and to increase the performance of organic solar cells. A widely employed HIL is Poly (3,4-ethylenedioxythiophene) : poly(styrenesulfonate) (PEDOT:PSS) [63-64]. But, in addition to its solution with acidic nature (pH=1) that corrodes the ITO surface, the aqueous PEDOT:PSS dispersion brings about degradation owing to the existence of moisture as well as reduction in the lifetime of device [65-68]. Furthermore, work function of PEDOT:PSS is 5.0-5.1 eV, which can restrict charge injection into materials carrying high amount of ionization energy. Hence, it is significant to offer stable, friendly and promising alternative materials to be used as HIL rather than PEDOT:PSS in OSC [69].

Metal oxides

It should be indicated that transition metal-oxides such as tungsten-, vanadium-, nickel-, rhenium-, and molybdenum-oxides (WO_3 , V_2O_5 , NiO , ReO_3 , MoO_3) are currently focus of intense research instead of PEDOT:PSS [70-75]. In particular, transition metal-oxides have been ubiquitous cathode electrodes for Gratzel type electrochemical solar cells, inverted solar cells, and organic light emitting diode. In organic solar cell application, these materials can act as a buffer layer on metal electrodes due to their high permeability in visible region of solar spectrum, high semiconducting features, and high charge mobility values. The first studies associated with application of metal-oxide as anode electrode or hole-transport buffer

layer appeared in design of organic light emitting diode. The subsequent researches have focused on metal oxides to be utilized as a hole-transport layer to increase efficiency of hole- mobility through electrodes. Specifically, MoO₃ has strongly n-doped by oxygen vacancies and indicate considerably deep lying electronic states [76]. It can evaporate at low temperature (~400oC) and therefore is feasible anode buffer layer for employing in OSC. According to the previous reports, vacuum-grown MoO₃ exhibit electron affinity (EA) of 6.7 eV, work function (WF) of 6.9eV and ionization energy (IE) of 9.7eV, respectively [76]. Its fermi energy level is lower within the range of 0.5-0.2 than conduction band limit [77,78]. On the other hand, depending on stoichiometry and surface contamination, MoO_x can possess various work functions. The example would be the exposure of oxygen and air, which lead to change in energy band levels. It can be concluded that since HOMO energy levels of polymers used in organic solar cells with high PCE chance within the range of -5.2eV to -5.6eV, thermally evaporated MoO₃ use as an anode interlayer provides matching energy levels with related polymers [79].

Self-assembled monolayers

Self-assembled monolayers (SAM) of organic molecules can be defined as the formation of spontaneous molecular assembly on any surface due to the adsorption. SAMs are an affordable and useful surface coating for applications including sensitization, bio compatibility, molecular recognition for sensors, control of wetting and etc. SAMs molecules, comprise three main groups namely head group, tail and functional end group. There are various types of head groups with specific affinity for a substrate and metal oxides. For example, silane head groups are convenient for the substrate including HfO₂ [80], ITO [81], PtO [82], TiO₂ [80], ZrO₂ [83] and alcohol based amphiphiles are suitable for the substrate such as Fe_xO_y [84], Si-H [85], Si [86]. Moreover, acidic head groups such as RCOO⁻/RCOOH have affinity to α -Al₂O₃ [87], Fe_xO_y [88], Ni [89], Ti/TiO₂ [90] type substrates. SAMs can be created from either the liquid or gas phase onto a substrate surface via chemisorption that leads to slow organization of tail group. Over the period of minutes or hours, the head group assembles together on the substrate surface and results in formation of areas of close- packed molecules until single monolayer formed on substrate surface. Van der Waals interactions give rise to tight monolayer packs and thus reduce free energy of the surface [91]. The first example of the application of SAM molecules in

organic electronic device was shown in the study of organic electroluminescence where ITO surface was used as anode substrate and modified with SAM molecules, thereby reducing energy level between hole-transport materials (HTM) and anode material as well as increasing current density [92-96].

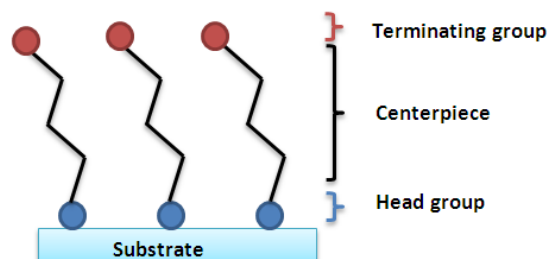


Figure 1.2 : A schematic diagram showing the different parts of the SAM molecule

1.1.2 Dye-synthesized solar cell

At the end of the last century, fabrication of robust large-scale solar cell based on molecular components for the feasible generation of electricity was considered to be utopic. But, the promising paper, written by O'Regan and Grätzel in 1991, encouraged researchers to compete in this challenge [97]. After the evolution of dye-sensitized solar cells (DSSCs), conventional solid-state photovoltaic technologies have confronted with big challenge by systems operating at a nano and molecular-level. DSSCs have proposed seminal features, for instance, for the small cells and minimodules, the obtained record efficiencies is about 12% and 9%, respectively as well as reached durable efficiency is of 8-9% with 1000h stability at 80oC. The cost-effective investments and easy fabrication are other advantages. Compare to other solar cell technologies, DSSCs operate relatively better under diffuse light condition and at elevated temperatures. DSSCs are also applicable to the flexible substrate with various shape, color, transparency and easy to integrate different products to come up with new commercial opportunities [98].

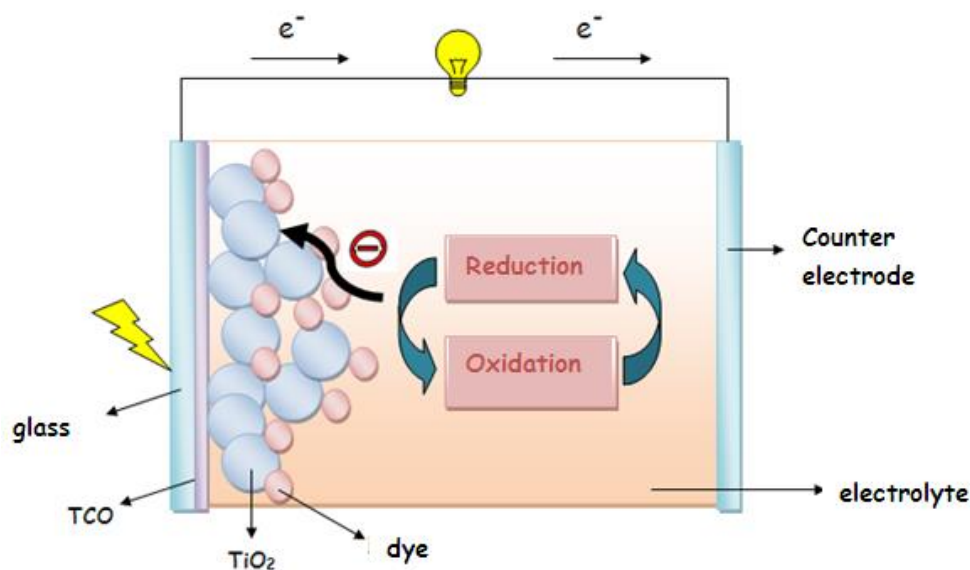


Figure 1.3 : DSSC's schematic diagram

After the work of Grätzel et al in the beginning of 1990s, high amount of work has been done for the development of a wealth of DSSC components and configurations. Essential working principles of the system have been understood through advanced characterization techniques and theoretical modelling of electrical and optical properties. The research in the synthesis of dyes (sensitizers) can be categorized into two main areas;

1-) Metal containing dyes; Functional ruthenium(II)-polypyridyl complexes such as N3 [99, 100], N719 (TBA+=tetra-n-butylammonium) [101, 99, 102], Z907 [103-105], and black dye [106- 108].

2-) Metal-free organic donor-acceptor (D-A) dyes.

The synthesis of the compounds in the former class entails expensive ruthenium metal, careful synthesis and complicated purification process. By contrast, the second class can be synthesized by means of low-cost and well-known synthesis method. The outstanding features of metal-free dyes are their tunable electrochemical and absorption properties through convenient molecular engineering [109].

Amongst metal containing sensitizers, ruthenium(II)-polypyridyl complexes produce high efficiencies due to the wide absorption range covering visible region and extending to the near-infrared (NIR) regime. Additionally, bipyridyl group bears carboxylate moieties that decrease the energy of the anti-bonding π^* orbital. Since

the electronic transition is defined as charge transfer from metal to ligand, excitation energy is efficiently given to the carboxylate moieties, from where electrons are poured into the conduction band of the semiconductor [110]. On the other hand, these dyes have moderate molar extinction coefficients ($\epsilon \leq 20000 \text{ L mol}^{-1} \text{ cm}^{-1}$). In spite of the low absorptivity of nanostructured titanium dioxide (TiO_2), its thickness on the conductive substrate can be changed to absorb almost all incoming light. But, with the help of fine engineering in structure of organic donor-acceptor dyes, high extinction coefficients can be obtained for all molecules [111]. Different from ruthenium (II) complexes, organic framework can be modified with various absorbing groups to adjust absorption and to achieve high extinction coefficients.

DSSCs consist of five components such as i) photoanode, ii) semiconductor metal oxide, iii) sensitizer, iv) hole transport material/electrolyte, and v) counter electrode. The sensitizer, anchored to the surface of semiconducting TiO_2 nanocrystals, absorbs the incoming light. The charge separation occurs at the border by the way of photoinduced electron injection from the excited sensitizer (dye) into the conductive band of the semiconductor (TiO_2). In the sensitizer's (dye) ground state holes are formed, and regenerated via reduction by the HTM, which is regenerated by electrons at the counterelectrode with an external circuit. The efficiency of DSSCs depends on a well-known principle, namely, a hole-transporter should regenerate the sensitizer more rapidly with respect to the recombination speed of the conduction band electrons with the oxidized sensitizer. In addition to this principle, in order to regenerate the oxidized dyes effectively formed after electron injection into the conduction band of semiconductor (TiO_2), by accepting electrons from hole transport material (HTM), the HOMO of sensitizer has to be found under the energy level of hole transporter.

1.1.2.1 Dyes

The following criteria can be satisfied in an ideal dssc, namely; i) the dye must have broad absorption band and high molar extinction coefficient, ii) with the aim of an easy electron transfer, the lowest unoccupied molecular orbital (LUMO) of dye has to be above than the conduction band of TiO_2 , iii) for an efficient electron transfer from redox couple to dye, the highest occupied molecular orbital (HOMO) of dye has to be less than the energy level of redox couple, iv) the dye must have anchoring

groups such as -COOH, -SO₃H, -PO₃H, and v) the dye must have high light and thermal stability for long life time.

Metallic dyes

Metallic dyes are very suitable molecules for DSSCs due to their broad absorption band. Until now the best photovoltaic performance was obtained by using Rutenium (Ru) polipyridil complexes (N3, N719 and black dye) by Gratzel et.al. Addition to their high light characteristics, Ru dyes have an advantage namely injection of photoelectric charge to TiO₂ via metal-ligand charge transfer. In Ru complexes, this transfer occurs faster than the recombination of oxidized electrons in dye [112].

Metal free organic dyes

There are some important factors for efficiencies of the dye and DSSC as follows:

- Absorption range of dye must include all visible region and part of the near-IR region. Molar extinction coefficient has to be high possibly.
- In order to provide an efficient electron injection into the anode, the LUMO of dye should be taken place near the anchoring group, i.e. a phosphonic or carboxylic acid, and, above the conduction band edge of the semiconductor electrode such as TiO₂.
- The energy level of redox couple must always be higher than HOMO of the dye.
- The dye should not be aggregated on the surface in order to prevent the nonradiative decay that is from the excited state to the ground state, which is usually observed with thicker films [113].
- In order to make the charge recombination minimum between the oxidized dye and the injected electrons, the positive charge occurred via electron injection process should be placed on the donor part, which is more away from the TiO₂ surface [114-118].

In recent years, metal free organic dyes are spotlighted because of their economic availability and being eco-friendly feature. As examples of these important organic dyes, Coumarine, indoline, merocyanine, and triphenylamine can be shown with

their 7-9% efficiency. For a metal-free organic dye, the highest power conversion efficiency ever detected is about 12% [119].

1.1.2.2. Electrolyte

DSSCs with Solid Electrolytes (ssDSSC)

In solid state DSSC, a hole transport material (HTM) is used instead of liquid electrolyte which reduce the oxidized dye. Solid HTMs have less diffusion distance than liquid redox couple. Disadvantages such as solvent evaporation and leakage, encountered in applications are prevented even better with respect to IL-DSSCs. After many kinds of hole-transporting materials have been experienced in ss-DSSCs, it is found that the inferior pore filling of porous TiO₂ films by the HTM makes the total efficiencies of solid state-DSSCs less than those for IL-DSSCs [120]. The efficiencies of above 5% have been reached by using solar cells which incorporate spiro-MeOTAD (2,2',7,7'-tetrakis-(N,N-di-p-methoxyphenylamine)-9,9'-spirobifluorene) or a highly conductive ionic polymer solid electrolyte as hole conductors and ruthenium(II)-polypyridyl complexes as sensitizers respectively [121-123].

DSSCs with Ionic Liquids as Electrolytes

In recent years, scientists have made Ionic liquids (ILs) to be useful as solvents or components of liquid and quasi-solid electrolytes for DSSCs [124-127]. Besides the reduced volatility due to negligible vapor pressure, the two important properties of ILs over organic solvents are thermal stability, and high ionic conductivity. These mentioned properties provide a better long-term stability in solar cells. In terms of performance, the experimental comparisons show that devices with liquid electrolytes degrade faster than cells with ILs, which is undesirable for practical applications. Additionally, the electrochemical stability is kept at a higher level if ILs are used instead of liquid electrolytes. On the other hand, as a main disadvantage ILs usually show worse performance in devices due to their high viscosity, which leads to mass-transfer limitations on the photocurrent under highest illumination [128]. A thin nanocrystalline TiO₂ film is required to approach high conversion efficiencies by virtue of the slow diffusion of I⁻ and I₃⁻ ions in ILs due to their high viscosity. Due to these aforementioned reasons, metal-free organic dyes exhibiting high absorptivity behavior are suitable for DSSCs with ionic liquids (ILDSSCs).

1.2 Characterization Of Solar Cells

The characterization of organic solar cells is made by using current-voltage curve under the standard value of 1.5 AM and 100 mW/cm² light. A solar simulator is needed for this purpose. Three parameters such as short circuit current (Isc), open circuit voltage (Voc) and fill factor (FF) are computed from current-voltage characterization. An example current-voltage curve of a photovoltaic cell is depicted in Figure 5. Short circuit current density (Isc) is measured under zero current. In this these, voltage applied to provide electromotor power is called Voc, I_{max} and V_{max} are current and voltage of maximum power point respectively. Power efficiency is calculated by multiplication of data.

$$\% \eta = \frac{V_{oc} I_{sc} FF}{P_{in}} \quad FF = \frac{I_{max} V_{max}}{I_{sc} V_{oc}} \quad (1)$$

P_{in}=light power from source

FF=fill factor

1.2.1 Short circuit current (Isc)

The short circuit current I_{sc} is calculated when the voltage is zero, namely I (V=0) = I_{SC}, and the short circuit condition occurs when there is low impedance. For an ideal cell, the highest current value is obtained when the total current is produced in the solar cell by photon excitation.

$$I_{SC} = I_{MAX} = I_{\ell} \text{ for forward-bias power quadrant}$$

1.2.2 Open circuit voltage (Voc)

The term of open circuit voltage (V_{OC}) determines the case of no current flowing through the cell, namely V (at I=0) = V_{OC}. On the other hand, V_{OC} corresponds to the maximum voltage difference across the cell for forward-bias sweep power quadrant, namely V_{OC} = V_{MAX}.

1.2.3 Maximum power (P_{MAX}), voltage at P_{MAX} (V_{MP}), current at P_{MAX} (I_{MP})

The computation of power producing by the cell can be easily made by making use of I-V sweep and utilizing the well known equation $P=IV$. The zero and maximum values of power are observed at the I_{SC} and V_{OC} points, and between the two points, respectively. The maximum value of power is marked by P_{MAX} point, and the voltage and current values at P_{MAX} point are shown as V_{MP} and I_{MP} respectively.

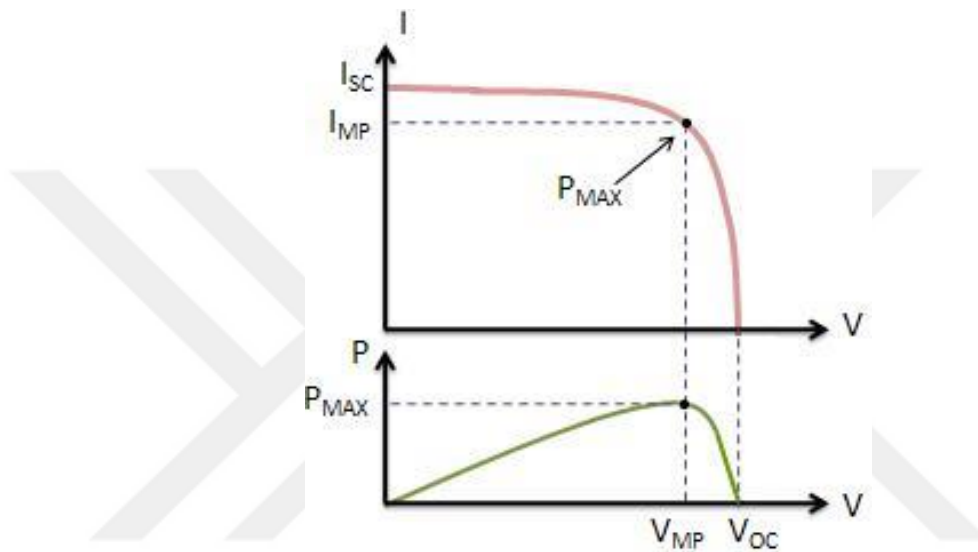


Figure 1.4 : An I-V Sweep also identified P_{MAX} [129]

1.2.4 Fill factor (FF)

The Fill Factor (FF) is used as the solar cell's quality indicator. The calculation of FF is made by comparing the maximum and theoretical power (P_T) with each other. The theoretical power (P_T) is calculated in the case of both the open circuit voltage and short circuit current being together. For another definition of FF, the graphical interpretation can also be made by using the rectangular areas's ratio depicted in Figure 1.5.

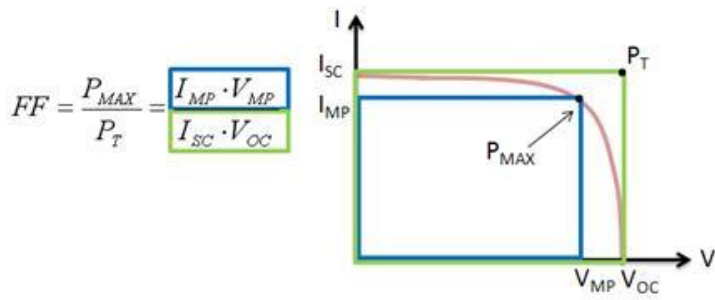


Figure 1.5 : Obtaining From the I-V Sweep The Fill Factor [129]

A higher FF corresponding a more square-like I-V sweep is desirable for optimum efficiency. Typical FF values range from 0.5 to 0.82, and are usually shown as a percentage.

1.2.5 Efficiency (η)

Efficiency is defined by the ratio of the output electrical power (P_{out}) to the input solar power (P_{in}) entering the PV cell. P_{out} can be assumed as to be P_{MAX} , because of the getting maximum efficiency capability of the solar cell that can be utilized up to its maximum power output.

$$\eta = P_{out} / P_{in} \rightarrow \eta_{max} = P_{max} / P_{in} \quad (3)$$

P_{in} is defined as the product of the irradiance of the incoming light with the surface area of solar cell. In calculations, the irradiance of the incoming light and the surface area of solar cell are measured in W/m^2 and m^2 respectively. The maximum efficiency exhibits a sensitive dependence on the following factors such as; (i) the performance of the device under test, (ii) temperature and (iii) the spectrum and intensity of the incoming light, which are called as ambient conditions. Therefore, for an acceptable test, PV cells should be compared by using similar lighting and temperature conditions as much as possible [129].

2. MATERIALS AND METHODE

2.1 Synthesis of Molecules

Supplier of 5-Bromo-5'-((4,4,5,5-tetramethyl-3,2-dioxaborolan-2-yl)-2,2'-bithiophene was purchased from TCI. [4-(methoxycarbonyl) phenyl] boronic acid, benzene boronic acid, 4-methoxybenzeneboronic acid, 3,5-dimethoxybenzene boronic acid, 3,4,5-trimethoxybenzene boronic acid, 4-iodophenol, 4-bromoaniline, 1,2-dimethoxy ethane (DME), and N,N-dimethylformamide (DMF) is Alfa-Aesar. Potassium carbonate was obtained from Riedel de Haen. Supplier of 1-bromohexane and copper (I) iodide is Fluka; Supplier of 18-crown-6, phenanthroline, n-butyllithium, tetrahydrofuran (THF), trimethylborate, 4-bromonaphthalene, 3,4-diaminobenzoic acid, [1,10-bis(diphenylphosphino)ferrocene]dichloropalladium(II), acetone, dichloromethane and toluene is Sigma-Aldrich. Supplier of Zinc acetate and potassium carbonate is Riedel de Haen

No purification is done on any chemicals, solvents, and reagents received from commercial source. All glassware was oven-dried and all reaction was performed under inert (N₂) environment.

2.2 UV-Visible Absorption and Cyclic Voltammetry

For the electrochemical measurements of MZ-341 and MZ-235 dyes CH 440B Instruments potentiometer was used. FT-IR measurements were made on a Thermo Scientific FT-IR Spectrometer with an ATR system (3000-650 cm⁻¹). ¹H and ¹³C NMR (Varian-400 MHz) data were made at 25 °C utilizing CHCl₃-d and d₆-DMSO as solvents and TMS as an internal standard. The absorption and fluorescence spectra were recorded utilizing a Termo Scientific UV-Vis spectrophotometer and a Hitachi F-2500 fluorescence spectrophotometer, respectively.

2.3 Kelvin Probe and Efficiency Analyses

Kelvin Probe analyses were carried out with NT-MDT Ntegra Solaris AFM. Xe light and a Solar Light Co. solar simulator (model 16S-300) was used for solar cells'

characterization by illuminating the samples.. The light intensity was 1000 W/m^2 for all device measurements. At the end, the J-V curves were made by connecting the cells to a Keithley Source Meter (model 2601A and 2200). Keithley computer software (LabTracer) controlled the process.

The ITO/MoO₃/P3HT:PCBM/LiF/Al structure was taken as reference solar cell, and the ITO/MoO₃/SAM/P3HT:PCBM/LiF/Al structure was prepared by using SAM molecules. In the first step DMSO solvent was used. Then the solvent was changed as DMF because of the wetness of DMSO.

In the solar cells a quasi-solid state electrolyte was used. This was preferred as it decreases the risk of leaks minimizing sealing problems in the cells while it combines the high ionic conductivity of liquids.



3. RESULTS AND DISCUSSION

3.1 Synthesis and Structural Analyses

3.1.1 SAM molecules

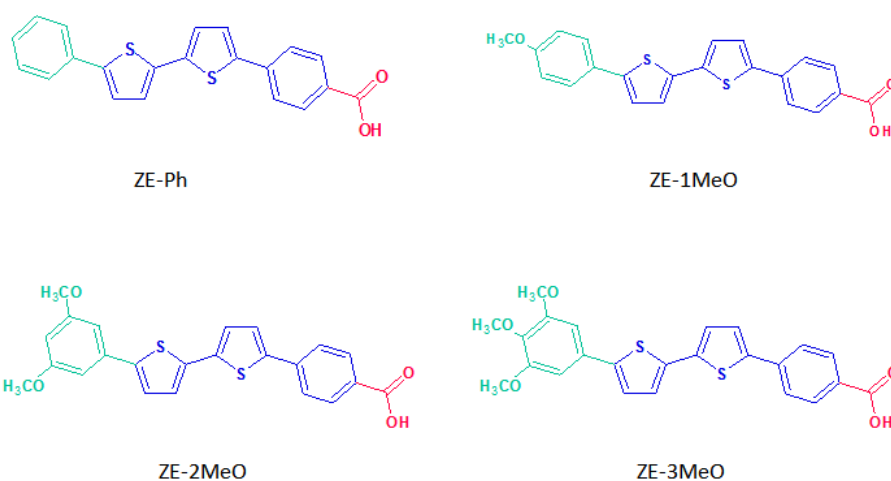


Figure 3.1: Molecule structures of SAM molecules

3.1.1.1 Synthesis of methyl 4-(5'-bromo[2,2'-bithien]-5-yl) benzoate

A mixture of methyl-4-iodobenzoate (200 mg, 0.53 mmol) and 2-(5'-bromo-2,2'-bithien-5-yl)-4,4,5,5-tetramethyl-1,3,2-dioxaborolane (96.3 mg, 0.79 mmol) were dissolved in DME (20 ml) in a Schlenk flask. Pd(dppf)Cl₂ and K₂CO₃ were added to the mixture after the temperature was reached to 50°C. The mixture was refluxed under N₂ overnight. The reaction was monitored with thin layer chromatography (TLC) to establish completion. The final solution was then extracted with an equal volume of CH₂Cl₂ and water. The organic solvent was removed under decreased pressure by utilizing a rotary evaporator and the obtained crude product was purified by column chromatography (SiO₂, CH₂Cl₂/n-Hexane:1/1) to afford a yellow powder as a product. ¹H NMR (400 MHz, CDCl₃): δ 8.0-7.98 (d, 2H), 7.85-7.80 (m, 2H), 7.42-7.40-7.38 (t, 1H), 7.25 (s, 2H), 3.86 (s, 3H).

3.1.1.2 Synthesis of 4-(5'-phenyl[2,2'-bithiophen]-5-yl) benzoic acid (ZE-Ph)

A mixture of 4-(5'-bromo-2,2'-bit-5-yl) benzoate (200 mg; 0.53 mmol) and benzenboranic acid (96.3 mg; 0.79 mmol) were dissolved in DME (20 ml) in a Schlenk flask. Pd(dppf)Cl₂ and K₂CO₃ (2 ml; 1M) were added to the mixture after the temperature was reached to 50°C. The mixture was refluxed under N₂ overnight. The reaction was observed with TLC to establish completion. The final solution was then extracted with an equal volume of CH₂Cl₂ and water. The organic solvent was removed and the obtained crude product was purified by column chromatography (SiO₂, CH₂Cl/n-Hexane:1/1) to afford a yellow powder. Then, the product was dissolved in (1:1, V:V) THF-Ethanol mixture in a round-bottom flask. KOH (0.5M; 1M) was added to the solution and refluxed overnight. After all organic solvents were removed, pure water (10 ml) and 1M HCl solution was added to the flask until the pH of the solution reached a region between 3 and 4. At the end, the organic yellow product was precipitated, filtered, washed with pure water and dried overnight. ¹H NMR (400 MHz CDCl₃): δ 7.96-7.98 (d, 2H), 7.82-7.79 (d, 2H), 7.68 (s, 3H), 7.54 (s, 1H), 7.44 (s, 4H), 7.37-7.31 (m, 1H).

3.1.1.3 4-[5'-(4-methoxyphenyl)-2,2'-bithiophen-5-yl] benzoic acid (ZE-1MeO)

A mixture of 4-(5'-bromo-2,2'-bit-5-yl) benzoate (200 mg; 0.53 mmol) and 4-methoxybenzene boronic acid (120.1 mg; 0.79 mmol) were dissolved in DME (20 ml) in a Schlenk flask. Pd(dppf)Cl₂ (22 mg; 0.03 mmol) and K₂CO₃ (1M; 1 ml) were added to the mixture after the temperature was reached to 50°C. The mixture was refluxed under N₂ overnight. The reaction was observed with TLC to establish completion. The final solution was then extracted with an equal volume of CH₂Cl₂ and water. The organic solvent was removed and the obtained crude product was purified by column chromatography (SiO₂, CH₂Cl/n-Hexane:1/1) to afford a yellow powder as a product. Then, the product was dissolved in (1:1, V:V) THF-Ethanol mixture in a round-bottom flask. KOH (0.5M; 1M) was added to the solution and refluxed overnight. After all organic solvents were removed under pressure, pure water (10 ml) and 1M HCl solution was added to the flask until the pH of the solution reached a region between 3 and

4. Finally, organic yellow product was precipitated, filtered, washed with pure water and dried overnight. ¹H NMR (400 MHz CDCl₃): δ 7.95 (s,2H), 7.80 (s,2H), 7.67-7.62 (d,3H), 7.39 (s,3H), 7.00 (s,2H), 3.79 (s,3H).

3.1.1.4 4-[5'-(3,5-dimethoxyphenyl)-2,2'-bithiophen-5-yl] benzoic acid (ZE-2MeO)

A mixture of 4-(5'-bromo-2,2'-bit-5-yl) benzoate (200 mg; 0.53 mmol) and 3,5-trimethoxybenzene boronic acid (143.8 mg; 0.79 mmol) were dissolved DME (20 ml) in schlenk flask. Pd(dppf)Cl₂ (22 mg; 0.03 mmol) and K₂CO₃ (1M; 1 ml) were added to the mixture after temperature was reached to 50°C. The mixture was refluxed under N₂ overnight. The reaction was observed with thin layer chromatography (TLC) to establish completion. The final solution was then extracted with equal volume of CH₂Cl₂ and water. The organic solvent evaporated and obtained crude product was purified by column chromatography (SiO₂, CH₂Cl/n-Hexane:1/1) to afford yellow powder as a product. Then, the product was dissolved in (1:1, V:V) THF-Ethanol mixture in round-bottom flask. KOH (0.5m; 1M) was added to solution and refluxed overnight. After all organic solvents were removed under pressure, the pure water (10ml) and 1M HCl solution was added to flask until pH of the solution reached to region between 3 and 4. Finally, organic yellow product was precipitated, filtered, washed with pure water and dried overnight. ¹H NMR (400 MHz CDCl₃): δ 7.97-7.95 (d, 2H), 7.80-7.78 (d,2H), 7.67 (s,1H), 7.56 (s,1H), 7.41 (s,2H), 6.80 (s,2H), 6.48 (s,1H), 3.80 (s, 6H).

3.1.1.5 4-[5'-(3,4,5-trimethoxyphenyl)-2,2'-bithiophen-5-yl] benzoic acid (ZE-3MeO)

A mixture of 4-(5'-bromo-2,2'-bit-5-yl) benzoate (200 mg; 0.53 mmol) and 3,4,5-trimethoxybenzene boronic acid (167.5 mg; 0.79 mmol) were dissolved DME (20 ml) in schlenk flask. Pd(dppf)Cl₂ (22 mg; 0.03 mmol) and K₂CO₃ (1M; 1 ml) were added to the mixture after temperature was reached to 50°C. The mixture was refluxed under N₂ overnight. The reaction was observed with TLC to establish completion. The final solution was then extracted with equal volume of CH₂Cl₂ and water. The organic solvent was evaporated and obtained crude product was purified by column chromatography (SiO₂, CH₂Cl/n-Hexane:1/1) to afford yellow powder as a product. Then, the product was dissolved in (1:1, V:V) THF-Ethanol mixture in

round-bottom flask. KOH (0.5m; 1M) was added to solution and refluxed overnight. After all organic solvents were removed under pressure, the pure water (10ml) and 1M HCl solution was added to flask until pH of the solution reached to region between 3 and 4. Finally, organic yellow product was precipitated, filtered, washed with pure water and dried overnight. ^1H NMR (400 MHz CDCl_3): δ 7.80-7.78 (d, 2H), 7.66 (s, 2H), 7.52 (s, 1H), 7.41 (s, 1H), 6.92 (s, 2H), 3.85 (s, 6H), 3.67 (s, 3H).

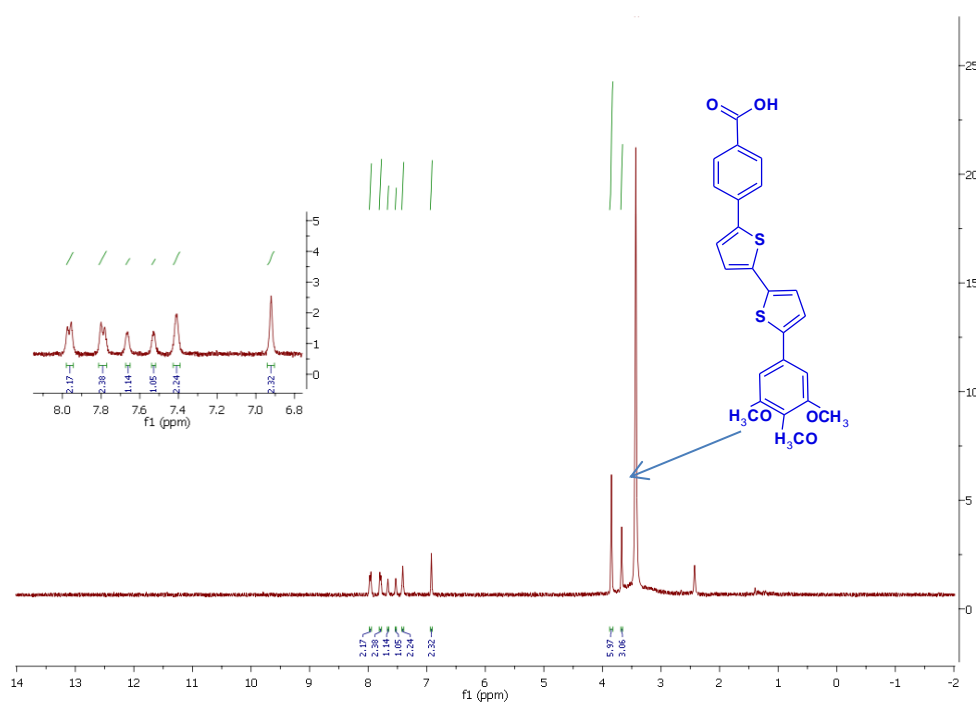


Figure 3.2: NMR spectrum of 4-[5'-(3,4,5-trimethoxyphenyl)-2,2'-bithiophen-5-yl] benzoic acid (ZE-3MeO)

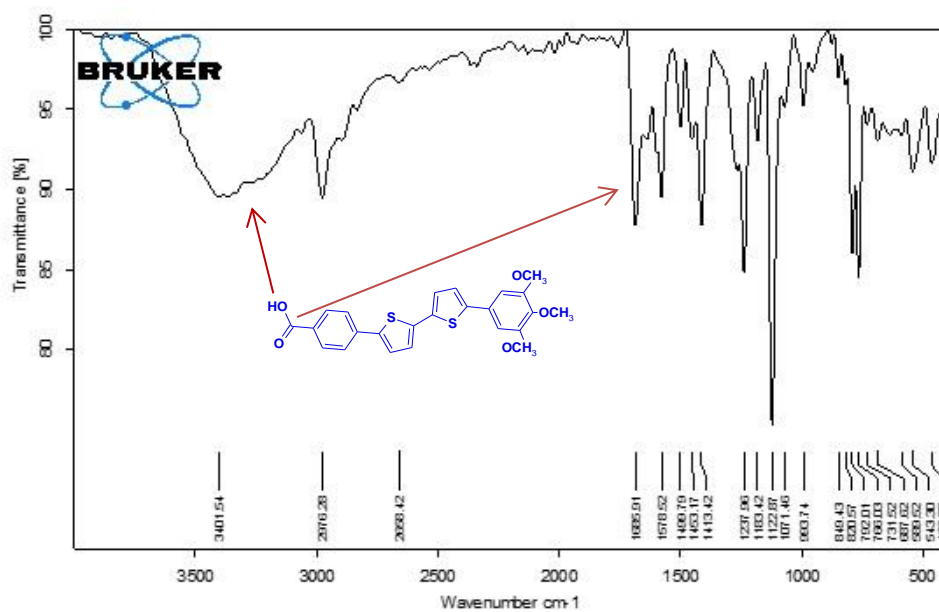


Figure 3.3: FT-IR spectrum of 4-[5'-(3,4,5-trimethoxyphenyl)-2,2'-bitien-5-yl]benzoic acid.

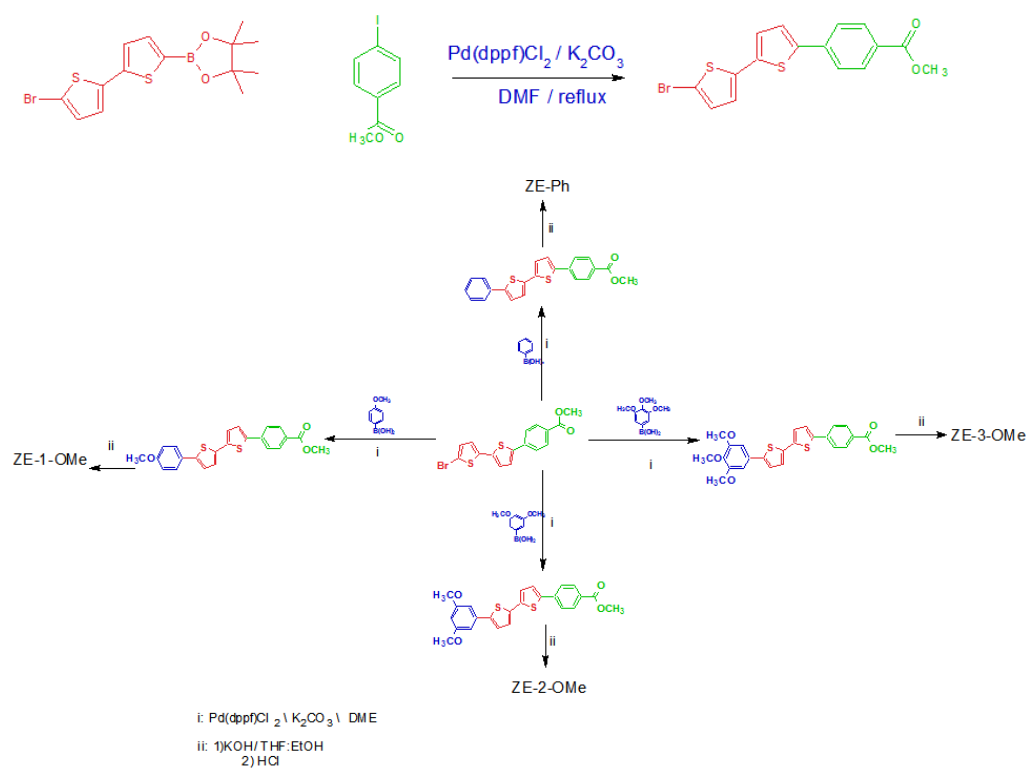
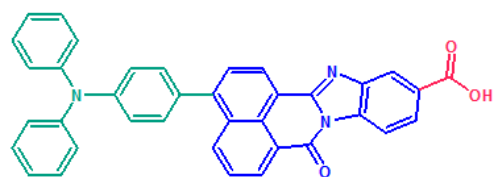
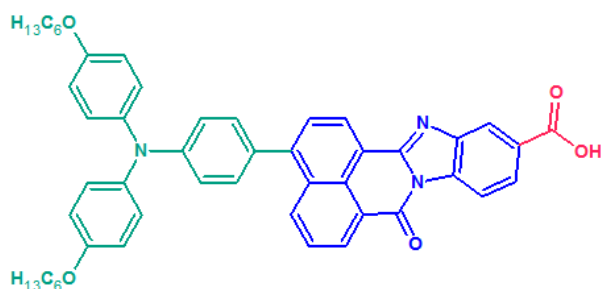


Figure 3.4: Synthesis procedure of SAM molecules

3.1.2 Dye molecules



MZ-341



MZ-235

Figure 3.5: Structures of dye molecules

3.1.2.1 Synthesis of 1-(hexyloxy)-4-iodophenol (1)

Potassium carbonate (5.6 g, 40 mmol), 18-Crown-6 (1 g, 4 mmol), 4-iodophenol (8.8 g, 40 mmol), and 1-bromohexane (6.6 g, 40 mmol) were dissolved in acetone (100 mL) in a round bottomed flask and refluxed with stirring overnight. The reaction was monitored with thin layer chromatography (TLC) to establish completion. The reaction was filtered after cooled down to room temperature, and the reaction mixture was extracted with diethylether (2 x 20 mL) and water (2 x 20 mL). The organic phase was separated then dried with sodium sulphate. The solvent was evaporated and column chromatography was used to purify crude product (dichloromethane/hexane: 1/1, V/V) to obtain a colorless oil (91%, yield). ¹H NMR (400 MHz CDCl₃): δ 7.50 (d, 2H), 6.63 (d, 2H), 3.87 (t, 2H), 1.76-1.70 (m, 2H), 1.44-1.39 (m, 2H), 1.34-1.29 (m, 4H), 0.89 (t, 3H). ¹³C NMR (400 MHz CDCl₃): δ 138.37, 117.18, 68.35, 31.84, 29.41, 25.96, 22.87, 14.30.

3.1.2.2 Synthesis of (4-bromophenyl)bis[4-(hexyloxy)phenyl]amine(2)

CuI (0.2 g, 1 mmol) and phenanthroline (0.18 g, 1 mmol) were dissolved in toluene (10 mL) in a round bottomed flask. The reaction mixture was stirred under Dean-Stark apparatus and for half an hour. Potassium hydroxide (4.8 g, 77 mmol), 4-bromoaniline (1.65 g, 9.6 mmol), 1-(hexyloxy)-iodobenzene (5 g, 16 mmol), and toluene (20 mL) were added in to the flask and the mixture was refluxed overnight. The reaction was monitored with thin layer chromatography (TLC) to establish completion. The reaction was cooled down to the room temperature, then filtered with celite and washed with dichloromethane. Then the extraction was made with dichloromethane (3 x 20 mL) and water (3x 20 mL). The organic phase was dried over sodium sulphate after separating and the solvent was evaporated. Column chromatography was used to purify crude product (dichloromethane/hexane: 1/4, V/V) on silica gel to yield yellow oil (66% yield). ¹H NMR (400 MHz CDCl₃): δ 7.21 (d, 2H), 7.00 (d, 2H), 6.8 (d, 6H), 3.91 (t, 4H), 1.78-1.72 (m, 4H), 1.46-1.42 (m, 4H), 1.36-1.32 (m, 8H), 0.90 (t, 6H). ¹³C NMR (400 MHz CDCl₃): δ 168.37, 134.67, 131.33, 130.50, 128.98, 127.89, 127.24, 125.16, 110.48, 40.43, 40.23, 40.02, 39.81, 39.60.

3.1.2.3 Synthesis of (4-{bis[4-(hexyloxy)phenyl]amino}phenyl) boronic acid (3)

(4-bromophenyl)bis[4-(hexyloxy) phenyl]amine (3.8 g, 7.3 mmol) was dissolved in dry THF (10 mL) and added to the round bottomed flask under argon atmosphere. The temperature was set to -80 °C with acetone and dry ice. N-butyl lithium (3.75 mL, 7.25 mmol) was dripped into the flask with care and stirred for thirty minutes. Trimethylborate (8.4 mL, 72.6 mmol) was dripped to the flask and stirred overnight. The reaction was monitored with thin layer chromatography (TLC) to establish completion. The product was extracted with 1 M hydrochloric acid aqueous solution (3 x 30 mL) and diethylether (3 x 30 mL). The organic phase was dried with sodium sulphate after separating, and the solvent was evaporated. Column chromatography was used to purify crude product (ethylacetate/ hexane: 3/1, V/V) on silica gel to obtain white solid (74% yield). ¹H NMR (400 MHz d₆-DMSO): δ 7.68 (s, 2H), 7.57 (d, 2H), 6.97 (d, 4H), 6.85 (d, 4H), 6.66 (d, 2H), 3.89 (t, 4H), 1.70-1.63 (m, 4H), 1.42-1.36 (m, 4H), 1.30-1.26 (m, 8H), 0.85 (t, 6H). ¹³C NMR (400 MHz CDCl₃): δ

156.03, 150.073, 140.37, 135.87, 127.65, 118.08, 116.07, 68.30, 31.66, 29.37, 25.87, 14.53.

3.1.2.4 Synthesis of 6-(4-{bis[4-(hexyloxy)phenyl]amino}phenyl)-1H,3H-benzo[de]isochromene-1,3-dione (4)

(4-{bis[4-(hexyloxy) phenyl] amino} phenyl) boronic acid (150 mg, 0.3 mmol) and 6-bromo-1,3- benzoisochromene-1,3-dione (103 mg, 0.4 mmol), was dissolved in 1,2-dimethoxyethane (15 mL) in a schlenk flask. After that, [1,10-Bis (diphenylphosphino) ferrocene] dichloropalladium (II) (20 mg, 0.022 mmol) and potassium carbonate aqueous solution (1 M, 2 mL) were added to flask. The mixture refluxed overnight. The reaction was monitored with thin layer chromatography (TLC) to establish completion. The reaction was extracted with dichloromethane (3 x 20 mL) and water (3 x 20 mL). The organic phase was dried over sodium sulphate after separating, the solvent was evaporated. Column chromatography was used to purify crude product (dichloromethane/hexane: 1/2, V/V) on silica gel to obtain red solid. ¹H NMR (400 MHz CDCl₃): δ 8.62 (m, 2H), 8.54 (dd, 1H), 7.74 (dd, 2H), 7.31 (d, 2H), 7.16 (d, 4H), 7.05 (d, 2H), 6.89 (d, 4H), 3.96 (t, 4H), 1.79 (m, 4H), 1.47 (m, 4H), 1.35 (m, 8H), 0.91 (t, 6H). ¹³C NMR (400 MHz CDCl₃): δ 156.56, 139.89, 134.90, 133.25, 130.65, 129.00, 128.07, 127.73, 127.34, 119.14, 115.91, 68.69, 31.61, 29.32, 26.00, 23.02, 14.23.

3.1.2.5 Synthesis of 4-(4-{bis[4-(hexyloxy)phenyl]amino}phenyl)-7- oxo-7H-benzimidazo[2,1-a]benzo[de]isoquinoline-11-carboxylic acid (5)

6-(4-{bis[4-(hexyloxy) phenyl]amino}phenyl)-1H,3H-benzo[de]isochromene-1,3-dione (70 mg, 0.1 mmol), zinc acetate (20 mg, 0.1 mmol) and 3,4-diaminobenzoic acid (33 mg, 0.2 mmol) was dissolved in pyridine (15 mL) in a round bottomed flask. The mixture was refluxed with stirring overnight. The reaction was monitored with thin layer chromatography (TLC) to establish completion. The reaction mixture was neutralized by 1 M hydrochloric acid aqueous solution then extracted with dichloromethane (3 x 20 mL) and water (3 x 20 mL). The organic phase was dried over sodium sulphate after separating, and the solvent was evaporated by rotary evaporator. Column chromatography was used to purify crude product

(dichloromethane/hexane: 9.5/0.5, V/V) on silica gel to obtain red solid. ¹H NMR (400 MHz CDCl₃): δ 8.86-8.75 (d, 1H), 8.60 (t, 1H), 8.18 (m, 1H), 8.01 (m, 1H), 7.90 (m, 1H), 7.72 (m, 2H), 7.47 (m, 2H), 7.34 (m, 2H), 7.14 (m, 4H), 7.07 (m, 2H), 6.89 (m, 4H), 3.96 (t, 4H), 1.35 (m, 16H), 0.91 (m, 6H). ¹³C NMR (400 MHz CDCl₃): δ 164.14, 156.28, 149.68, 140.53, 130.65, 129.64, 127.41, 119.45, 115.70, 68.67, 31.82, 29.90, 29.55, 25.98, 22.69, 14.55.

3.1.2.6 Synthesis of methyl 4-bromo-7-oxo-7H-benzimidazo[2,1-a]benzo[de]isoquinoline-11-carboxylate(6)

6-bromo-1H,3H-benzo[de]isochromene-1,3-dione (28 mg, 0.1 mmol), zinc acetate (20 mg, 0.1 mmol) and methyl 3,4-diaminobenzoate (33 mg, 0.2 mmol), were dissolved in pyridine (15 mL) in a round bottomed flask. The reaction was monitored with thin layer chromatography (TLC) to establish completion. The reaction mixture was neutralized using 1M hydrochloric acid aqueous solution then extracted with dichloromethane (3 x 20 mL) and water (3 x 20 mL). The organic phase was dried with sodium sulphate and the solvent was evaporated. Column chromatography was used to purify crude product (dichloromethane/hexane: 9.5/0.5, V/V) on silica gel to obtain a yellow solid. ¹H NMR (400 MHz d₆-DMSO): δ 8.88 (m, 1H), 8.71 (t, 1H), 8.56-8.46-8.45 (m, 1H), 8.20 (m, 1H), 8.09 (m, 1H), 8.08 (m, 1H), 7.98-7.91 (m, 1H), 7.89-7.85 (m, 1H), 4.00 (s, 3H). ¹³C NMR (400 MHz CDCl₃): δ 163.51, 148.41, 147.31, 133.32, 131.96, 131.68, 131.43, 130.34, 129.49, 128.46, 127.62, 127.10, 125.48, 124.12, 122.50, 116.28, 51.75.

3.1.2.7 Synthesis of methyl 4-[4-(diphenylamino)phenyl]-7-oxo-7H-benzimidazo[2,1-a]benzo[de]isoquinoline-11-carboxylate (7)

4-(diphenylamino)phenylboronic acid (90 mg, 0.3 mmol) and methyl 4-bromo-7-oxo-7H-benzimidazo[2,1-a]benzo[de]isoquinoline-11-carboxylate (123 mg, 0.3 mmol) were dissolved in 1,2-dimethoxyethane (10 mL) in a schlenk flask. After that potassium carbonate aqueous solution (1 M, 2 mL) and [1,10-bis(diphenylphosphino)ferrocene] dichloropalladium (II) (12 mg, 0.02 mmol) were added to the mixture. The system was isolated under argon atmosphere and stirred overnight at boiling temperature. The reaction was monitored with thin layer

chromatography (TLC) to establish completion. The extraction was made with dichloromethane (3 x 20 mL) and water (3 x 20 mL). The organic phase was dried with sodium sulphate and the solvent was evaporated. Column chromatography was used to purify crude product (dichloromethane/hexane: 1/2, V/V) on silica gel to obtain orange solid. ¹H NMR (400 MHz CDCl₃): δ 8.90-8.84 (m, 2H), 8.65-8.64-8.57 (m, 1H), 8.48 (d, 1H), 8.19 (t, 1H), 7.97-7.86 (d, 1H), 7.81-7.72 (m, 1H), 7.42-7.37-7.34 (m, 6H), 7.27-7.21 (m, 6H), 7.11 (t, 2H), 6.93 (t, 2H), 4.00 (s, 3H). ¹³C NMR (400 MHz CDCl₃): δ 164.31, 163.60, 148.33, 147.26, 134.54, 133.64, 133.48, 131.99, 131.82, 131.57, 131.00, 130.79, 129.58, 128.31, 127.94, 127.77, 127.17, 126.79, 125.04, 123.71, 122.68, 122.57, 122.38, 122.27, 120.95, 120.62, 116.09, 51.66.

3.1.2.8 Synthesis of 4-[4-(diphenylamino)phenyl]-7-oxo-7H-benzimidazo[2,1-a]benzo[de]isoquinoline-11-carboxylic acid (8)

Methyl 4-[4-(diphenylamino)phenyl]-7-oxo-7H-benzimidazo [2,1-a]benzo[de]isoquinoline-11-carboxylate was dissolved in THF:ethanol (1:1) mixture in a round bottomed flask. The reaction was refluxed overnight after adding 1 M KOH solution. The reaction was monitored with thin layer chromatography (TLC) to establish completion then the organic solvent was evaporated and the mixture was acidified using 1 M HCl. The precipitate was filtered and washed with pure water. Column chromatography was used to purify crude product (dichloromethane/methanol: 9.5/0.5, V/V) on silica gel to obtain red solid. ¹H NMR (400 MHz CDCl₃): δ 8.96-8.89 (m, 1H), 8.67-8.56 (m, 1H), 8.26 (t, 1H), 7.82 (m, 2H), 7.71 (m, 1H), 7.54 (m, 1H), 7.42-7.41 (m, 2H), 7.34 (m, 4H), 7.23 (m, 8H), 7.11 (t, 2H). ¹³C NMR (400 MHz CDCl₃): δ 166.39, 163.96, 163.77, 153.38, 148.43, 147.46, 147.26, 133.49, 131.99, 131.82, 131.58, 130.98, 130.80, 129.49, 128.30, 127.76, 126.76, 125.09, 123.71, 122.52, 122.38, 120.95, 116.09.

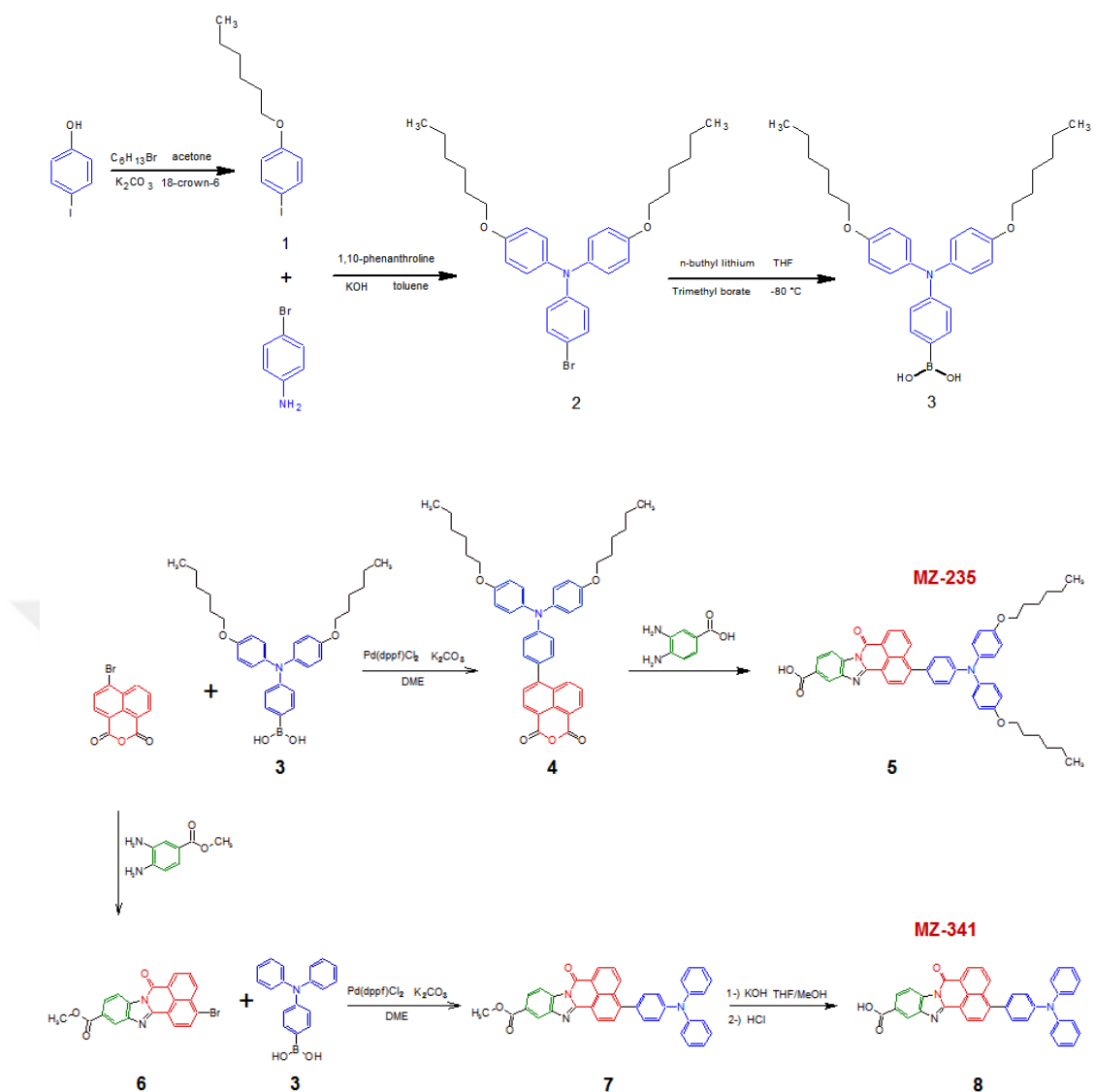


Figure 3.6: Synthesis procedure of MZ dyes.

3.2 UV-Visible Absorption Spectrums of SAM Molecules

3.2.1 SAM molecules

Absorption spectrum of SAM molecules is given at figure 3.7, it is clearly shown that all the molecules absorb between approximately 325-450 nm range. Absorption peaks are between 393 nm and 399 nm. Since the SAM molecules' absorptions are in the UV range, they don't affect P3HT's absorption in the visible range. ZE-Ph molecule has the minimum absorption and ZE-3MeO has the maximum absorption intensity. Electron donor methoxy groups increase the absorption intensity.

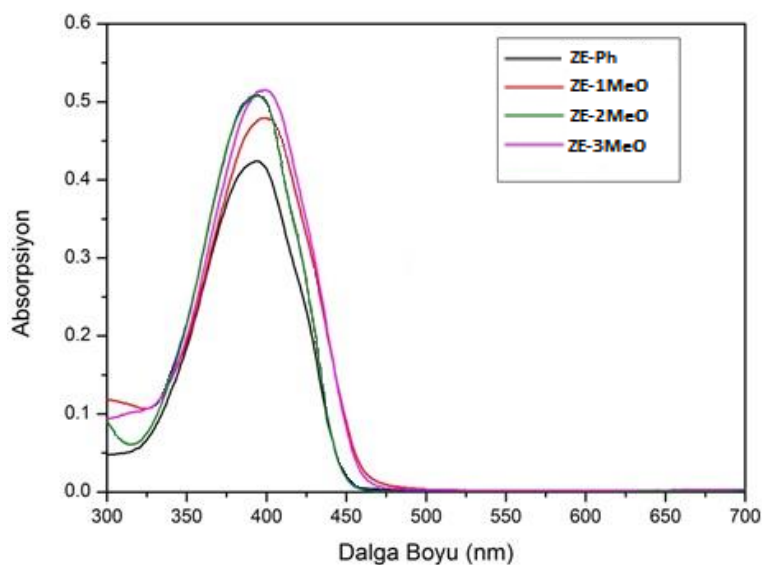


Figure 3.7: Absorption spectrum of SAM Molecules

3.2.2 Dye molecules

Fig. 8a and b present the absorption and fluorescence spectra of dyes MZ-341 and MZ-235 in toluene and THF dilute solutions, respectively. The photophysical parameters are shown in Table 3.1. The dyes display almost identical absorption spectra, regardless of the solvent used, with peaks at 441-443 nm for MZ-341 and at 459 nm for MZ-235. A red-shift (~ 17 - 19 nm) of the absorption's peak for MZ-235 in comparison with MZ-341 in both solvents is observed. This causes from the hexyloxy substituents on the para position of the two benzenes of the triphenylamine donor. The addition of these extra electron donating hexyloxy groups on the triphenylamine donor, reduces the oxidation potential by giving triphenylamine an enhanced nucleophilic character, and results in an increased HOMO level of the dye. As a result of this a red shift of the absorption maximum for MZ-235 compared to MZ-341 where these substitution groups are absent is seen. Otherwise, the fluorescence spectra in toluene and THF display several differences in both dyes, with those in toluene being narrower and hypsochromically shifted compared to those in THF. The fluorescence spectra in toluene show peaks at 547 and 576 nm for MZ-341 and MZ-235, respectively. The corresponding values in THF are 595 and 613 nm. The bathochromic shift as well as the broader spectrum in THF compared to toluene, is an indication that the excited state presents an intense charge transfer character. Finally, a bathochromic shift (18-29 nm) of the fluorescence peak

accompanied by a broader spectrum in both solvents is evident for MZ-235 with the extra electron donating groups.

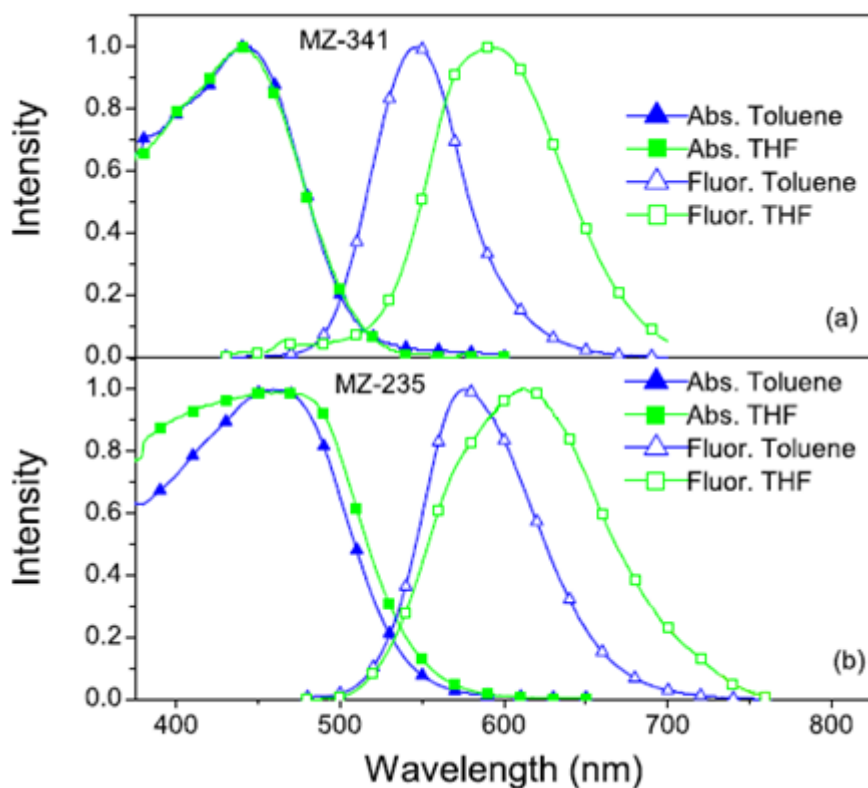


Figure 3.8: Absorption and Fluorescence spectrums of MZ dyes a)MZ-341 b)MZ-235

Table 3.1 : Photophysical parameters of MZ-341 and MZ-235 dyes. The molar extinction coefficients in $M^{-1} cm^{-1}$ are shown in parentheses.

| | MZ-341 | | MZ-235 | |
|----------------|--------------------|----------------------|--------------------|----------------------|
| | λ abs (nm) | λ fluor (nm) | λ abs (nm) | λ fluor (nm) |
| Toluene | 443 (3240) | 547 | 460 (5840) | 576 |
| THF | 441 (9050) | 595 | 460 (4870) | 613 |

3.3 Cyclic Voltammetry Results of SAM Molecules

3.3.1 SAM molecules

Measurement of the oxidation and reduction potentials of SAM molecules were done with cyclic voltammetry method. Tetra butyl ammonium hexa fluoro phosphate (TBAPF6) was solved in acetonitrile solvent and used as electrolyte. Glassy carbon was utilized as working electrode, Pt was utilized as counter electrode and Ag/AgCl was utilized as reference electrode. The HOMO and LUMO energy levels were calculated from oxidation and reduction potentials, respectively. The following equivalents were used to compute the HOMO and LUMO energy levels [130].

$$E_{\text{LUMO}} = -e(E_{1/2(\text{red.})} + 4,4) \quad (4)$$

$$E_{\text{HOMO}} = -e(E_{1/2(\text{ox.})} + 4,4)$$

The oxidation potentials, which assigned to the oxidation of the thiophene are between 0.80 V and 0.90 V. The reduction potentials which assigned to the reduction of the carboxyl are between -1.73 V and -1.77 V. The band gaps are decreasing when electron donor methoxy groups are added to SAM molecules.

Table 3.2 : HOMO and LUMO energy levels of SAM molecules

| Molecule | V _{reduction} (V) | V _{oxidation} (V) | E _{HOMO} (eV) | E _{LUMO} (eV) | ΔE _g (eV) |
|-----------------|----------------------------|----------------------------|------------------------|------------------------|----------------------|
| ZE-Ph | -1.75 | 0.90 | -5.30 | -2.65 | 2.65 |
| ZE-1 MeO | -1.76 | 0.88 | -5.28 | -2.64 | 2.64 |
| ZE-2 MeO | -1.73 | 0.85 | -5.25 | -2.67 | 2.58 |
| ZE-3 MeO | -1.77 | 0.80 | -5.20 | -2.63 | 2.57 |

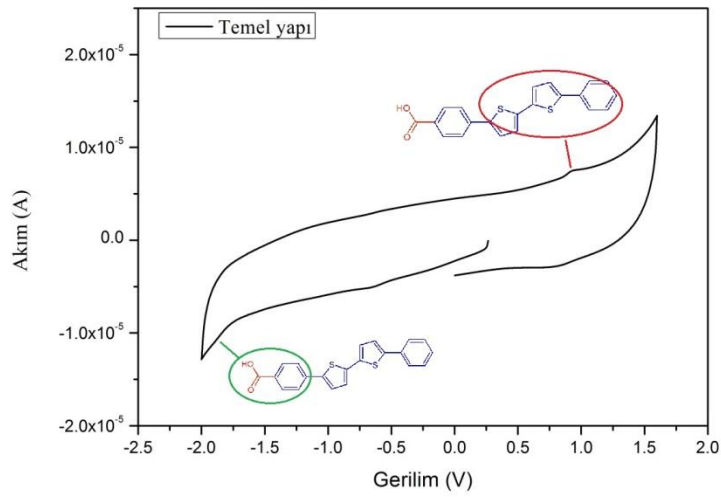


Figure 3.9: Cyclic voltammogram of ZE-Ph

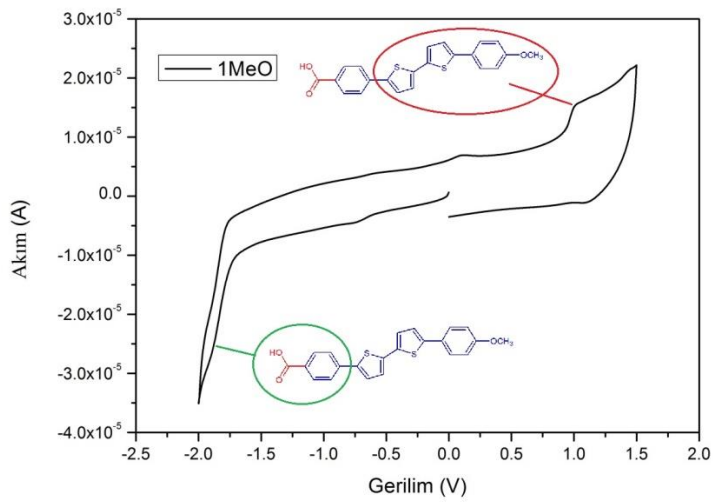


Figure 3.10: Cyclic voltammogram of ZE-1MeO

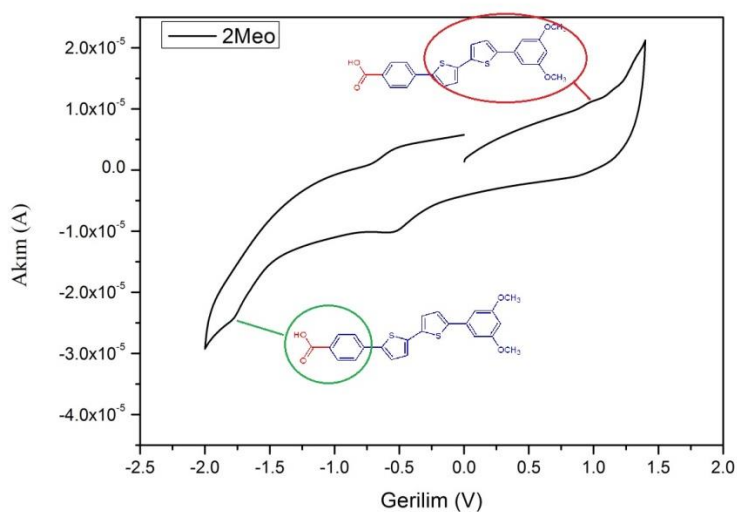


Figure 3.11: Cyclic voltammogram of ZE-2MeO

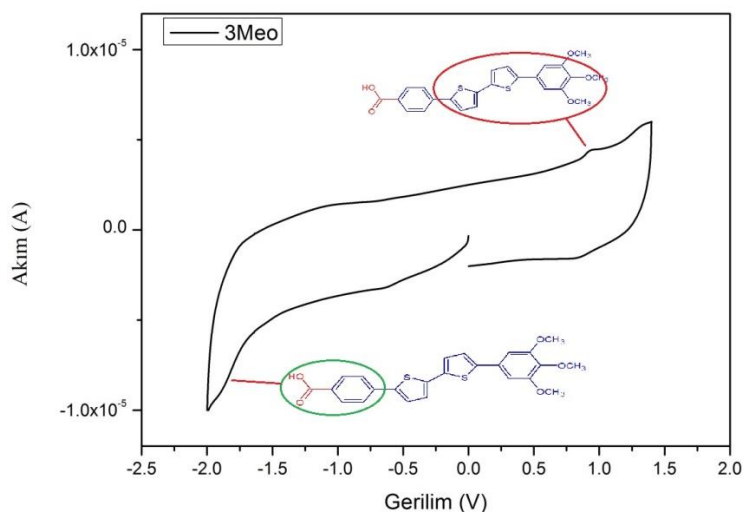


Figure 3.12: Cyclic voltammogram of ZE-3MeO

3.3.2 Cyclic voltammetry results of SAM molecules on ITO surface

ITO substrats were kept in 1×10^{-4} M concentrated SAM solutions overnight and used as working electrode. In the case of the scanning process in negative side, since the molecules adsorbed on ITO surface are separated from the surface, the measurement is only made in positive side. When the methoxy groups are added to molecule, oxidation potentials have been increased. Differences of cyclic voltammetry results show that the SAM molecules coated on ITO surface.

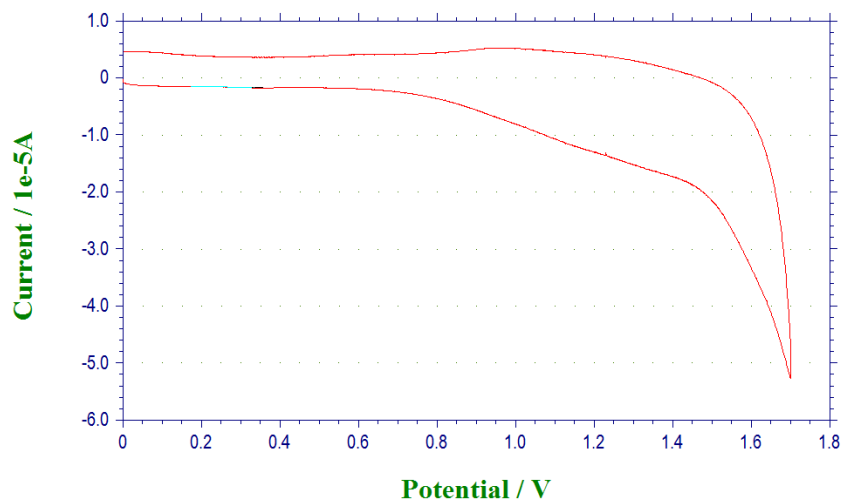


Figure 3.13: Cyclic voltammogram of ITO/ZE-1MeO

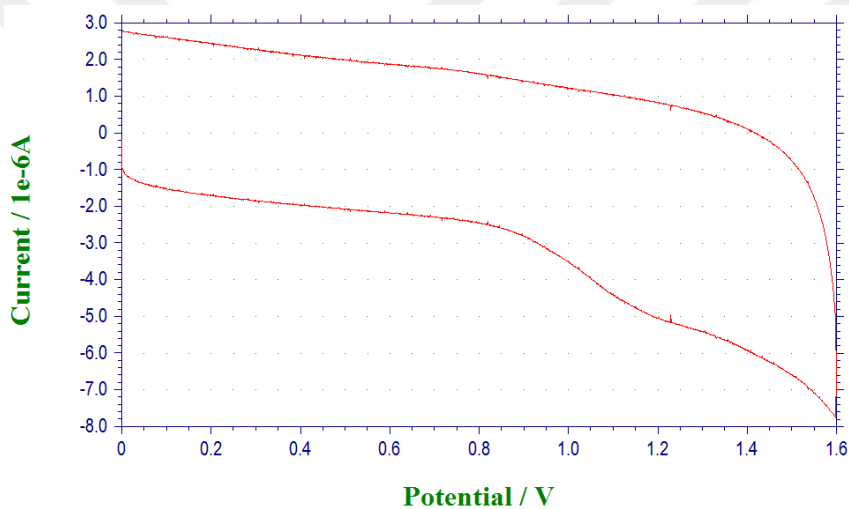


Figure 3.14: Cyclic voltammogram of ITO/ZE-2MeO

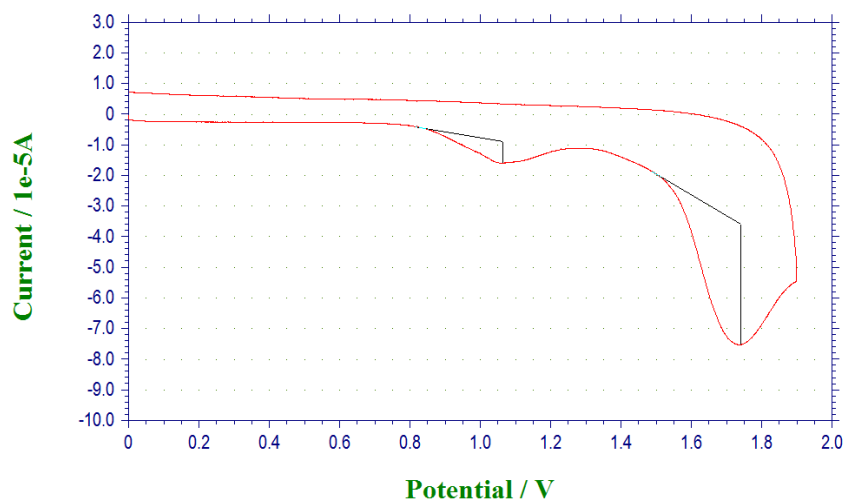


Figure 15: Cyclic voltammogram of ITO/ZE-3MeO

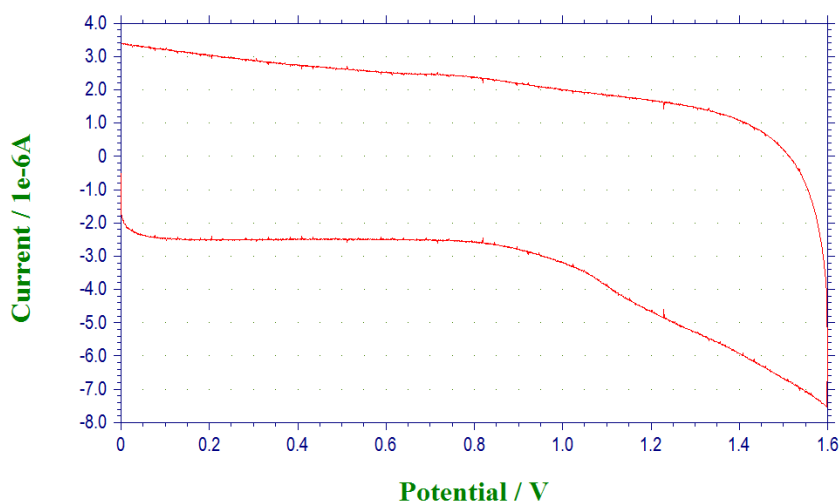


Figure 3.16: Cyclic voltammogram of ITO/ZE-Ph

Table 3.3 : Oxidation potentials and HOMO energy levels of ITOs with SAM molecules

| Molecule | $V_{\text{oxidation}}$ (V) | E_{HOMO} (eV) |
|----------------|----------------------------|------------------------|
| ZE-Ph | 1.1 | 5.5 |
| ZE-1MeO | 1.0 | 5.4 |
| ZE-2MeO | 0.95 | 5.35 |
| ZE-3MeO | 0.9 | 5.3 |

3.3.3 Dye molecules

Cyclic voltammetry method was used to measure the electrochemical properties of MZ dyes. The measurement was done in a 0.1M solution of Bu_4NPF_6 in acetonitrile. The scan rate was 100 mV s^{-1} . A glassy-carbon was utilized as the working electrode while platinum was used as the counter electrode and Ag/AgCl as the reference electrode. The oxidation potentials which caused by the triphenylamine donor moiety, were found at 0.89 V for MZ-341 and 0.78 V for MZ-235. The reduction potentials caused by benzimidazole were found at -1.13 V and -1.16V for MZ-341 and MZ-235, respectively. The reduction potentials caused by carboxylic acid acceptor that can be anchored to the TiO_2 surface were found at -1.67 V for MZ-341 and -1.56 V for MZ-235. The electron donating hexyloxy groups on triphenylamine reduces the oxidation potential. HOMO levels were calculated from the oxidation and LUMO levels were calculated from the reduction potentials for both dyes.

HOMO and LUMO levels are located at 5.18 and 3.24 eV for MZ-235, 5.30 and 3.27 eV for MZ-341. Cyclic voltammograms for both dyes are presented in Figure 17.

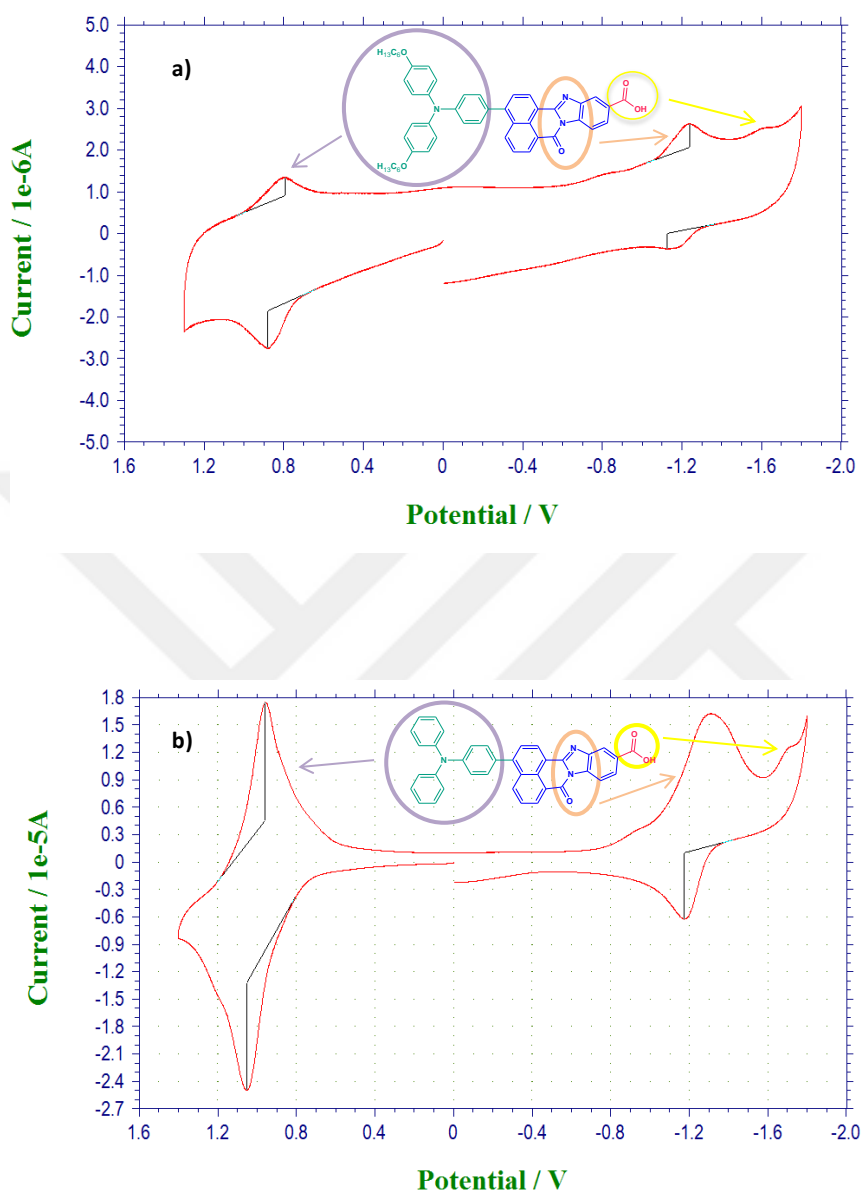


Figure 3.17: Cyclic Voltammograms of MZ dyes a) MZ-235 b) MZ-341

3.4 ITO/SAM Kelvin Probe Microscope Analyses

To measure of contact potential difference of ITO surface with and without SAM, Kelvin Probe Force Microscope was used. Contact potential difference (CPD) was analyzed between ITO, ITO/SAM electrodes and AFM conductive tip (Pt). CPD was

measured from 4 different points as 0.020 V between ITO and Pt. The potential difference of ZE-1MeO, ZE-2MeO, ZE-3MeO, ZE-Ph, coated ITO electrodes are 0.324 V, 0.225 V, 0.187 V, 0.162 V, respectively. It is seen from the potential differences, the SAM molecules were arranged on ITO surface. Work functions of modified ITO electrodes were increased with respect to work function of ITO electrode.

Table 3.4 : Contact potential difference between conductive tip Pt and substrate

| Anode Electode | CPD (V) |
|----------------|---------|
| ITO | 0.020 |
| ITO/ZE-1MeO | 0.324 |
| ITO/ZE-2MeO | 0.225 |
| ITO/ZE-3MeO | 0.187 |
| ITO/ZE-Ph | 0.162 |

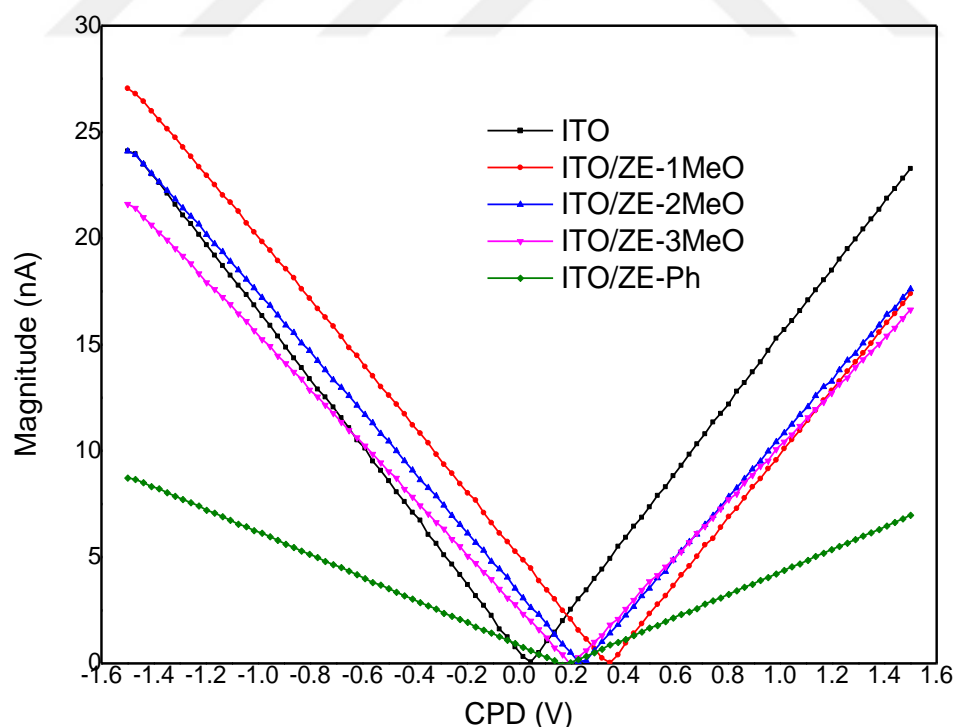


Figure 3.18: CPD Results of ITO substrate and SAM coated ITOs

3.5 Contact Angle Results

When we contemplate a liquid drop resting on a flat, horizontal surface, we can describe the contact angle as the angle created by intersection of the liquid-solid interface. Figure 3.19 shows the contact angle values when the liquid spread and is bead on the surface. If the contact angle less than 90° that means wetting is available so the liquid spread on the surface. If the contact angle higher than 90° that means wetting is inconvenient so the liquid is bead on the surface [131].

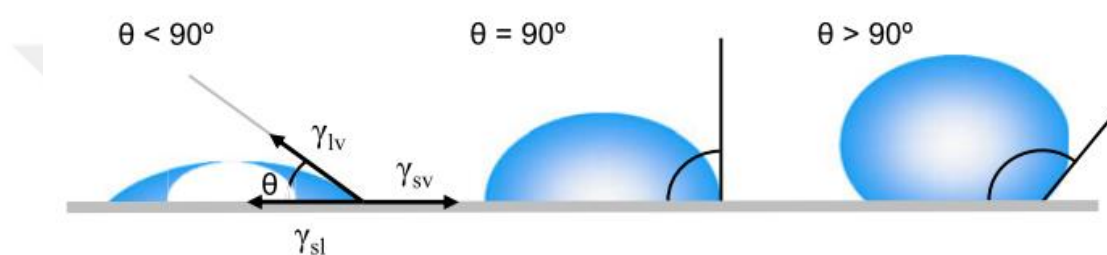
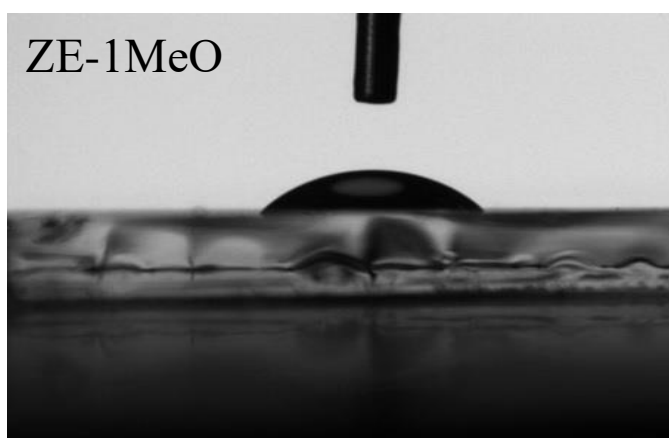
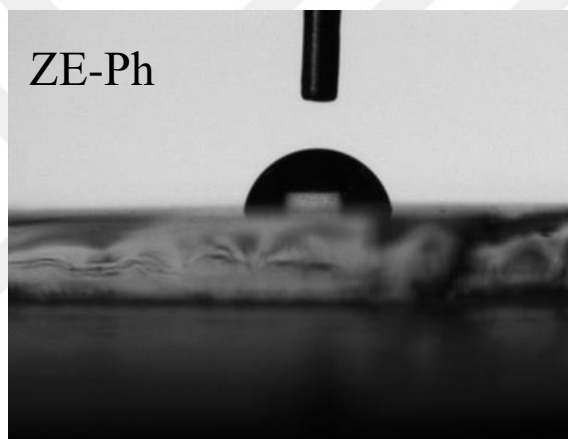
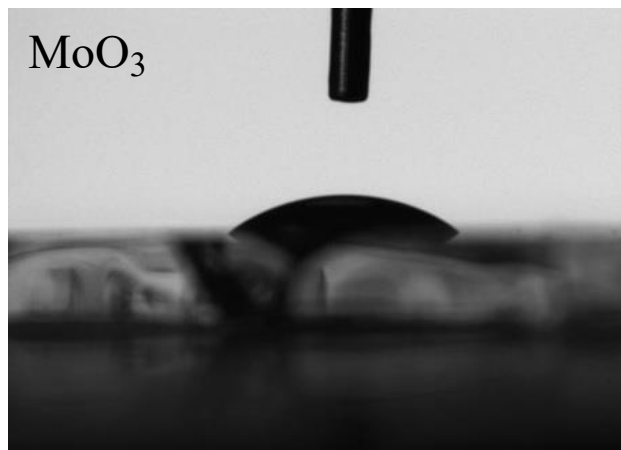


Figure 3.19: Illustration of contact angles formed by sessile liquid drops on a smooth homogeneous solid surface [131].

Contact angle results of MoO_3 and SAM molecules are given at figure x and table x. the results show that the higher ZE-Ph has the highest contact angle value. ZE-Ph molecule has a phenyl as functional group so it doesn't make H-bond with water. On the other hand, the methoxy groups make H-bond with water molecules, therefore SAM molecules with methoxy groups have less contact angle values. On the basis of this, we can say the ZE-Ph molecule is the most hydrophobic molecule among the SAM molecules.



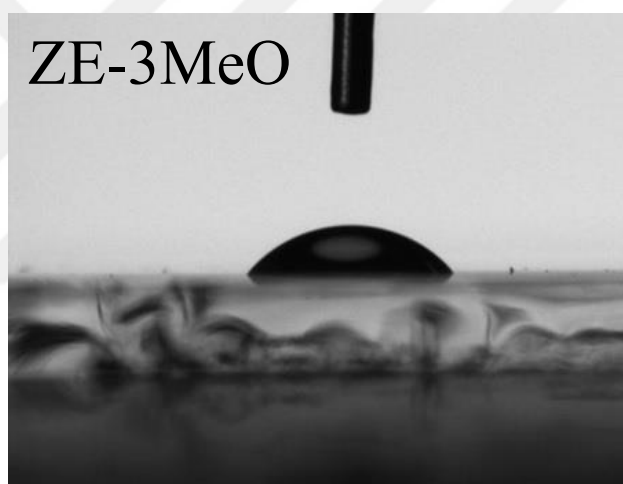
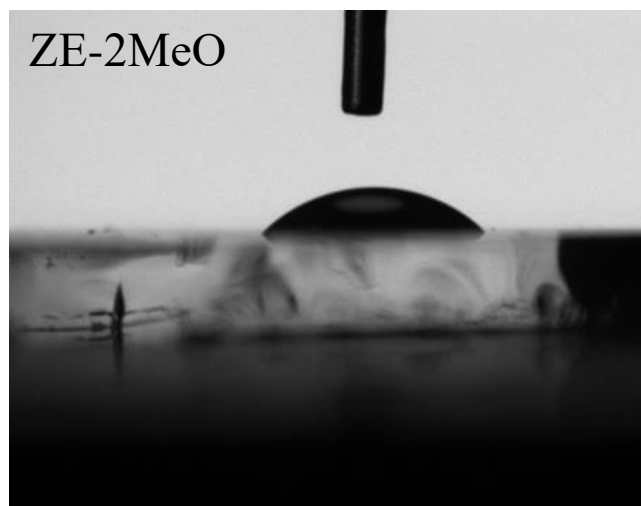


Figure 3.20: Contact angle measuring photo of MoO₃ and SAM molecules

Table 3.5 : Contact angle values of MoO₃ and SAM coated MoO₃

| Materials | Contact angle values |
|-----------------------------|-----------------------------|
| MoO₃ | 38.2 ⁰ |
| MoO₃/Ph | 79.4 ⁰ |
| MoO₃/1MeO | 46.4 ⁰ |
| MoO₃/2MeO | 43.2 ⁰ |
| MoO₃/3MeO | 49.5 ⁰ |

3.6 Investigaiton of Solar Cell's Electrical Characterization

3.6.1 SAM molecules

3.6.1.1 The solar cells experiments of the electrode prepared by adsorbing SAM molecules on MoO₃ coated ITO

The ITO/MoO₃/P3HT:PCBM/LiF/Al structure was taken as reference solar cell, and the ITO/MoO₃/SAM/P3HT:PCBM/LiF/Al structure was prepared by using SAM molecules. After the MoO₃ films coated on ITO at 4500 rpm with the spin coating technique was annealed at 470 degrees for 3 minutes in the air environment, the films with MoO₃ were incubated for 24 hours in 5x10⁻⁵ M concentrated SAM solutions prepared in DMSO solvent in nitrogen atmosphere. Solutions prepared in 1,2-dichlorobenzene by using 1:1 w/v ratios of poly(3-hexylthiophene) (P3HT) and phenyl(6,6) C₆₁ Butyric acid methyl ester (PCBM) as the active layer were coated on SAM coated films at 800 rpm with a spin coating technique in nitrogen atmosphere. P3HT: PCBM coated films were annealed at 110 degrees for 10 minutes. With the use of a mask, LiF(0,6nm)/Al(80nm) cathode electrode were coated on the active layer under vacuum (1.3x10⁻⁶ Torr) by thermal evaporation technique. For LiF and Al, the evaporation rates are 0.1 Å/s and 0.8-1.2 Å/s respectively. The electrical characteristics of the solar cells under the light were taken at room temperature and under the conditions of air mass A.M1.5 and radiation power 100 mW / cm² (these standards are used for radiation in all measurements). The obtained current density-voltage graphs and electrical parameters are given in Fig. 3.21 and Table 3.6.

Table 3.6 : Electrical parameters obtained from solar cells using different SAM materials. MoO₃ coated films were left in SAM for 24 hours.

| Parameters | Standard | ZE-2MEO | ZE-3MEO | ZE-Ph |
|------------------------------|----------|---------|---------|-------|
| J (mA/cm²) | 6.41 | 5.91 | 6.16 | 6.47 |
| V_{oc}(mV) | 550 | 530 | 540 | 540 |
| Efficiency(%) | 1.71 | 1.5 | 1.76 | 1.66 |
| Fill Factor | 0.486 | 0.368 | 0.528 | 0.474 |

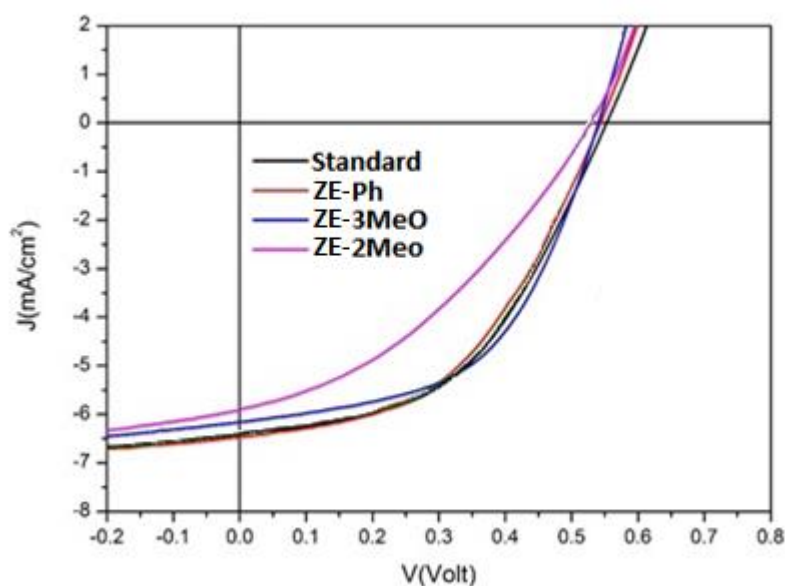


Figure 3.21: J-V graphs of solar cells prepared using different SAM materials

It is understood from table 3.6 that the efficiency of cells prepared with ZE-3MeO increased the efficiency of the standard cell. Despite the low current, the increase in the fill factor has increased the efficiency.

Since the active terminals of all the molecular structures are carboxylic acids, starting from the ZE-3MeO material, optimization studies were carried out depending on the waiting time in the optimum solution. In studies conducted, MoO₃ coated films were stored in the ZE-3MeO solution for 9 hours and 15 hours, and the waiting time in the optimum SAM solution was determined from the efficiency values of the solar cells. In order to remove organic SAM molecules clustered outside the single-coat from the film surface, electrodes retained in the solution were subjected to agitation process in DMSO solvent. One of the main problems occurs due to the MoO₃ thin films obtained by the sol-gel technique turns into hydrate form in a solution containing water.

Table 3.7 : Electrical parameters obtained from solar cells using different ZE-3MeO SAM molecule. MoO₃ coated films were left in SAM for 9 and 15 hours.

| Parameters | Standard | 15hours-6min | 15hours-10min | 9hours-6min |
|-------------------------|----------|--------------|---------------|-------------|
| J (mA/cm ²) | 5,64 | 5,84 | 6,33 | 6,2 |
| V _{oc} (mV) | 520 | 550 | 550 | 560 |
| Efficiency(%) | 1,4 | 1,55 | 1,8 | 2 |
| Fill Factor | 0,474 | 0,484 | 0,515 | 0,575 |

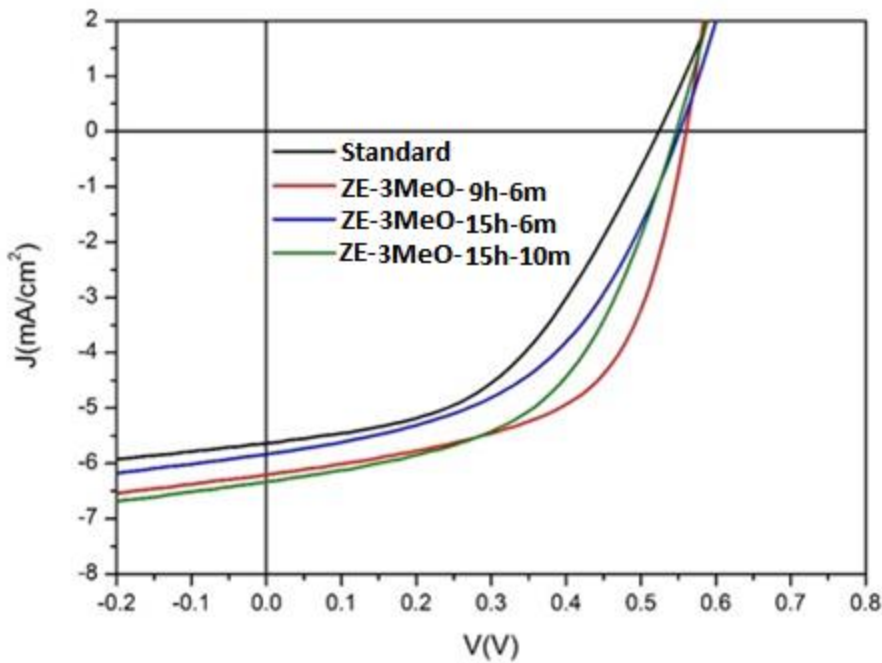


Figure 3.22: J-V graphs of solar cells prepared using ZE-3MeO SAM molecule.

The best efficiencies are obtained on cells which kept in SAM solutions for 9 hours 6 minutes. Despite the current lower than cell which kept 15 hours in SAM, efficiency is higher than the other cells. The higher values of Voc and FF increase the power conversion efficiency.

Table 3.8 : Electrical parameters obtained from solar cells using different SAM materials. MoO₃ coated films were left in SAM for 9 hours.

| Parameters | Standart | ZE-2MEO | ZE-3MEO | ZE-Ph |
|------------------------------|----------|---------|---------|-------|
| J (mA/cm²) | 6,31 | 6,09 | 6,3 | 6,7 |
| V_{oc}(mV) | 570 | 580 | 580 | 570 |
| Efficiency(%) | 2,06 | 2 | 1,96 | 2,14 |
| Fill Factor | 0.571 | 0.564 | 0.534 | 0.559 |

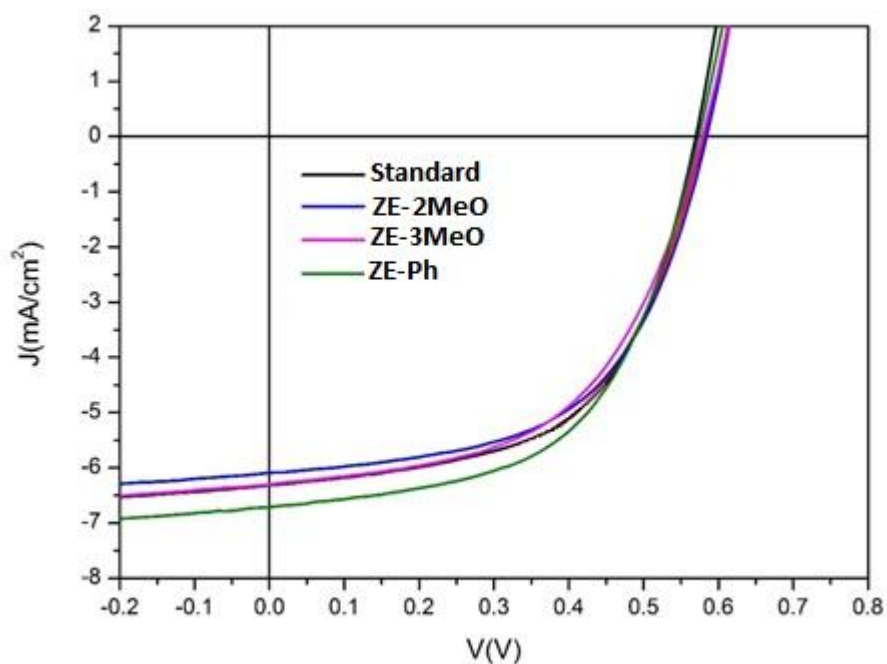


Figure 3.23: J-V graphs of solar cells prepared using different SAM materials.

It is understood from table 3.8 that when the cells kept in SAM solution 9 hours the efficiency of cells prepared with ZE-Ph increased the efficiency of the standard cell. The highest current values increase the efficiency to 2.14%.

Because of the high order sulfoxy groups of the DMSO solvent absorbs moisture very much. To remove this effect, DMF solvent were used in the next studies.

Boiling point of DMSO is higher than DMF, this is causing to films to remain wet. However same problems were seen when DMF was used.

Table 3.9 : Electrical parameters obtained from solar cells using different SAM materials. MoO₃ coated films were left in SAM for 24 hours

| Parameters | Standart | ZE-1MeO | ZE-2MEO | ZE-3MEO | ZE-Ph |
|------------------------------|----------|---------|---------|---------|-------|
| J (mA/cm²) | 6.24 | 5.68 | 6.30 | 5.82 | 5.63 |
| V_{oc}(mV) | 570 | 490 | 490 | 450 | 420 |
| Efficiency(%) | 1.75 | 0.75 | 1.05 | 0.68 | 0.72 |
| Fill Factor | 0.49 | 0.28 | 0.34 | 0.26 | 0.325 |

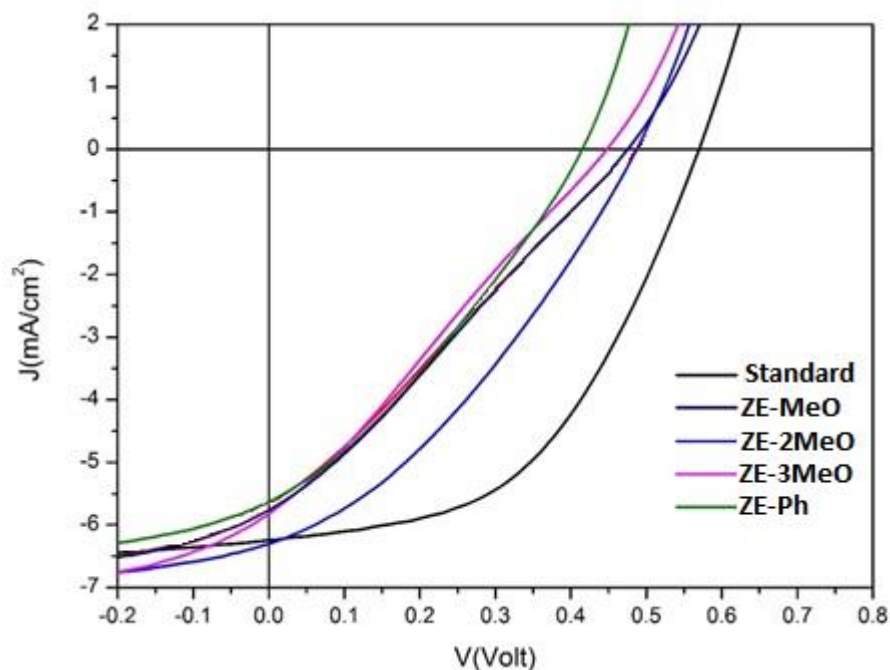


Figure 3.24: J-V graphs of solar cells prepared using different SAM materials

As table 3.9 and figure 3.24 show, the efficiency is very low of the cells which kept in SAM solutions for 24 hours. Fill factors of cells are very low and this is decreased the efficiency.

Because of the aluminium is a wet metal, the pots can be oxidized and the lifetime of potas will be very short. Due to this problem Ca/Ag katode electrode, which can create ohmic contact with PCBM was thermally evaporated on solar cells.

ITO/MoO₃/P3HT:PCBM/Ca/Ag structure was created as reference solar cell and ITO/MoO₃/SAM/P3HT:PCBM/Ca/Ag structure was created with using SAM solutions. Firstly, MoO₃ was coated on ITO with spin coater at 4500 rpm and annealed at 470 C^o for 6 minutes. Then MoO₃ films were kept in 1x10⁻⁴ M SAM solutions (in DMF) for 12 hours. In order to remove the SAM molecules which aggregate on film, the films were mixed in DMF solution for 6 minutes. P3HT:PCBM/chlorobenzene (1:0.8 w/w) solutions were coated on SAM films with spin coater at 800 rpm. Then the films were annealed at 110°C for 10 minutes. Ca(10nm)/Ag(80nm) as cathode electrode was thermally evaporated (evaporation rates are 0.2 Å/s for Ca and 0.7-1 Å /s for Ag) on the active layer under vacuum (8x10⁻⁷ Torr). Measurement of power conversion efficiencies of solar cells were made at A.M 1.5, room temperature and 100 mW/cm² sun light.

Table 3.10 : Electrical parameters obtained from solar cells using different SAM materials. MoO₃ coated films were left in SAM for 12 hours.

| Parameters | Standart | ZE-2MeO | ZE-3MeO | ZE-Ph |
|---|----------|---------|---------|-------|
| J_{sc} (mA/cm²) | 5.00 | 5.00 | 5.36 | 5.51 |
| V_{oc}(mV) | 480 | 510 | 520 | 530 |
| Efficiency(%) | 1.34 | 1.19 | 1.32 | 1.49 |
| Fill Factor | 0.558 | 0.467 | 0.474 | 0.501 |

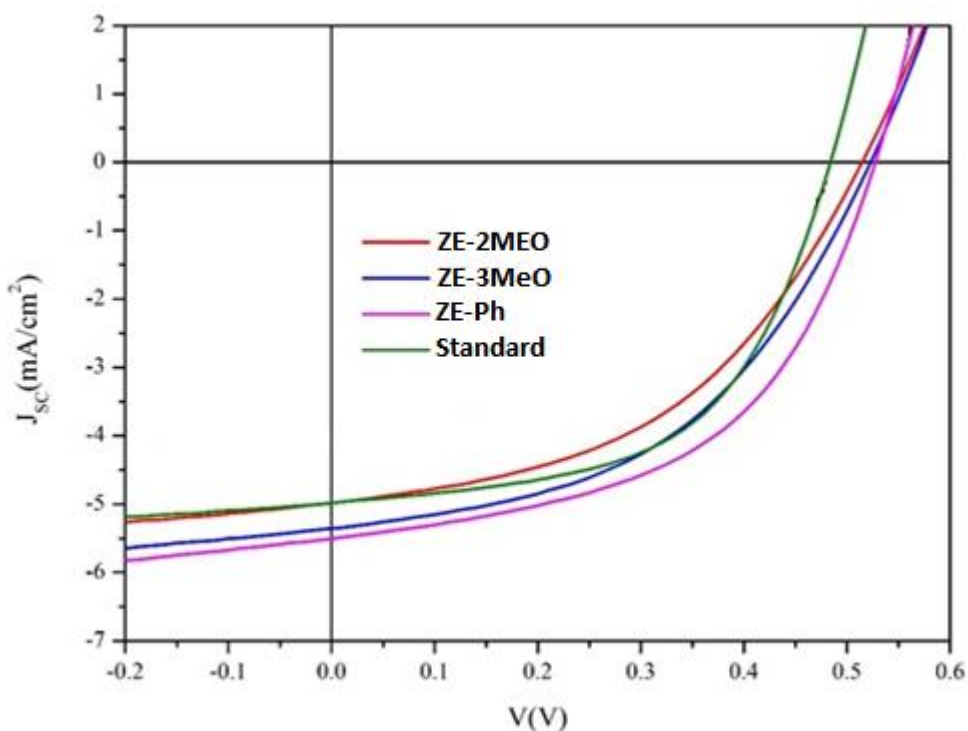


Figure 3.25: J-V graphs of solar cells prepared using different SAM materials.

As the table 3.10 and figure 3.25 show, the ZE-Ph has the best efficiency with 1.49%. The higher current and voltage values increase the efficiency of ZE-Ph solar cell.

MoO₃ electrodes were kept in SAM solutions for 9 hours, the results are shown at table 3.11 and figure 3.26. The experimental part is same with the part which the cells kept in SAMs for 12 hours.

Table 3.11 : Electrical parameters obtained from solar cells using different SAM materials. MoO₃ coated films were left in SAM for 9 hours.

| Parameters | Standart | ZE-2MeO | ZE-3MeO | ZE-Ph |
|---|----------|---------|---------|-------|
| J_{sc} (mA/cm²) | 4.75 | 4.60 | 5.40 | 4.67 |
| V_{oc}(mV) | 490 | 500 | 520 | 510 |
| Efficiency(%) | 1.25 | 1.20 | 1.38 | 1.27 |
| Fill Factor | 0.538 | 0.516 | 0.49 | 0.534 |

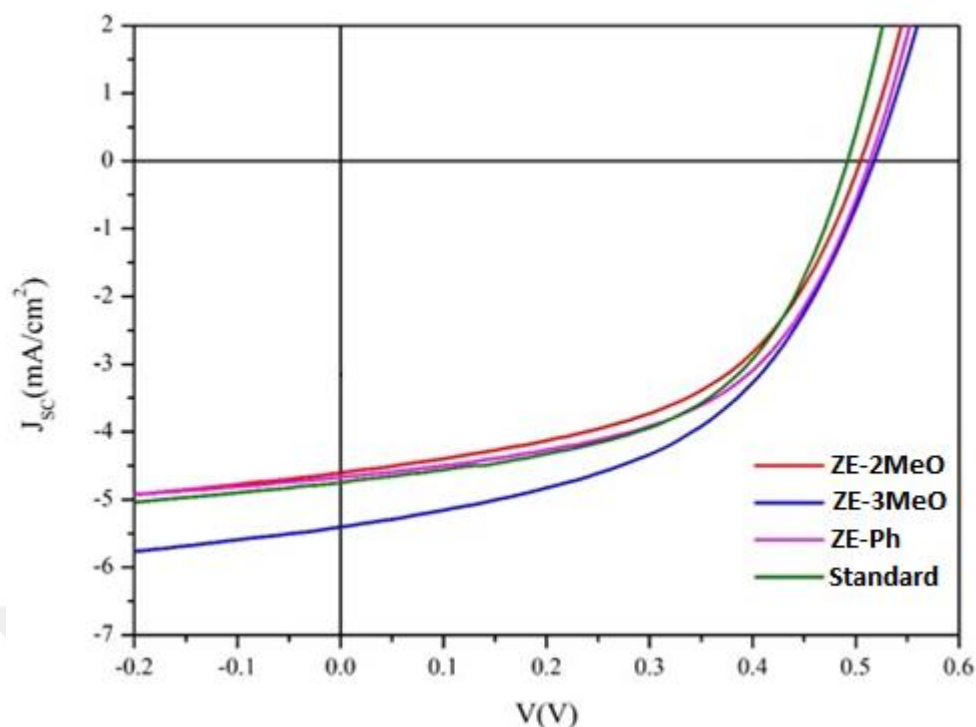


Figure 3.26: J-V graphs of solar cells prepared using different SAM materials

When the table 3.11 and figure 3.26 is examined, only the ZE-3MeO from the solar cells which MoO₃ films were left in SAM solution for 9 hours resulting in increased yield. Despite the drop in the fill factor, current density and open circuit voltage values increase.

It is seen that the efficiencies of ZE-Ph and ZE-3MeO were reached the higher values than the other cells. The solar cell with ZE-3MeO SAM was achieved the highest 1.76% efficiency and the solar cell with ZE-Ph SAM was achieved the highest 2.14% efficiency. 2.14% is the best performance of the organic solar cells which have ZE SAM molecules.

3.6.1.2. The solar cells experiments of the electrode prepared by evaporating MoO₃ thin film on SAM coated ITO

For the reason of stability problems in the cells with single layer SAM molecules on MoO₃ electrode, the new cells were made. SAM molecules coated on ITO and MoO₃ was coated on SAM. The potential barrier between layers were thought to decrease on new cells. The objective of this study is to shift the fossil level of the ITO towards the MoO₃ conductivity band to provide load carriers with step band levels in the solar cell to achieve effective load transfer. The electrical characteristics of solar

cells with hybrid buffer anode electrode structure prepared by coating the SAM molecules on the ITO substrate and evaporating the MoO₃ thin film were investigated. ITO/ SAM / MoO₃ / P3HT: PCBM / Ca / Ag structure was prepared by using SAM molecules with ITO / MoO₃ / P3HT: PCBM / Ca / Ag structure as reference solar cell in order to see the effects of SAM molecules. As a first trial, ITO substrates were incubated for 20 hours in 1×10^{-4} M concentrated SAM solutions prepared in DMF solvent in nitrogen. In order to remove the organic SAM molecules clustered on the surface, the films were rinsed in DMF wash for 4 minutes. Then a 5 nm thick MoO₃ thin film was evaporated by physical evaporation technique on SAM coated ITO at 7×10^{-7} Torr. On MoO₃ coated films, solutions prepared in chlorobenzene in the ratio 1: 0.8 w / w of P3HT and PCBM organic solutions as the active layer were coated at 800 rpm with a rotary coating technique in nitrogen atmosphere. P3HT: PCBM coated films were annealed in a nitrogen atmosphere at 110 ° C for 10 minutes on a heater. Ca (20nm) / Ag (100nm) contacts as a cathode electrode are covered with a thermal evaporation technique in vacuum (8×10^{-7} Torr) on the active layer using a shading mask (evaporating ratios are 0.2 Å/s for Ca, 0,7-1 Å/s for Ag). The electrical characteristics of the solar cells under the light were taken at air mass A.M1.5, room temperature and 100 mW / cm² radiation power. Obtained current density-voltage graphics and electrical parameters are given in Figure 3.27 and Table 3.12.

Table 3.12 : Electrical parameters obtained from solar cells using different SAM materials. ITO substrats were left in SAM for 20 hours.

| Parameters | Standard | ZE-1MeO | ZE-2MeO | ZE-3MeO | ZE-Ph |
|---|----------|---------|---------|---------|-------|
| J_{sc} (mA/cm²) | 4.48 | 4.54 | 4.55 | 4.58 | 4.72 |
| V_{oc}(mV) | 525 | 523 | 525 | 528 | 527 |
| Efficiency (%) | 1.47 | 1.49 | 1.50 | 1.52 | 1.60 |
| Fill Factor (%) | 62.0 | 63.0 | 63.0 | 63.0 | 62.0 |

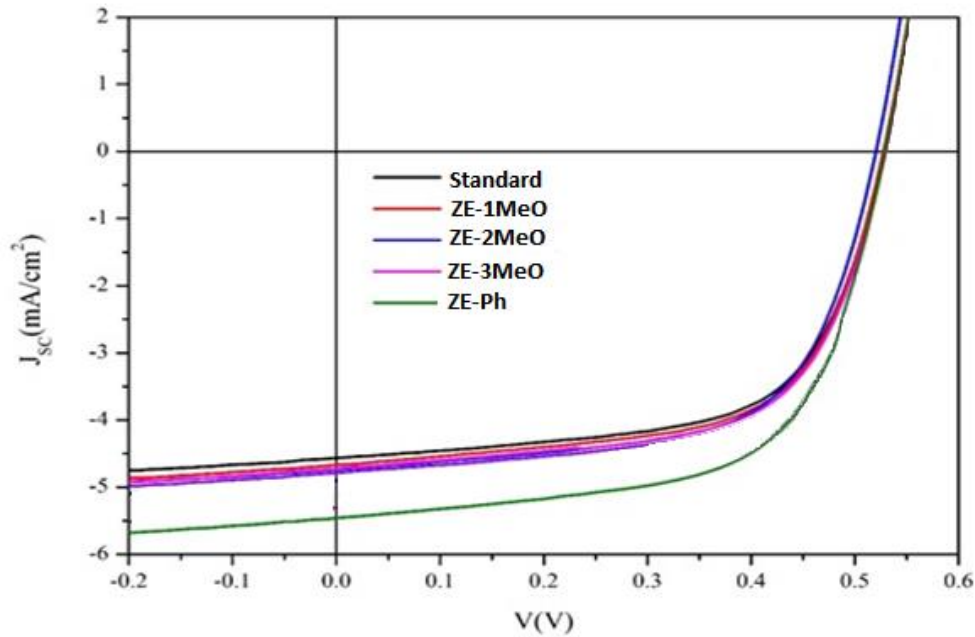


Figure 3.27: J-V graphics of solar cells with ITO/SAM/MoO₃ electrode configuration

When Table 3.12 and Figure 3.27 are examined, the yield of cells prepared by incubating ITO substrates in SAM solutions for 20 hours and rinsing in DMF solvent for 4 minutes increased the yield of standard cell. An increase was observed for all materials in current density, open circuit voltage and fill factors. The obtained data and the subsequent studies are based on the determination of the optimum conditions that can increase efficiency. Experimental study yielding the highest efficiency gains with the optimization of the thin film thicknesses of MoO₃ and the retention time of the ITO electrodes in the SAM solutions is shown below.

The ITO substrates were incubated for 24 hours in SAM solutions at a concentration of 1×10^{-4} M prepared in DMF solvent in nitrogen atmosphere and the films were rinsed in DMF solvent for 6 minutes in order to remove aggregated SAM molecules from the film surface. MoO₃ thin film with a thickness of 10 nm was evaporated on ITO coated with SAM at 7×10^{-7} Torr and annealed in nitrogen atmosphere on the heater at 100 °C for 15 minutes. Solvents prepared in chlorobenzene in the ratio of 1: 0.8 w / w of P3HT and PCBM organic solutions as the active layer were coated at 800 rpm with a rotary coating technique in nitrogen atmosphere and annealed on a heater at 110 °C for 10 minutes in a nitrogen atmosphere. The Ca (20nm) / Ag (100nm) contacts were coated as cathode electrodes by thermal evaporation technique (8×10^{-7} Torr) on the active layer using evaporation masks (evaporation

rates of 0.2 Å / s for Ca and 0.7-1 Å / s for Ag). The electrical characteristics of the solar cells under the light were taken at air mass A.M1.5, room temperature and 100 mW / cm² radiation power. The obtained current density-voltage graphs and electrical parameters are given in Table 3.13, Table 3.14 and Figure 3.28. The values given in Table 3.13 are the average of the data obtained from 5 solar cells prepared for each electrode structure. When the table 3.13, table 3.14 ve figure 3.28 examined it is seen that the efficiencies of SAM coated cells increases in contrast to standard cells.

Table 3.13: Average electrical parameters of cells with ITO/SAM/MoO₃ anode electrode configuration

| Anode Electrode Configuration | J _{sc} (mA/cm ²) | V _{oc} (mV) | FF (%) | PCE (%) |
|-------------------------------|---------------------------------------|----------------------|--------|---------|
| ITO/MoO ₃ | 6.02 | 533 | 57.4 | 1.85 |
| ITO/ZE-1MeO/MoO ₃ | 6.09 | 537 | 57.7 | 1.88 |
| ITO/ZE-2MeO/MoO ₃ | 6.64 | 533 | 57.5 | 2.03 |
| ITO/ZE-3MeO/MoO ₃ | 6.21 | 540 | 58.4 | 1.95 |
| ITO/ZE-Ph/MoO ₃ | 6.93 | 540 | 56.6 | 2.12 |

Table 1.14: The highest electrical parameters of cells with ITO/SAM/MoO₃ anode electrode configuration

| Anode Electrode Configuration | J _{sc} (mA/cm ²) | V _{oc} (mV) | FF (%) | R _s (Ω.cm ²) | R _p (Ω.cm ²) | PCE (%) |
|-------------------------------|---------------------------------------|----------------------|--------|-------------------------------------|-------------------------------------|---------|
| ITO/MoO ₃ | 6.16 | 540 | 57.9 | 20.7 | 772.2 | 1.93 |
| ITO/ZE-1MeO/MoO ₃ | 6.09 | 540 | 58.4 | 19.7 | 799.2 | 1.93 |
| ITO/ZE-2MeO/MoO ₃ | 6.71 | 540 | 57.4 | 17.2 | 718.3 | 2.08 |
| ITO/ZE-3MeO/MoO ₃ | 6.34 | 540 | 58.7 | 17.5 | 812.1 | 2.01 |
| ITO/ZE-Ph/MoO ₃ | 7,10 | 540 | 57.3 | 15.0 | 710.0 | 2.20 |

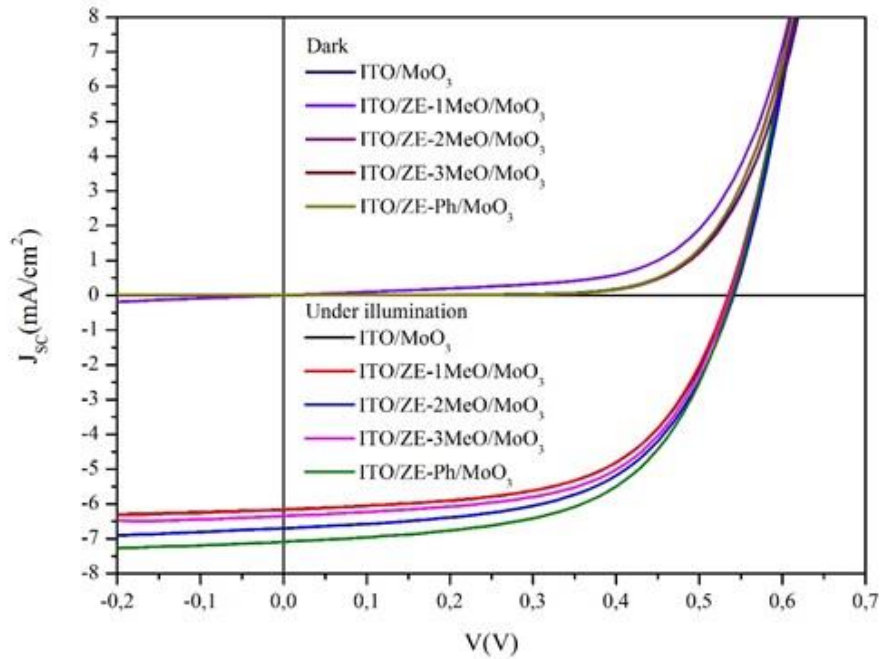


Figure 3.28: J-V graphics of solar cells with ITO/SAM/MoO₃ electrode configuration under illumination and dark

The change of the potential from the HOMO level of the P3HT molecule to the ITO electrode takes place in steps via decreasing the work function of ITO electrode at interface. Thus, the transfer of the load carriers from the OSC structure to the outer electrodes is increased compared to the ITO / MoO₃ structure without recombination. In particular, as the energy level difference between the HOMO band of the P3HT donor organic semiconductor and the work function value of the ITO electrode increases, the effective charge transfer decreases. The increase in the open circuit voltage values indicates the increase of the hole charge carriers reaching the anode electrode without recombination. Compared to the standard cell, the solar cell series resistance is reduced and matches the promised target in the thesis. Parallel resistance increase in OSC is a desirable feature and it is obvious that parallel resistances increase in ITO / SAM / MoO₃ structures compared to standard ITO / MoO₃ electrodes. Successful achievement of the aim of decreasing series resistances and increasing parallel resistances as envisaged in the thesis. The study shows that the SAM / MoO₃ hybrid anode electrode structure shows improvements in OSC efficiency and electrical properties.

3.7. Incident Photon to Current Efficiency (IPCE) of SAM Molecules

Incident photon to current efficiency is a measure of the ratio of the photocurrent (converted to an electron transfer rate) versus the rate of incident photons (converted from the calibrated power of a light source) as a function of wavelength. IPCE takes into consideration the efficiencies for photon absorption/charge excitation and separation, charge transport within the solid to the solid-liquid interface, and interfacial charge transfer across the solid-liquid interface. IPCE values is calculated with equation 5.

$$\text{IPCE}\% = \frac{I_{\text{sc}}(\text{A})}{P(\text{W})} \times \frac{1240}{\lambda(\text{nm})} \times 100 \quad (5)$$

P is radiation power, I_{sc} is photocurrent of solar cell, λ is wavelength of incident photon. IPCE values of organic solar cells with and without SAM molecules is shown at figure 8. IPCE value of OSC without SAM is 49.95% at 510 nm, this IPCE value corresponds to P3HT's maximum absorption. IPCE values of solar cells with SAM are higher than solar cells without SAM molecules.

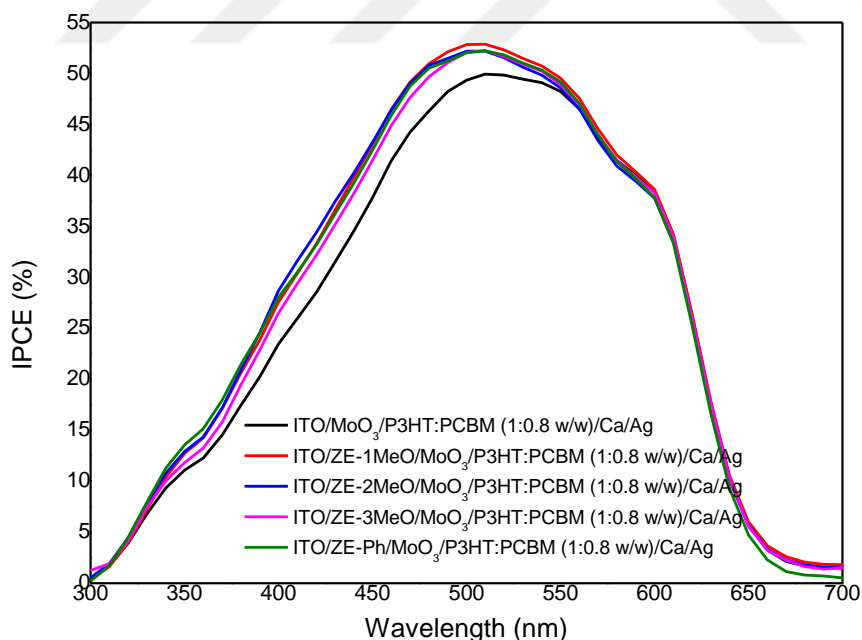


Figure 3.29: IPCE curves of solar cells with/without SAM molecules

3.6.2 Dye molecules

0.7 g ICS-PPG230 (functionalized alkoxide precursor) were dissolved in 0.8 g of 3-methoxypropionitrile and 1.6 g of sulfolane to prepare the electrolyte. Then, 0.368 g acetic acid, 0.3 M 1-methyl-3-propylimidazolium iodide, 0.05 M I₂ and 0.1 M LiI were added. After that, 0.204 g of tertbutyl pyridine and 0.036 g of guanidine were added to mixture and stirred a few hours. One drop solution was placed on the dye adsorbed titania electrode and platinized FTO counter electrode was pushed. The platinized FTO glass was made by H₂PtCl₆ solution (5 mg/1 mL of i-PrOH) followed by heating at 450 °C for 10 min. Two electrodes stuck together. The cell active area for the electrical measurements was 0.28 cm². In table 3.12 the electrical characteristics and in figure 27 current-voltage (J-V) characteristic curves of DSSCs are given. The efficiencies are 3.0% and 3.4% for MZ-235 and MZ-341, respectively. Approximately 660mV open circuit voltage was measured for both dyes. The short circuit current density was 6.83 mA/cm² for MZ-341 and 6.45 mA/cm² for MZ-235. The extinction coefficient's low value and visible light's ineffective exploitation causes short circuit current. Otherwise, MZ-235 cell's lower absorption of dye adsorbed TiO₂ photo electrode respect to MZ-341, causes relatively lower values for electrical characteristics (seen in te inset of Figure 27a). The dark current density in the cells which seen in Figure 27b, doesn't have significant differences but, the electron leakage of MZ-235 is higher compared to MZ-341.

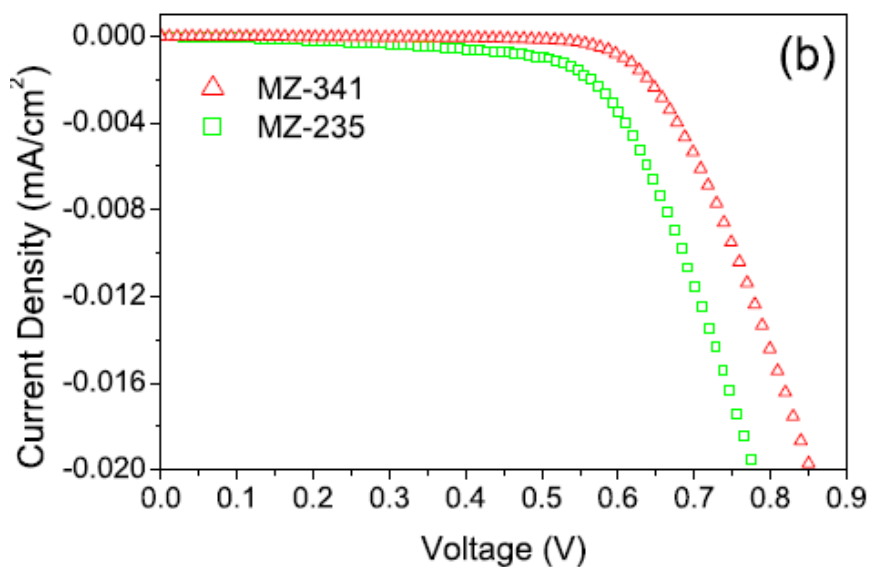
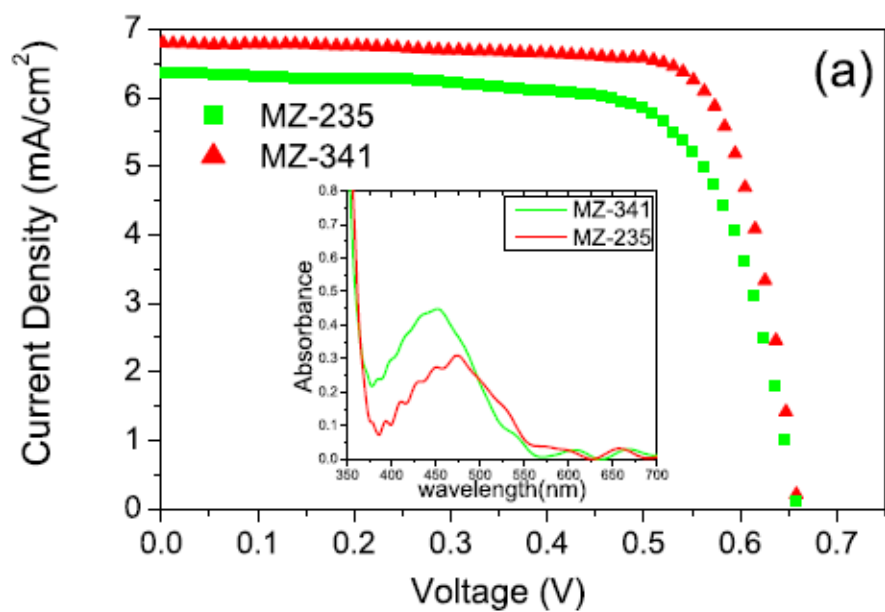


Figure 3.30: J-V curves of MZ dyes a) under light illumination (1.5 A.M 1000 W/m²) b) in dark

Table 3.15: Solar cell parameters for DSSC with MZ dyes.

| Dye | Voc (mV) | Jsc (mA/cm ²) | FF | η (%) |
|--------|----------|---------------------------|------|------------|
| MZ-341 | 663 | 6.83 | 0.74 | 3.4 |
| MZ-235 | 662 | 6.45 | 0.69 | 3.0 |

4. CONCLUSION

Organic solar cells and dye sensitized solar cells are challenging rival routes for silicon based solar cells with their easy manufacturing. Inserting a boundary layer between the ITO and P3HT: PCBM, the potential barrier will reduce, leading to an enhanced efficiency with hole injection from P3HT to ITO. As anode buffer layer, PEDOT:PSS is used for electron injection process in organic solar cells. PEDOT:PSS is considerably coated on ITO electrodes to improve hole injection in organic solar cells. However, PEDOT:PSS has some disadvantages on device lifetime because of the chemical reactions between PEDOT:PSS and ITO interface. Besides PEDOT:PSS, metal oxides and SAMs are efficient applicants for the anode buffer layers in organic solar cells. Coating SAM molecules on ITO surface tune ITO energy level coherently with active layer and smooth its surface. Additionally, diffusion of electron charge carriers to anode is blocked and hole-electron recombination is decreased. On the other hand, DSSC performance is better than the other solar cell technologies under diffuse light conditions and at higher temperatures. DSSCs offer wide range opportunities like; design solar cells with a large flexibility in shape, color, and transparency. Trying various molecules opens up new commercial opportunities.

The aim of this thesis is to synthesis of new SAM and dye molecules for OSC and DSSC application. The head group of SAMs (-COOH) binds to the substrate surface. The centerpiece of molecule is electron donating bithiophene group. Terminating side has four group; benzene, one methoxy, two methoxy and three methoxy benzene. NMR results and FT-IR results show that SAM molecules were synthesized efficiently.

Electrochemical characterization of SAM molecules were made by cyclic voltammetry. Electron donor methoxy groups made the oxidation potentials of molecules to be decreased. The oxidation potentials of SAM molecules are changing between 0.80 and 0.90 V. COOH groups of SAM molecules shows irreversible reduction potentials. Band gaps of SAM molecules are decreased when the methoxy groups were added. The band gaps are changing between 2.65 and 2.57 eV. Cyclic voltammetry analyses of SAM molecules on ITO were made only in positive voltage

since the molecules adsorbed on ITO surface are separated from the surface. HOMO energy levels are 5.5 eV, 5.4 eV, 5.35 eV and 5.30 eV for ZE-Ph, ZE-1MeO, ZE-2MeO and ZE-3MeO, respectively. UV-Visible absorption spectrums show that SAM molecules give absorption in UV range and they don't venture to P3HT's absorption area. Thus, P3HT can absorb the visible area of the solar spectrum. The absorptions of SAM molecules are between 300 and 475 nm.

Kelvin Probe Force Microscopy was used to analyze the contact potential difference (CPD) of ITO/SAM structures. CPD values are changed when SAM molecules adsorbed on ITO surface. By making use of MoO₃ and SAM molecules, the potential barrier between ITO and P3HT is decreased and thus efficiency is increased. MoO₃ coated ITO films were kept in SAM solutions for 9, 12, 15 and 24 hours. Best performance was acquired for 9 hours samples with 2.14% efficiency. The highest electrical parameters of cells with ITO/SAM/MoO₃ anode electrode configuration was seen at the solar cell with ZE-Ph molecule for 24 hours. The efficiency of cell with ZE-Ph is 2.20%. It was seen that the SAM molecules were increased the efficiency. When an increase seen at reaching of the hole charge carriers to the anode electrode without recombination the increase is seen at open circuit voltage values. In solar cells series resistance is decreased compared to the standard cell and parallel resistance is increased. IPCE value of OSC without SAM is 49.95% at 510 nm and IPCE values of solar cells with SAM are higher than solar cells without SAM molecules.

As experimental results, increase in short circuit currents of OSC structures, where electrodes are used which are modified by SAM molecules, is obtained. Each potential change in structure ITO anode electrode with SAM molecule performs a task on transfers the hall charge carrier and resultant energy catalyzed charge transfer band profile and hall charge carrier at ITO electrode. Here the value of function work decreases with SAM molecules created effect of molecular dipol moment on the interface. The magnitude of the molecular dipol moment have been changing depending on the intensity of the electronegative bands. In the methoxy terminal groups of SAM molecules the dipol moment direction is radially outwards from the ITO electrode. Here is located on the carboxylic acid, carbonil groups according to the methoxy groups, since it is more electronegative, the part methoxy

groups being positive and dipole moments of methoxy groups towards the direction (outward from the ITO electrode). As methoxy groups increased, the magnitude of the dipole moment increases and the value of the function work decreases according to 1-MeO group.

The dyes for DSSC have D- π -A structure. Donor sides are triphenylamine groups with/without hexyloxy. The p-conjugated bridge between donor and acceptor is benzimidazole derivative. The electron acceptor is a carboxyl group which anchoring to TiO₂. NMR and FT-IR results shows the dye molecules were synthesized efficiently. The OH and C=O peaks were seen on FT-IR results.

Electrochemical characterization is made by cyclic voltammetry. Electron donor hexyloxy groups made the oxidation potentials of molecules to be decreased. The oxidation potentials are 0.78 and 0.89 V for MZ235 and MZ-341, respectively. The MZ dyes have two reduction potentials. The first reversible peaks are originated from the benzimidazole derivative. The second irreversible peaks are originated from the COOH groups. Dye molecules have absorption at UV-Visible range. The dye MZ-235 shows a bathochromic shift of its absorption spectrum thus exhibiting a better coverage of the visible spectrum. The absorption maximums of MZ-235 are 460 nm in THF and toluene. For the MZ341 dye absorption maximums are 441 and 443 nm in THF and toluene, respectively.

The DSSC with MZ-341 dye showed an overall efficiency of 3.4% and MZ-235 showed an efficiency of 3.0%. The higher absorption intensity of MZ-341 coated TiO₂ result in higher instrument performance. The results prove that efficient dye molecules and SAM molecules were synthesized for DSSC and OSC.

REFERENCES

1. **Yang, L.**, (2014) Hole Transport Materials for Solid-State Mesoscopic Solar Cells UPPSALA UNIVERSITY.
2. IEA Key World Energy Statistics (2013), International Energy Agency, OECD publishing, Paris, France.
3. **Xu, B.**, (2015) - Advanced Organic Hole Transport Materials for Solution-Processed Photovoltaic Devices.
4. Statistical Review of World Energy, Workbook, London, **2013**
5. IMATE CHANGE 2014: Synthesis Report. Summary for Policymakers. IPCC. Retrieved 7 March, **2015**.
6. **Lundberg, O.**, Band Gap Profiling and High Speed Deposition of Cu(In, Ga)Se₂ for Thin Film Solar Cells.
7. **Lindqvist, C.**, (2014) Stability of Bulk-Heterojunction Blends for Solar Cell Applications CHALMERS UNIVERSITY OF TECHNOLOGY.
8. <http://www.eia.gov/forecasts/aeo/er/?src=Total-f3>, accessed 20/05/13.
9. http://ec.europa.eu/clima/policies/brief/causes/index_en.htm, accessed 23/12/13.
10. **Sartori, S.**, (2013), *MRS Bulletin*, **38**, 1011.
11. Nordic Energy Technology Perspective - Pathways to a Carbon Neutral Energy Future; International Energy Agency and Norden (Nordic EnergyResearch), 2013.
12. **Yang, L.**, (2014), Hole transport materials for solid-state mesoscopic solar cells.
13. **Nozik, A. J., Miller, J.**, (2010) *Chem. Rev.*, **110**, 6443–6445
14. Key World Energy Statistics. IEA. 2014. pp. 6, 28. Archived from the original on 5 May, 2014.
15. Solar Energy Perspectives: Executive Summary. International Energy Agency. 2011.
16. **Chapin, D. M., Fuller, C. S., Pearson, G. L.** (1954), *J. Appl. Phys.*, **25**.
17. **M.A. Green, K.Emery, D.L.King, S. Igari, and W.Warta**, (2003), Solar Cell Efficiency Tables (version 22) *Progress in Photovoltaics: Research and Applications*, **11**, p.347-352
18. **Gregg, B.A.**, (2003), Excitonic Solar, Cells. *J Phys Chem B*, **107**, 4688–98.
19. **Yu, G., Gao, J., Hummelen, J, Wudl, F, Heeger, A.**, (1995), Polymer photovoltaic cells: enhanced efficiencies via a network of internal donor-acceptor heterojunctions. *Science*, **270**, 1789–91.
20. **Zhu, R., Chung, C.H., Cha, K.C., Yang, W., Zheng, Y.B., Zhou, H., Song, T.B., Chen, C.C., Weiss, P.S., Li, G., Yang, Y.**, (2011), Fused silver nanowires with metaloxide nanoparticles and organic polymers for highly transparent conductors. *ACS Nano*, **5**, 9877–82.
21. **Chen, K.S., Salinas, J.F., Yip, H.L., Hou, J., Hou, J., Jen, A.K.**, (2012), Semi-transparent polymer solar cells with 6% PCE, 25% average visible transmittance and color rendering index close to 100 for power generating win-dow applications. *Energy Environ Sci*, **5**, 9551–7.
22. **Kallman, H., Pope, M.** (1959), *Journal of Chemical Physics*, **30**, 585-586.

23. Shirakawa, H., Louis, E. J., MacDiarmid, A. G., Chiang, C. K., Heeger, A., (1977), *J. Journal of the Chemical Society, Chemical Communications*, 578-580.
24. The Nobel Prize in Chemistry 2000 (http://nobelprize.org/nobel_prizes/chemistry/laureates/2000/). *The Nobel Foundation* available online 27/06/2011.
25. Tang, C. W., (1986), *Applied Physics Letters*, 48, 183-185.
26. Sariciftci, N. S., Smilowitz, L., Heeger, A. J. H., Wudl, F., (1992), *Science*, 258, 1474-1476.
27. Winder, C., Sariciftci, N.S., (2004), *J. Mater. Chem.*, 14, 1077p.
28. Peumans, P., Forrest, S. R., (2001), *Very-High Efficiency Double Heterostructure Copper Phthalocyanine/C60 photovoltaic Cells*, *Appl. Phys. Lett.* 79, 126-128.
29. Drechsel J., Mannig B., Kozlovski F., et al., (2004), *High Efficiency Organic Solar Cells Based on Single or Multiple PIN Structures*, *Thin Solid Films* 451, 515-517.
30. Rand B. P., Xue J., Yang F., and Forrest S. R., (2005), *Organic Solar Cells with Sensitivity Extending into the Near-Infrared Region*, *Appl. Phys. Lett.* 87 (23) 233508.
31. Mutolo K. L., Mayo E. I., Rand B.P., Forrest S. R., and Thompson M. E., (2006), *Enhanced Open-Circuit Voltage in Subphthalocyanine/C60 Organic Photovoltaic Cells*, *J. Am. Chem. Soc.* 128 (25), 8108-8109.
32. Gommans H., Cheyens D., Aernouts T. et al., (2007), *Electro-Optical Study of Subphthalocyanine in a Bilayer Organic Solar Cell*, *Adv. Funct. Mater.* 17, 2653-2658.
33. Troshin P. A., Troyanov S. I. and Boiko G. N. et al., (2004), *Efficient [2+3]-Cycloaddition Approach to Synthesis of Pyridinyl Based [60]-Fullerene Ligands, Fullerenes, Nanotubes*, *Carbon Nanostruct.* 12, 435-441.
34. Koeppe R., Troshin P. A., Lyubovskaya R. N., and Sariciftci N. S., (2005), *Complexation of Pyrrolidinofullerenes and Zinc-Phthalocyanine in a Bilayer Organic Solar Cell Structure*, *Appl. Phys. Lett.* 87, (24), 244102
35. Troshin P. A., Koeppe R. and Peregudov A. S. et. al., (2007), *Supramolecular Association of Pyrrolidinofullerenes Bearing Chelating Pyridyl Groups and Zinc Phthalocyanine for Organic Solar Cells*, *Chem. Mater.*, 19, 5363-5372.
36. Troshin P. A., Lyubovskaya R. N. and Razumov V. F., (2008), *Nanotechnologies in Russia*, Vol. 3 Nos. 5–6 242-271p.
37. You J, Dou L, Yoshimura K, Kato T, Ohya K, Moriarty T, Emery K, Chen CC, Gao J, Li G, Yang Y., (2013), *A polymer tandem solar cell with 10.6%*, *Nat Commun*, 4, 1446/1-10.
38. Zitzler-Kunkel, A., Lenze, M. R., Meerholz, K., and Würthner, F., (2013), *Enhanced photocurrent generation by folding-driven H-aggregate formation*, *Chem. Sci.*, 4, 2071.
39. Bhosale, R., Misek, J., Sakai, N., and Matile, S., (2010), *Chem. Soc. Rev.*, 39, 138–149.
40. Bassani, D. M., Jonusauskaitė, L., Lavie-Cambot, A., McClenaghan, N. D., Pozzo, J.-L., Ray, D. and Vives, G., (2010), *Coord. Chem. Rev.*, 254, 2429–2445

41. **Brunetti, F. G.; Kumar, R.; Wudl, F.**, (2010), *Organic electronics from perylene to organic photovoltaics: painting a brief history with a broad brush*. *J. Mater. Chem.*, 20, 2934
42. **Matsuo, Y., Kawai, J., Inada, H., Nakagawa, T., Ota, H., Otsubo, S., Nakamura, E.**, (2013), *Addition of dihydromethano group to fullerenes to improve the performance of bulk heterojunction organic solar cells*, *Adv. Mater.*, 25, 6266
43. **Yu, G., Gao, J., Hummelen, J. C., Wudl, F., Heeger, A. J.**, (1995), *Science*, 270,1789
44. **Sariciftci, N. S., Baun, D., Zhang, C., Srdanov, V. I., Heeger, A. J., Stucky, G., Wudl, F.**, (1993), *Appl. Phys. Lett.*, 62, 585
45. **Shaheen, S. E., Brabec, C. J., Sariciftci, N. S., Padinger, F., Fromherz, T., Hummelen, J. C.**, (2001), *Appl. Phys. Lett.*, 78, 841
46. **Brabec, C. J., Shaheen, S. E., Winder, C., Sariciftci, N. S., Denk, P.**, (2002), *Appl. Phys. Lett.*, 80, 1288.
47. **Blom, P. W. M., De Jong, M. J. M., Breedijk, S.**, (1997), *App. Phys. Lett.*, 71, 930.
48. **Dennler, G., Scharber, M. C., and Brabec, C. J.**, (2009), *Polymer-Fullerene Bulk-Heterojunction Solar Cells*, *Adv. Mater.*, 21, 1323–1338.
49. **Gendron, D., Leclerc, M.**, (2011), *New conjugated polymers for plastic solar cells.*, *Energy Environ. Sci.*, 4, 1225
50. **Li, G., Zhu, R., Yang, Y.**, (2012), *Polymer solar cells*. *Nat. Photonics*, 6, 153–161.
51. **Roncali, J.**, (2009), *Molecular Bulk Heterojunctions: An Emerging Approach to Organic Solar Cells.*, *Acc. Chem. Res.*, 42, 1719–1730
52. **Sariciftci, N. S., Smilowitz, L., Heeger, A. J., Wudl, F.**, (1992), *Photoinduced electron transfer from a conducting polymer to buckminsterfullerene.*, *Science*, 258, 1474–1476
53. **Scharber, M. C., Muhlbacher, D., Koppe, M., Denk, P., Waldauf, C., Heeger, A. J. and Brabec, C. J.**, (2006), *Adv. Mater.*, 18, 789.
54. **Park, S. H., Roy, A., Beaupre, S., Cho, S., Coates, N., Moon, J. S., Moses, D., Leclerc, M., Lee, K., and Heeger, A. J.**, (2009), *Bulk heterojunction solar cells with internal quantum efficiency approaching 100%*, *Nat. Photonics*, 3, 297–302.
55. **Chen, H.Y., Hou, J., Zhang, S., Liang, Y., Yang, G., Yang, Y., Yu, L., Wu, Y., and Li, G.**, (2009), *Polymer solar cells with enhanced open-circuit voltage and efficiency*, *Nat. Photonics*, 3, 649–653
56. **Liang, Y., Xu, Z., Xia, J., Tsai, S. T., Wu, Y., Li, G., Ray, C., and Yu, L.**, (2010), *For the bright future—bulk heterojunction polymer solar cells with power conversion efficiency of 7.4%*, *Adv. Mater.*, 22, E135–E138
57. **Piliago, C., Holcombe, T. W., Douglas, J. D., Woo, C. H., Beaujuge, P. M., and Fréchet, J. M. J.**, (2010), *Synthetic control of structural order in N-alkylthieno[3,4-c]pyrrole-4,6-dionebased polymers for efficient solar cells*, *J. Am. Chem. Soc.*, 132, 7595–7597.
58. **Chu, T.Y., Lu, J., Beaupré, S., Zhang, Y., Pouliot, J.R. M., Wakim, S., Zhou, J., Leclerc, M., Li, Z., Ding, J. and Tao, Y.**, (2011), *Bulk heterojunction solar cells using thieno[3,4-c]pyrrole- 4,6-dione and dithieno[3,2-b:2',3'-d]silole copolymer with a power conversion efficiency of 7.3%*, *J. Am. Chem. Soc.*, 133, 4250–4253

59. Zhou, H., Yang, L., Stuart, A. C., Price, S. C., Liu, S., and You, W., (2011), *Development of fluorinated benzothiadiazole as a structural unit for a polymer solar cell of 7% efficiency*, *Angew. Chem., Int. Ed.*, 50, 2995–2998.
60. Liang, Y. and Yu, L., (2010), *A new class of semiconducting polymers for bulk heterojunction solar cells with exceptionally high performance*, *Acc. Chem. Res.*, 43, 1227–1236.
61. Xue, J., (2010), *Perspectives on organic photovoltaics*, *Polym. Rev.*, 50, 411–419.
62. Hu, H., Jiang, K., Yang, G., Liu, J., Li, Z., Lin, H., Liu, Y., Zhao, J., Zhang, J., Huang, F., Qu, Y., Ma, W., and Yan, H., (2012), *J. Am. Chem. Soc.*, DOI: 10.1021/jacs.5b08556.
63. Cao, Y., Yu, G., Zhang, C., Menon, R., Heeger, A. J., (1997), *Synth. Met.*, 87, 171
64. Heithecker, D., Kammoun, A., Dobbertin, T., Riedl, T., Becker, E., Metzendorf, D., Schneider, D., Johannes, H. H., Kowalsky, W., (2003), *Appl. Phys. Lett.*, 82, 4178
65. So, F., Kondakov, D., (2010), *Adv. Mater.*, 22, 3762.
66. de Jong, M. P., van IJzendoorn, L. J., de Voigt, M. J. A., (2000), *Appl. Phys. Lett.*, 77, 2255.
67. Balendhran, S., Deng, J., Ou, J. Z., Walia, S., Scott, J., Tang, J., Wang, K. L., Field, M. R., Russo, S., Zhuiykov, S., Strano, M. S., Medhekar, N., Sriram, S., Bhaskaran, M., Kalantarzadeh, K., (2013), *Enhanced Charge Carrier Mobility in Two-dimensional High Dielectric Molybdenum Oxide*. *Adv. Mater.*, 25, 109-114.
68. Seiichiro, M., Yang, Y., (2012), *Solution Processed MoO₃ Interfacial Layer for Organic Photovoltaics Prepared by a Facile Synthesis Method*. *Adv. Mater.* 24, 2459-2462.
69. Meyer, J., Khalandovsky, R., Görrn, P., and Kahn, A., (2011), *Adv. Mater.*, 23, 70–73.
70. Chu, C. W., Li, S.H., Chen, C.W., Shrotriya, V., Yang, Y., (2005), *Appl. Phys. Lett.*, 87, 193508.
71. Meyer, J., Hamwi, S., Bülow, T., Johannes, H. H., Riedl, T., Kowalsky, W., (2007), *Appl. Phys. Lett.*, 91, 113506.
72. Kanai, K., Koizumi, K., Ouchi, S., Tsukamoto, Y., Sakanoue, K., Ouchi, Y., Seki, K., (2010), *Org. Elect.*, 11, 188.
73. Lee, H., Cho, S. W., Han, K., Jeon, P. E., Whang, C. N., Jeong, K., Cho, K., Yi, Y., (2008), *Appl. Phys. Lett.*, 93, 043308
74. Leem, D. S., Park, H. D., Kang, J. W., Lee, J. H., Kim, J. W., Kim, J. J., (2007), *Appl. Phys. Lett.*, 91, 011113.
75. Steirer, K. X., Chesin, J. P., Widjonarko, N. E., Berry, J. J., Miedaner, A., Ginley, D. S., Olson, D. C., (2010), *Org. Elect.*, 11, 1414.
76. Kröger, M., Hamwi, S., Meyer, J., Riedl, T., Kowalsky, W., Kahn, A., (2009), *Org. Elect.*, 10, 932.
77. Kim, D.Y., Subbiah, J., Sarasqueta, G., So, F., Ding, H.J. and Gao, Y.L., (2009), *The effect of molybdenum oxide interlayer on organic photovoltaic cells*, *Appl. Phys. Lett.*, 95, 093304.
78. Kanai, K., Koizumi, K., Ouchi, S., Tsukamoto, Y., Sakanoue, K., Ouchi, Y. and Sek, K., (2010), *Electronic structure of anode interface with molybdenum oxide buffer layer*, *Org. Electron.*, 11, 188-194.

79. **Markus C.S., Mühlbacher D., Koppe M., Denk P., Waldauf C., Heeger A.J. and Brabec C.J.**, (2006), *Design Rules for Donors in Bulk-Heterojunction Solar Cells—Towards 10 % Energy-Conversion Efficiency*, *Adv. Mater.*, 18, 789.
80. **Fadeev, A. Y., Helmy, R. and Marcinko, S.**, (2002), *Self-assembled monolayers of organosilicon hydrides supported on titanium, zirconium, and hafnium dioxides*. *Langmuir*, 18(20), 7521–7529.
81. **Koide, Y., Such, M. W., Basu, R., Evmenenko, G., Cui, J., Dutta, P., Hersam, M. C. and Marks, T. J.**, (2003), *Hot microcontact printing for patterning ITO surfaces. Methodology, morphology, microstructure, and OLED charge injection barrier imaging*. *Langmuir*, 19(1), 86–93.
82. **Long, Y. T., Herrwerth, S., Eck, W. and Grunze, M.**, (2002), *Synthesis and characterization of self-assembled monolayers based on redox-active silane compounds on platinum surfaces*. *Physical Chemistry Chemical Physics*, 4(3), 522–526.
83. **Marcinko, S., Helmy, R. and Fadeev, A. Y.** (2003), *Adsorption properties of SAMs supported on TiO₂ and ZrO₂*. *Langmuir*, 19(7), 2752–2755.
84. **Boal, A. K., Das, K., Gray, M. and Rotello, V. M.**, (2002), *Monolayer exchange chemistry of gamma-Fe₂O₃ nanoparticles*. *Chemistry of Materials*, 14(6), 2628–2636.
85. **Zharnikov, M., Kuller, A., Shaporenko, A., Schmidt, E. and Eck, W.** (2003), *Aromatic self-assembled monolayers on hydrogenated silicon*. *Langmuir*, 19(11), 4682–4687.
86. **Niederhauser, T. L., Lua, Y. Y., Jiang, G. L., Davis, S. D., Matheson, R., Hess, D. A., Mowat, I. A. and Linford, M. R.**, (2002), *Arrays of chemomechanically patterned patches of homogeneous and mixed monolayers of 1-alkenes and alcohols on single silicon surfaces*. *Angewandte Chemie-International Edition*, 41(13), 2353–2356.
87. **Taylor, C. E. and Schwartz, D. K.** (2003), *Octadecanoic acid self-assembled monolayer growth at sapphire surfaces*. *Langmuir*, 19(7), 2665–2672.
88. **Hyeon, T., Lee, S. S., Park, J., Chung, Y. and Bin Na, H.**, (2001), *Synthesis of highly crystalline and monodisperse maghemite nanocrystallites without a size-selection process*. *Journal of the American Chemical Society*, 123(51), 12798–12801.
89. **Salem, A. K., Searson, P. C. and Leong, K. W.**, (2003), *Multifunctional nanorods for gene delivery*. *Nature Materials*, 2(10), 668–671.
90. **Chen, H. G., Wu, X. D., Yu, Q. Q., Yang, S. R., Wang, D. P. and Shen, W. Z.**, (2002), *Selfassembled monolayers of n-hexadecanoic acid and alpha-hydroxyl n-hexadecanoic acid on titanium surfaces*. *Chinese Journal of Chemistry*, 20(12), 1467–1471.
91. **Aswal D.K., Lenfant S., Guerin D., Yakhmi J.V. and Vuillaume D.**, (2006), *Self assembled monolayers on silicon for molecular electronics*, *Analytica Chimica Acta*, 568, 84–108.

92. **Susan F., Appleyard J., Day S.R., Pickford R.F. and Willis M.R.**, (2000), *Organic electroluminescent devices: enhanced carrier injection using SAM derivatized ITO electrodes*, J. Mater. Chem., 10, 169-173.
93. **Choi B., Rhee J. and Lee H.H.**, (2001), *Tailoring of self assembled monolayer for polymer light emitting diodes*, Appl. Phys. Lett., 79, 2109.
94. **Hsiao C.C., Chang C.H., Hung M.C., Yang N.J. and Chen S.A.**, (2005), *Self-assembled monolayer modification of indium tin oxide anode surface for polymer light-emitting diodes with poly[2-methoxy-5-(2-ethylhexyloxy)-1,4-phenylene vinylene] for high performance*, Appl. Phys. Lett., 86, 223505.
95. **Chong L.W., Lee Y.L. and Wen T.C.**, (2007), *Surface modification of indium tin oxide anodes by self-assembly monolayers: Effects on interfacial morphology and charge injection in organic light-emitting diodes*, Thin Solid Films, 515, 2833–284.
96. **Bedis O.H., Koukia F., Langb P., Ouadac H.B. and Bouchriha H.**, (2009), *Self-assembled monolayer effect on the characteristics of organic diodes*, Synthetic Metals, 159, 551–555.
97. **O'Regan, B., Gratzel, M.**, (1991), Nature, 353, 737
98. **Hagfeldt, A., Boschloo, G., Sun, L., Kloo, L., and Pettersson, H.**, (2010), Chem. Rev., 110, 6595–6663.
99. **Gratzel, M.**, (2004), J. Photochem. Photobiol. A, 164, 3.
100. **Nazeeruddin, M. K., Kay, A., Rodicio, I., Humphry-Baker, R., Mueller, E., Liska, P., Vlachopoulos, N., Gratzel, M.**, (1993), J. Am. Chem. Soc., 115, 6382.
101. **Nazeeruddin M. K., De Angelis, F., Fantacci, S., Selloni, A., Viscardi, G., Liska, P., Ito, S., Takeru, B., Gratzel, M.**, (2005), J. Am. Chem. Soc., 127, 16835.
102. **Nazeeruddin, M. K., Splivallo, R., Liska, P., Comte, P., Gratzel, M.**, (2003), Chem. Commun., 1456.
103. **Wang, P., Zakeeruddin, S. M., Exnar, I., Gratzel, M.**, (2002), Chem. Commun., 2972.
104. **Wang, P., Zakeeruddin, S. M., Moser, J. E., Nazeeruddin, M. K., Sekiguchi, T., Gratzel, M.**, (2003), Nat. Mater., 2, 402.
105. **Wang, P., Wenger, B., Humphry-Baker, R., Moser, J. E., Teuscher, J., Kandlehner, W., Mezger, J., Stoyanov, E. V., Zakeeruddin, S. M., Gratzel, M.**, (2005), J. Am. Chem. Soc., 127, 6850.
106. **Nazeeruddin, M. K., Pechy, P., Renouard, T., Zakeeruddin, S. M., Humphry-Baker, R., Comte, P., Liska, P., Cevey, L., Costa, E., Shklover, V., Spiccia, L., Deacon, G. B., Bignozzi, C. A., Gratzel, M.**, (2001), J. Am. Chem. Soc., 123, 1613.
107. **Chiba, Y., Islam, A., Watanabe, Y., Komiya, R., Koide, N., Han, L.**, (2006), Jpn. J. Appl. Phys., 45, L638.
108. **Nazeeruddin, M. K., Pchy, P., Gratzel, M.**, (1997), Chem. Commun., 1705.

109. **Tian, H., Meng, F.** (2005), in *Organic Photovoltaics: Mechanisms, Materials, and Devices* (Eds.: S.-S. Sun, N. S. Sariciftci), CRC, London, p. 313.
110. **Hagfeldt, A., Graetzel, M.**, (1995), *Chem. Rev.*, 95, 49.
111. **Zollinger, H.**, (2003), *Color Chemistry: Syntheses, Properties, and Applications of Organic Dyes and Pigments*, 3rd ed., Verlag Helvetica Chimica Acta, Zurich, and Wiley-VCH, Weinheim,.
112. **Ryan M.**, (2009), *Progress in Ruthenium Complexes for Dye Sensitized Solar Cells.*, *Platinum Metals Review*, 53, 216-218.
113. **Yum, J. H., Chen, P., Gratzel, M., Nazeeruddin, M. K.**, (2008), *Chem- SusChem*, 1, 699.
114. **Argazzi, R., Bignozzi, C. A., Heimer, T. A., Castellano, F. N., Meyer, G. J.**, (1995), *J. Am. Chem. Soc.*, 117, 11815.
115. **Clifford, J. N., Yahioglu, G., Milgrom, L. R., Durrant, J. R.**, (2002), *Chem. Commun.*, 1260.
116. **Hirata, N., Lagref, J. J., Palomares, E. J., Durrant, J. R., Nazeeruddin, M. K., Gratzel, M., Di Censo, D.**, (2004), *Chem. Eur. J.*, 10, 595.
117. **Clifford, J. N., Palomares, E., Nazeeruddin, M. K., Gratzel, M., Nelson, J., Li, X., Long, N. J., Durrant, J. R.**, (2004), *J. Am. Chem. Soc.*, 126, 5225.
118. **Haque, S. A., Handa, S., Peter, K., Palomares, E., Thelakkat, M., Durrant, J. R.**, (2005), *Angew. Chem.*, 117, 5886; *Angew. Chem. Int. Ed.* 2005, 44, 5740.
119. **Yao, Z., Zhang, M., Li, R., Yang, L., Qiao, Y., and Wang, P.**, (2015), *Angew. Chem. Int. Ed.*, 54.
120. **Kroeze, J. E., Hirata, N., Schmidt-Mende, L., Orizu, C., Ogier, S. D., Carr, K., Gratzel, M., Durrant, J. R.**, (2006), *Adv. Funct. Mater.*, 16, 1832.
121. **Nogueira, A. F., Longo, C., Paoli, M.-A. D.**, (2004), *Coord. Chem. Rev.*, 248, 1455.
122. **Snaith, H. J., Moule, A. J., Klein, C., Meerholz, K., Friend, R. H., Gratzel, M.**, (2007), *Nano Lett.*, 7, 3372.
123. **Wu, J., Hao, S., Lan, Z., Lin, J., Huang, M., Huang, Y., Li, P., Yin, S., Sato, T.**, (2008), *J. Am. Chem. Soc.*, 130, 11568.
124. **Kong, F.T., Dai S.Y., Wang K.J.**, (2007), *Adv. OptoElectron.*, Article ID 75384.
125. **M. Gorlov, L. Kloo**, *Dalton Trans.* 2008, 2655.
126. **Y. Cao, J. Zhang, Y. Bai, R. Li, S. M. Zakeeruddin, G. Michael, P. Wang**, *J. Phys. Chem. C* 2008, 112, 13775.
127. **Y. Bai, Y. Cao, J. Zhang, M. Wang, R. Li, P. Wang, S. M. Zakeeruddin, M. Gratzel**, *Nat. Mater.* 2008, 7, 626.
128. **D. Kuang, S. Uchida, R. Humphry-Baker, S. M. Zakeeruddin, M. Gratzel**, *Angew. Chem.* 2008, 120, 1949; *Angew. Chem. Int. Ed.* 2008, 47, 1923.
129. <http://www.ni.com/white-paper/7230/en/>
130. **Yu D., Yang Y., Durstock M., Baek J. B., and Dai L.**, 2010, Soluble P₃HT-Grafted Graphene for Efficient Bilayer Heterojunction Photovoltaic Devices, *ACS Nano*, 4, 10, 5633p

131. **Yuehua Yuan and T. Randall Lee**, 2013, Contact Angle and Wetting Properties, Surface Science Techniques, Springer Series in Surface Sciences, 51



APPENDIX

Figure 1. NMR spectrum of methyl 4-(5'-bromo[2,2'-bithien]-5-yl) benzoate

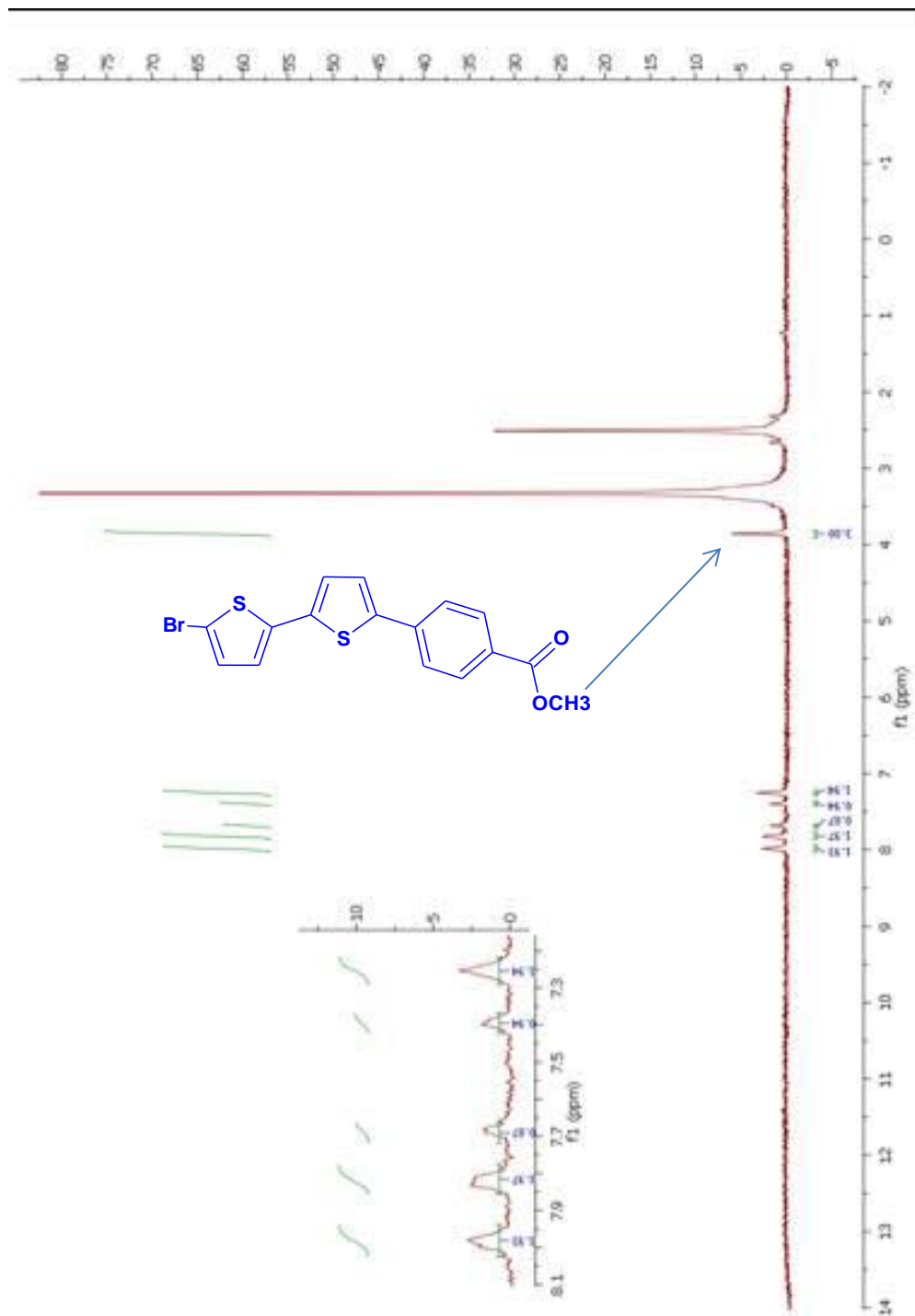


Figure 2. NMR spectrum of 4-(5'-phenyl[2,2'-bithiophen]-5-yl) benzoic acid (ZE-Ph)

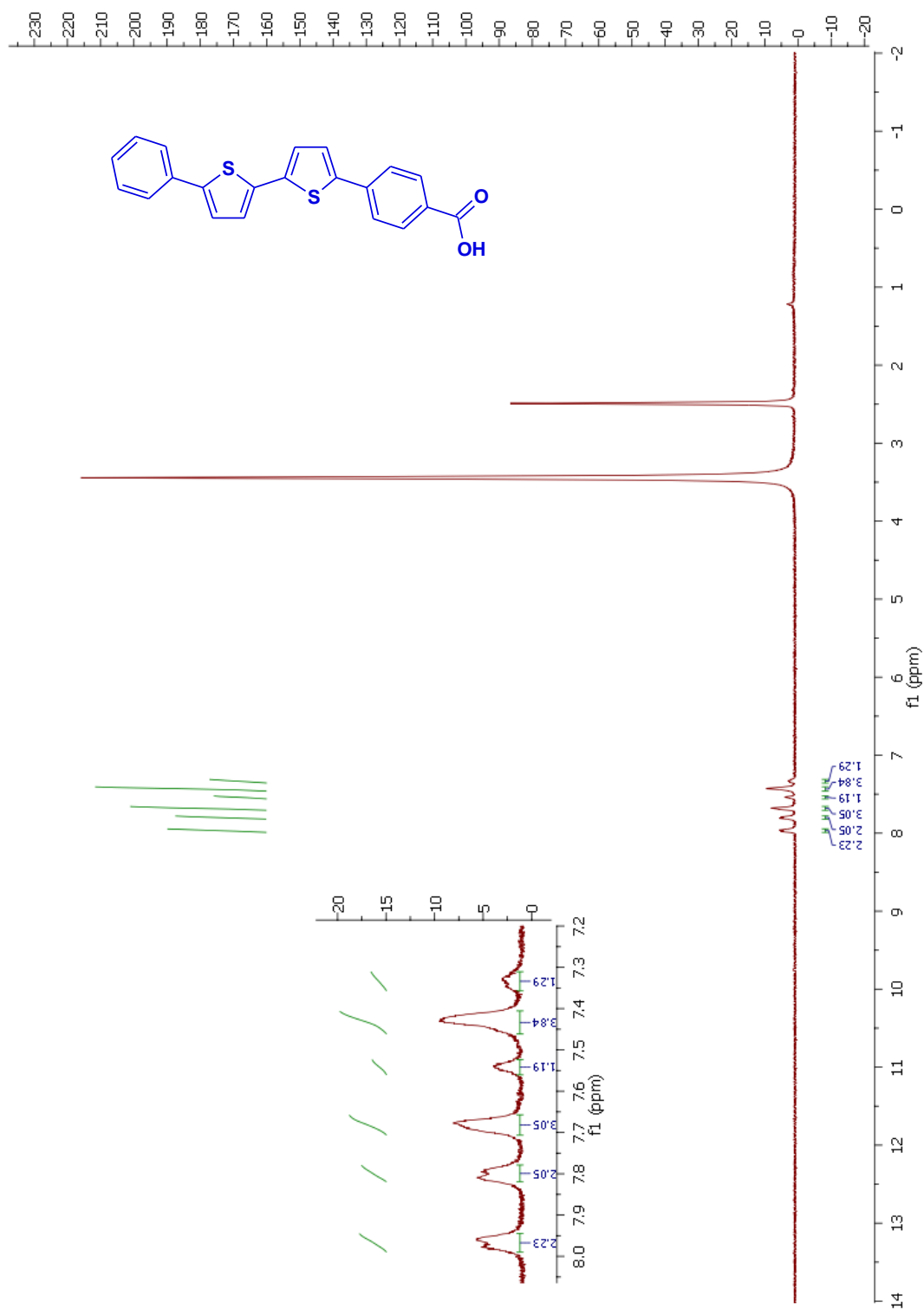


Figure 3. FT-IR spectrum of 4-(5'-phenyl-[2,2'-bithiopen]-5-yl)benzoic acid

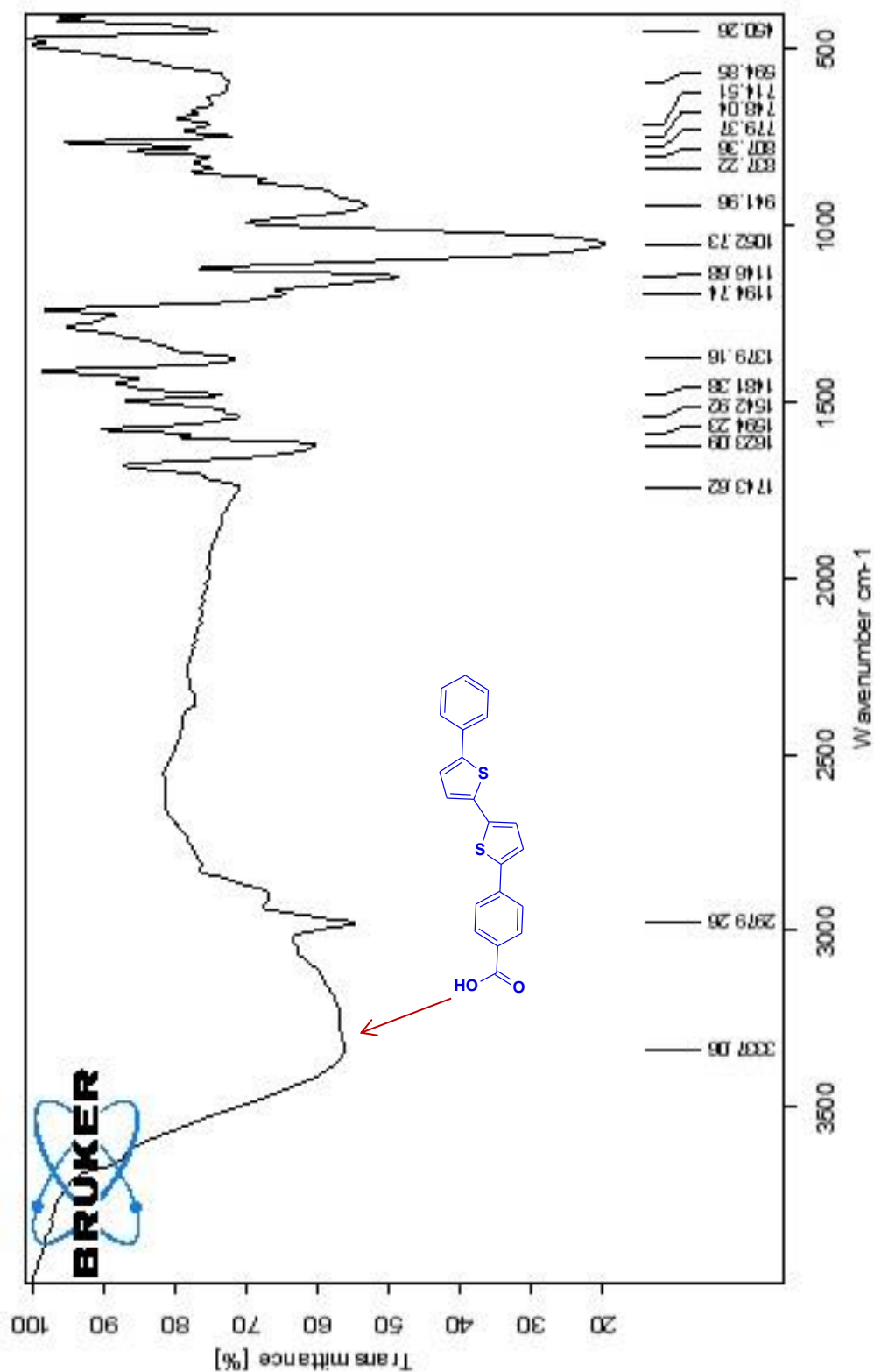


Figure 4. 4- [5' - (4-methoxyphenyl) -2,2'-bithiophen-5-yl] benzoic acid (ZE-1MeO)

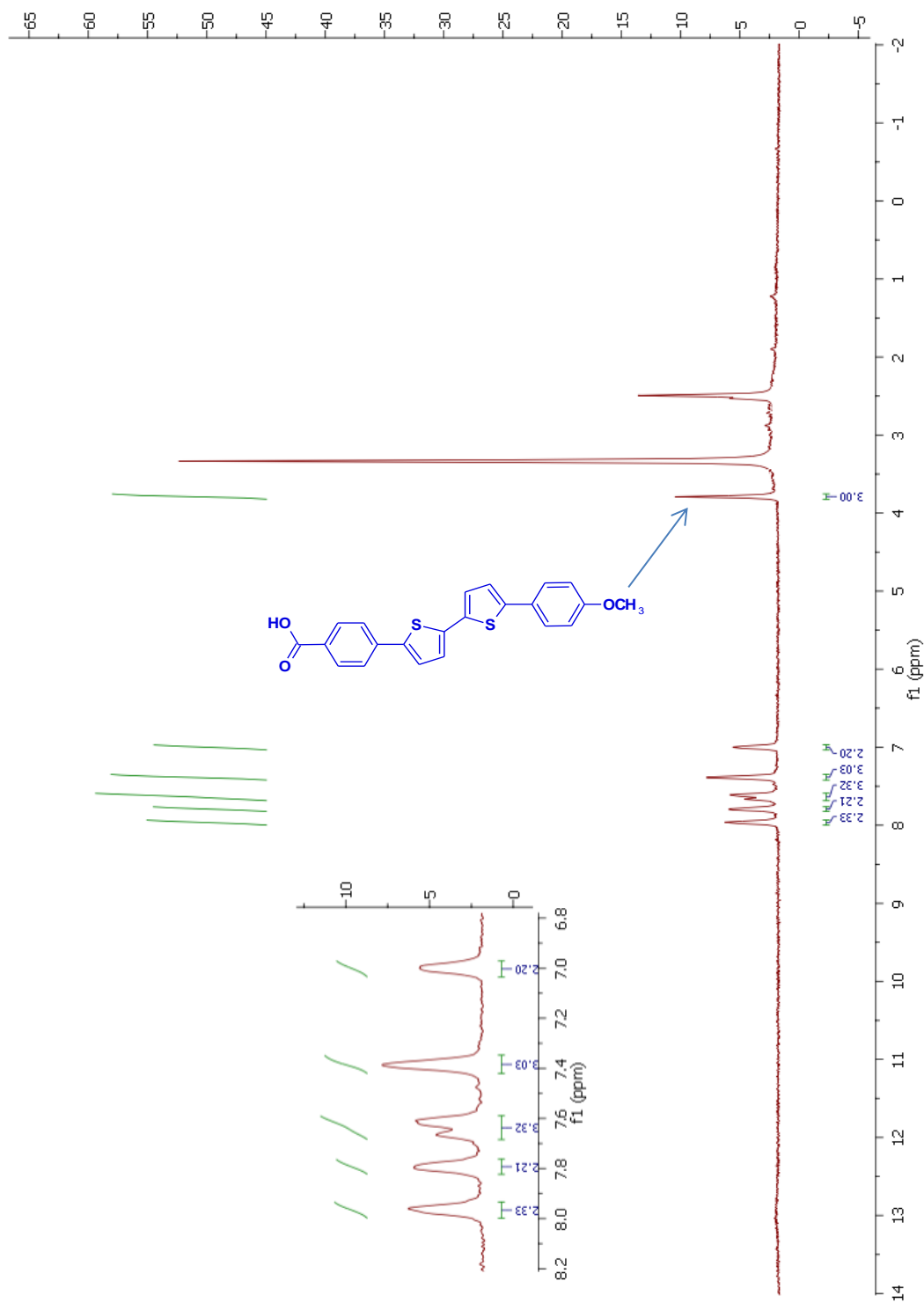


Figure 5. FT-IR spectrum of 4-[5'-(4-methoxyphenyl)-2,2'-bitien-5-il]benzoic acid

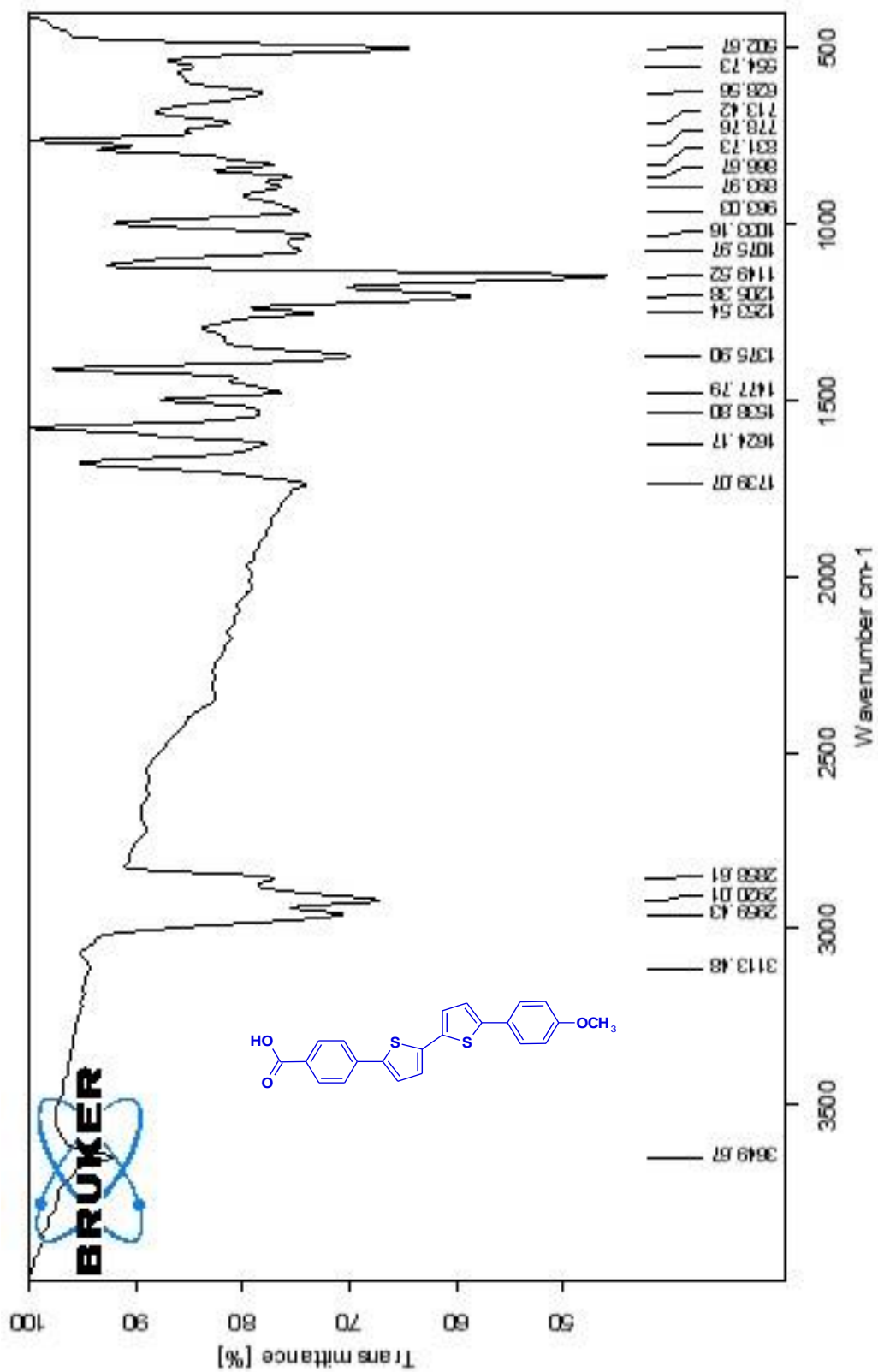


Figure 6. 4- [5'-(3,5-dimethoxyphenyl)-2,2-bithiophen-5-yl] benzoic acid (ZE-2MeO)

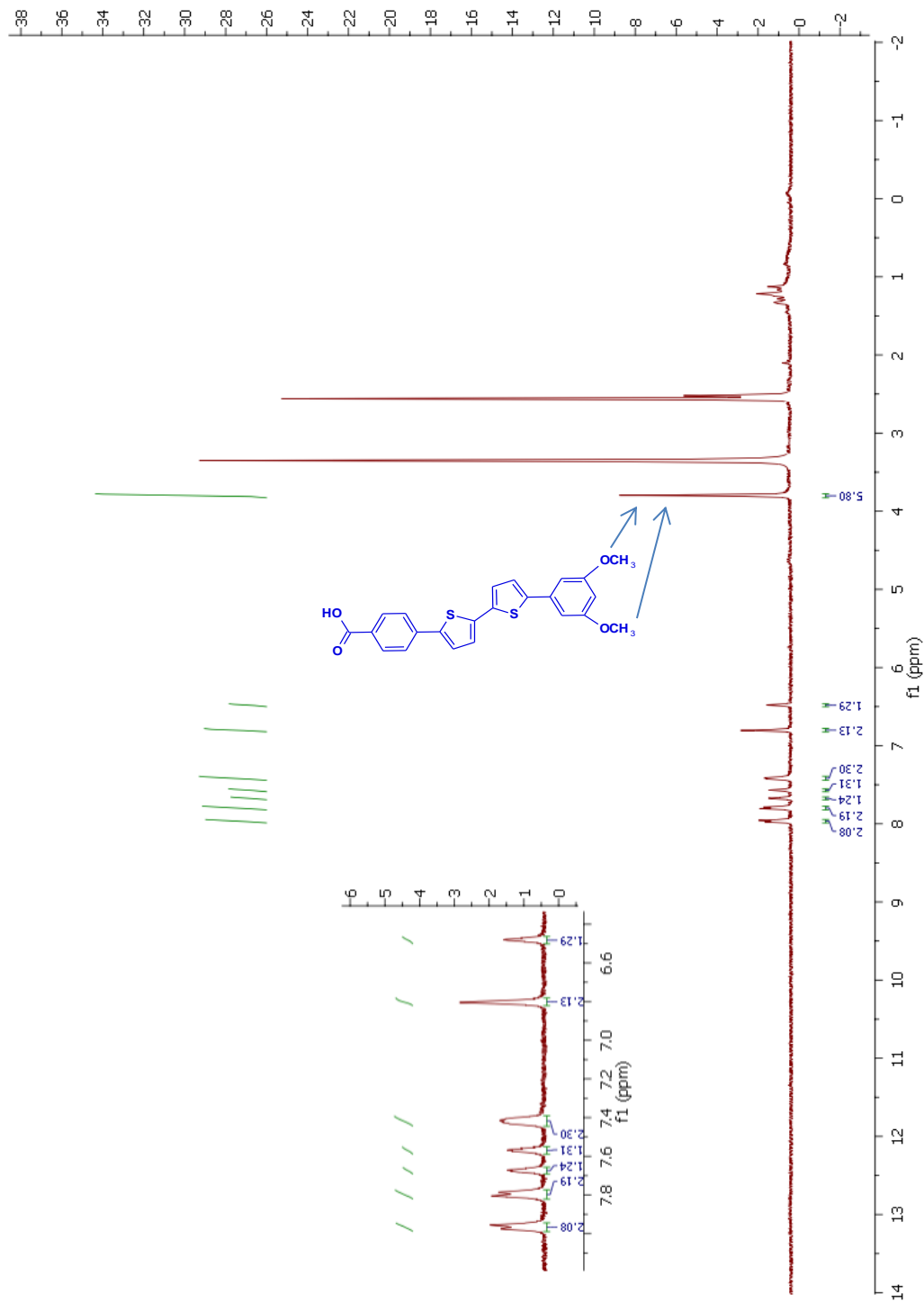


Figure 7. FT-IR spectrum of 4-[5'-(3,5-dimethoxyphenyl)-2,2'-bitien-5-yl]benzoic acid

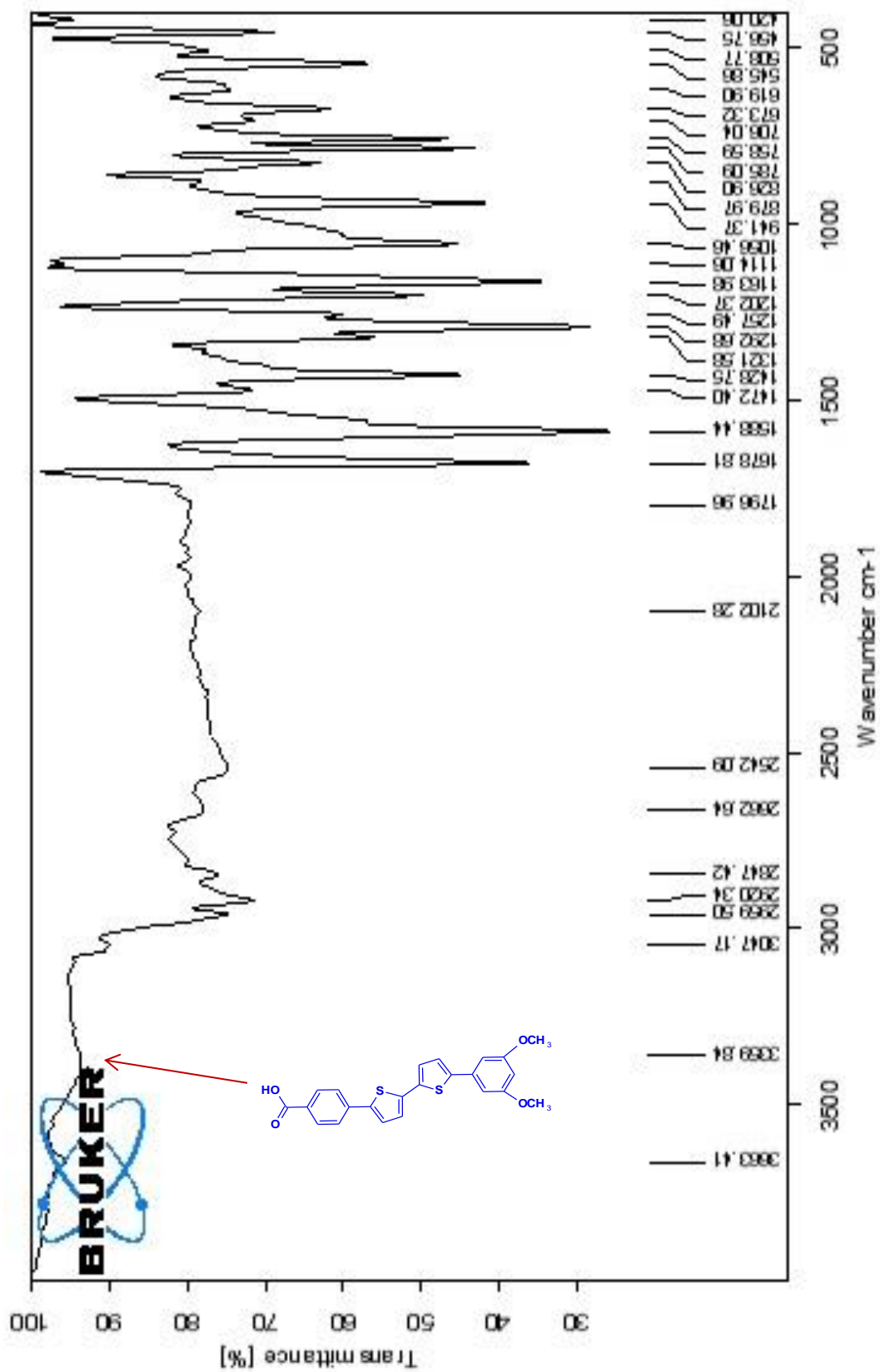


Figure 8. NMR spectrum of 4-[5'-(3,4,5-trimethoxyphenyl)-2,2'-bithiophen-5-yl] benzoic acid (ZE-3MeO)

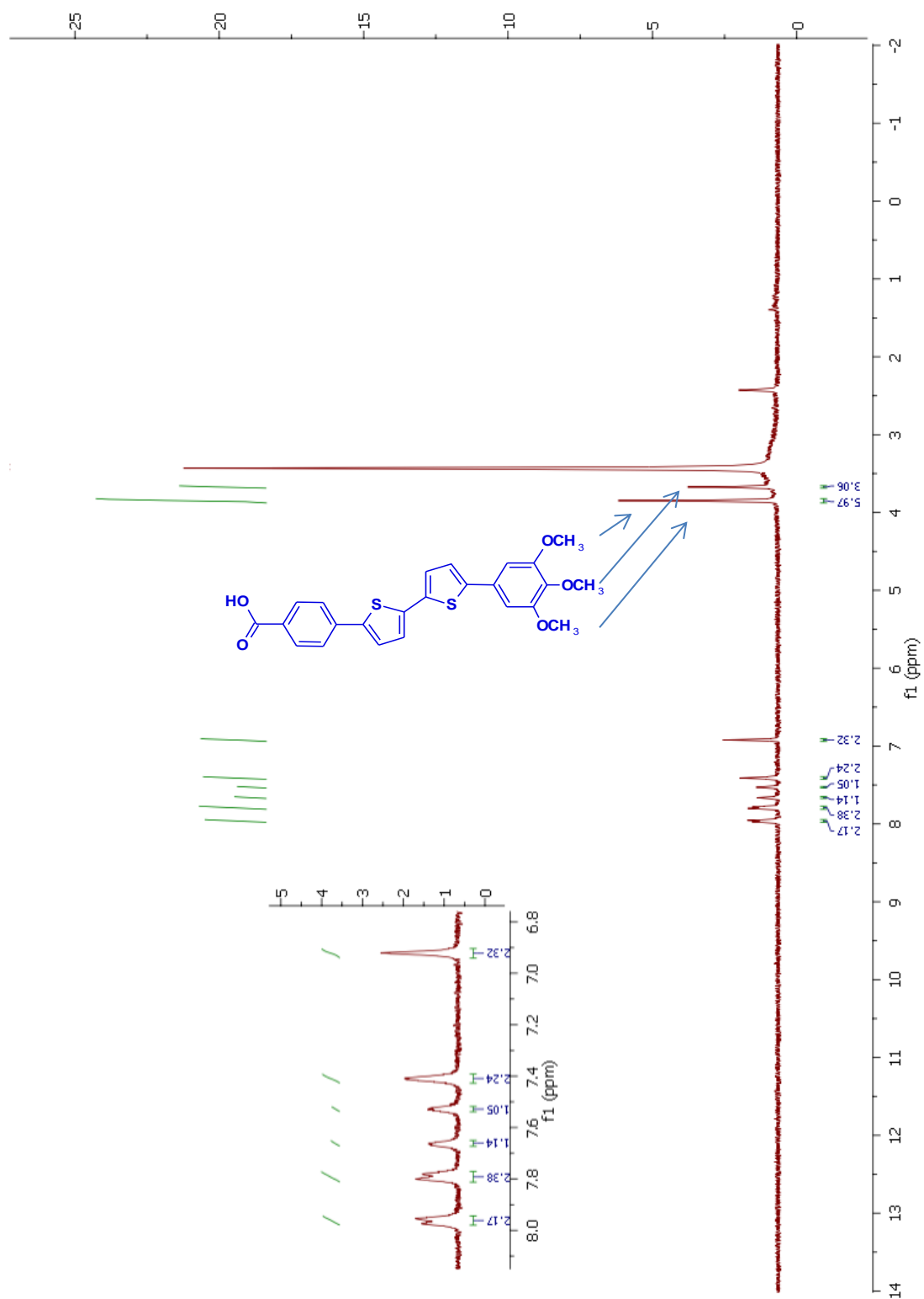


Figure 9. FT-IR spectrum of 4-[5'-(3,4,5-trimethoxyphenyl)-2,2'-bitien-5-il]benzoic acid

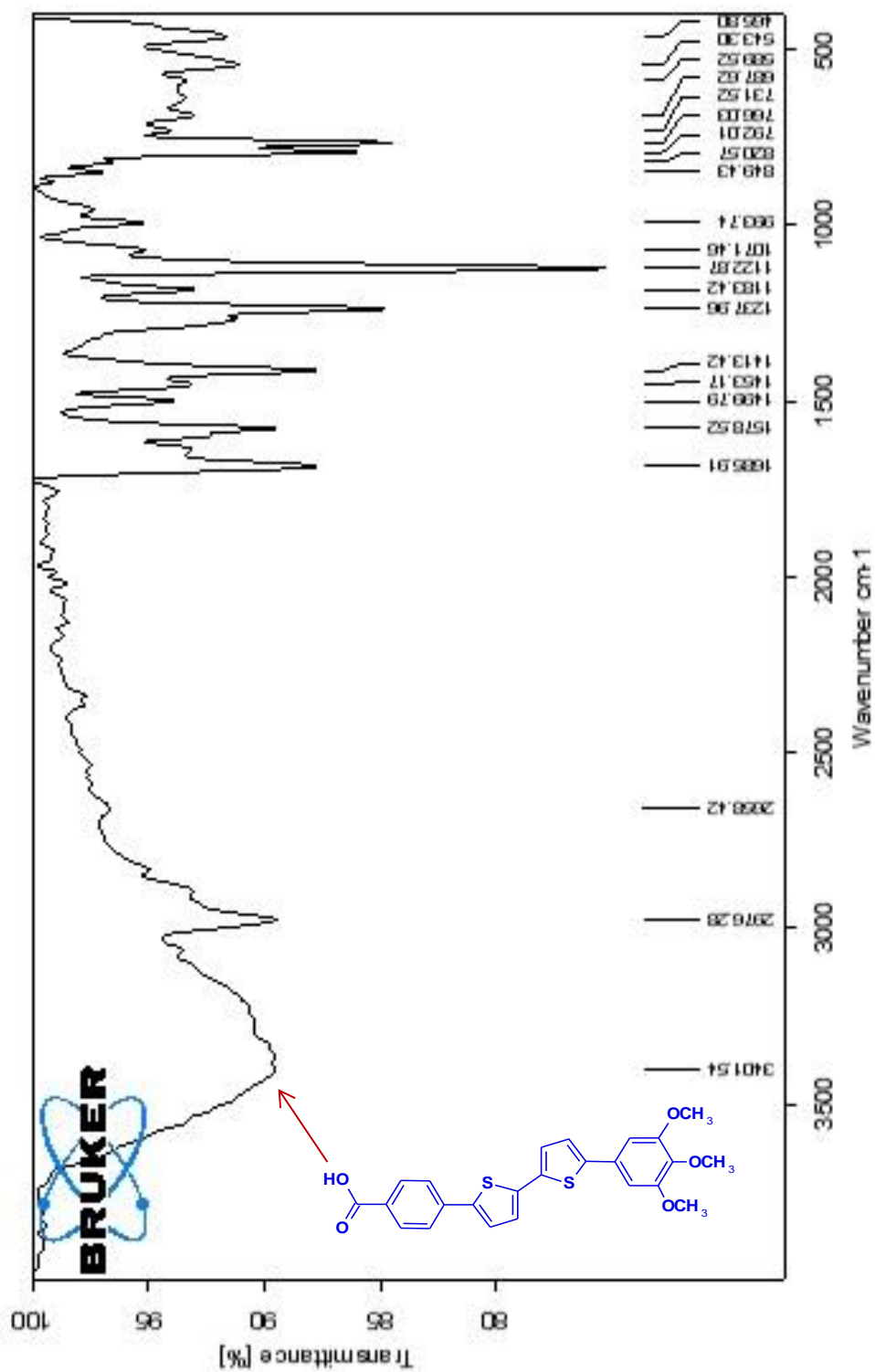


Figure 10. ^1H NMR spectrum of 1-(hexyloxy)-4-iodophenol

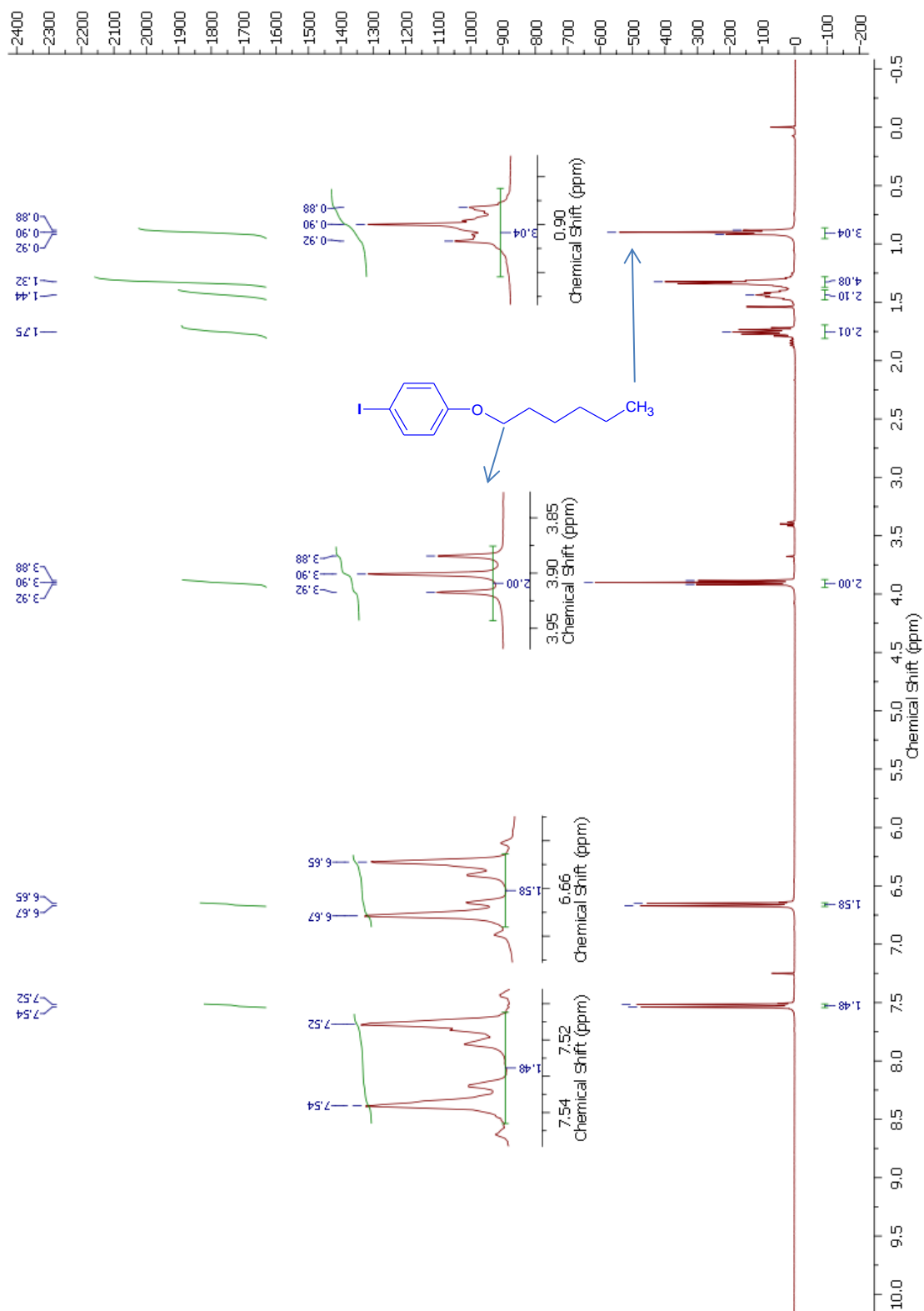


Figure 11. ^{13}C NMR spectrum of 1-(hexyloxy)- 4-iodophenol

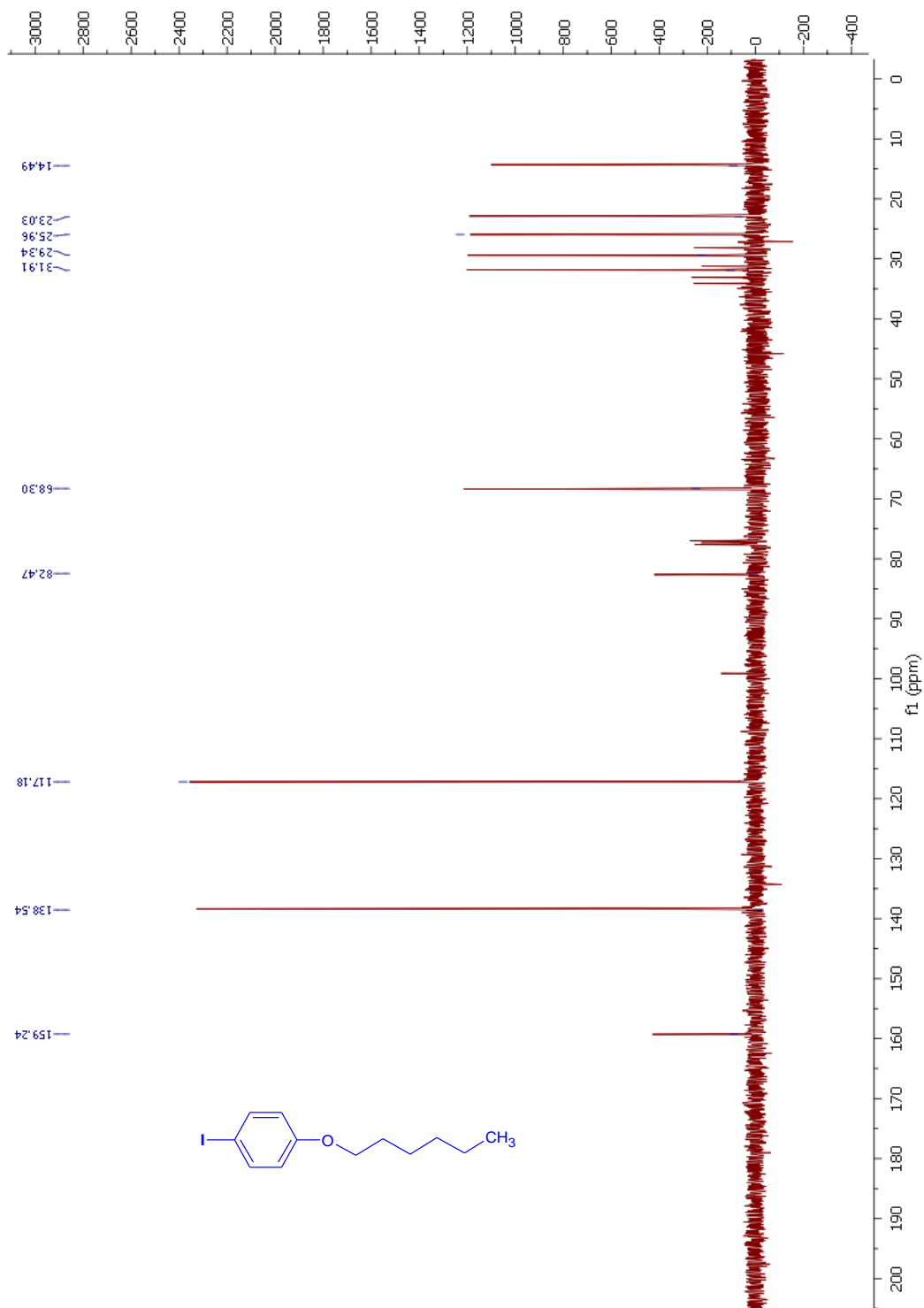


Figure 12. ^1H NMR spectrum of (4-bromophenyl)bis[4-(hexyloxy)phenyl]amin

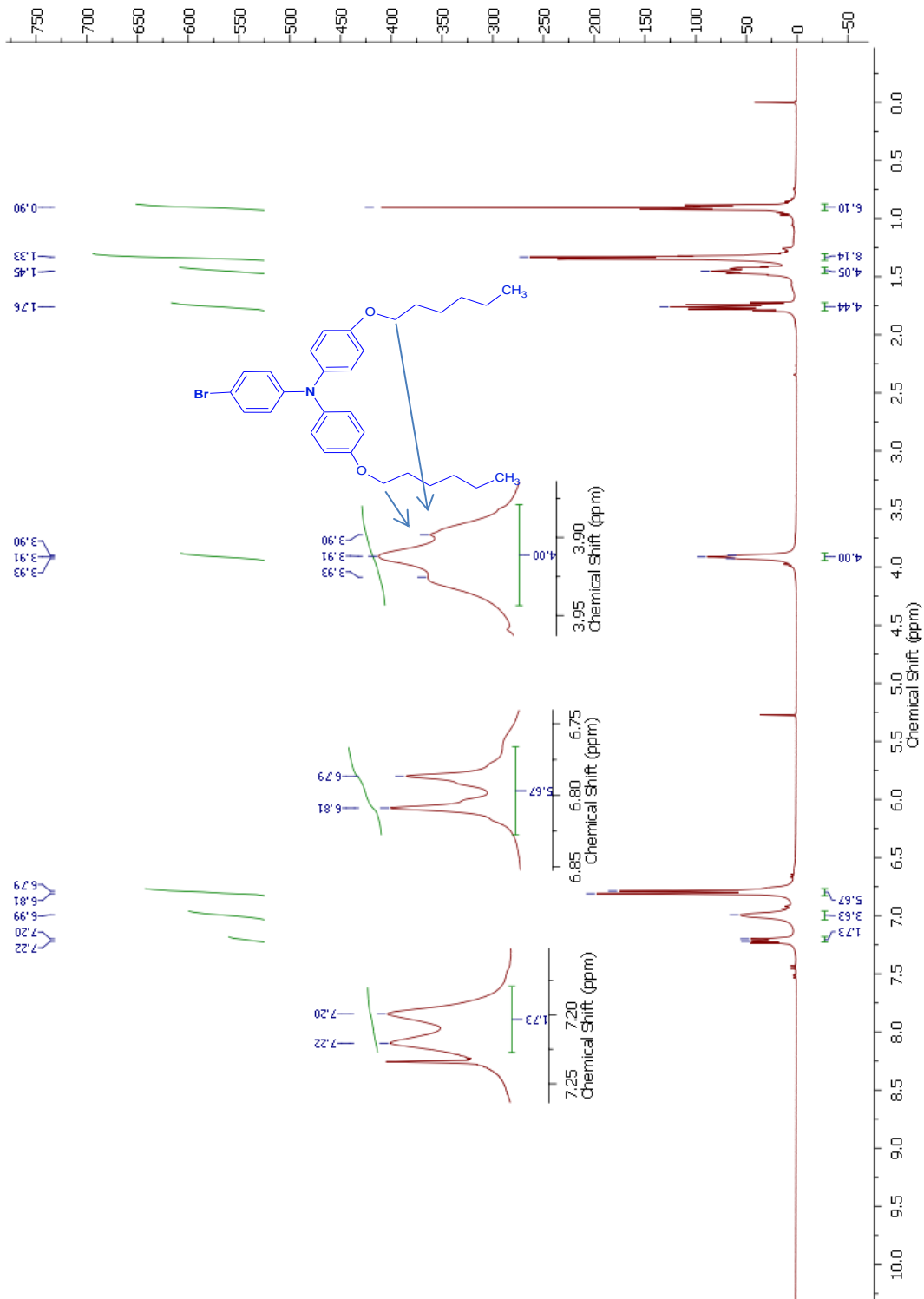


Figure 13. ^{13}C NMR spectrum of (4-bromophenyl)bis[4-(hexyloxy)phenyl]amin

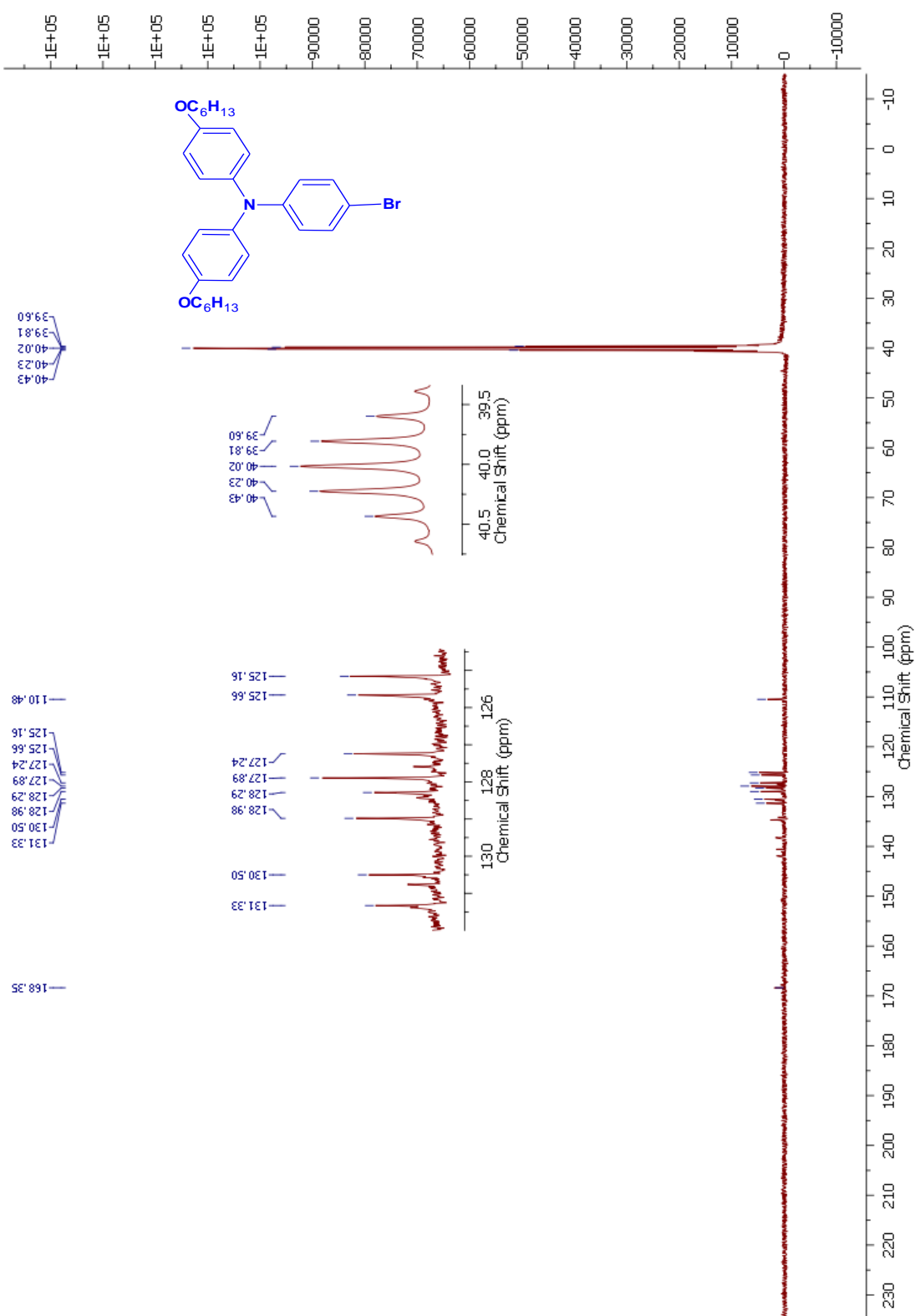


Figure 14. ^1H NMR spectrum of (4-{bis[4-(hexyloxy)phenyl]amino}phenyl)boronic acid

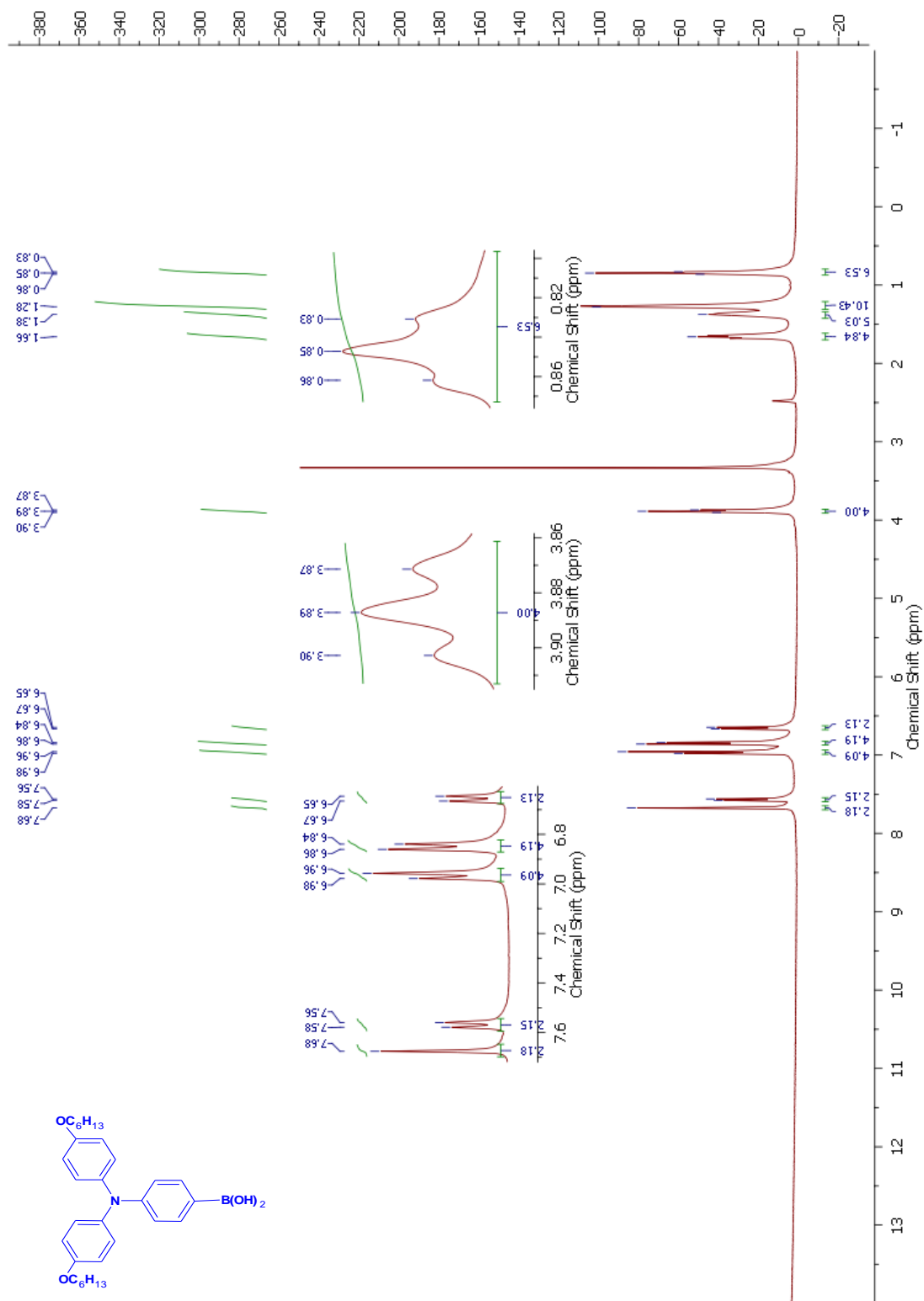


Figure 15. ^{13}C NMR spectrum of (4-{bis[4-(hexyloxy)phenyl]amino}phenyl)boronic acid.

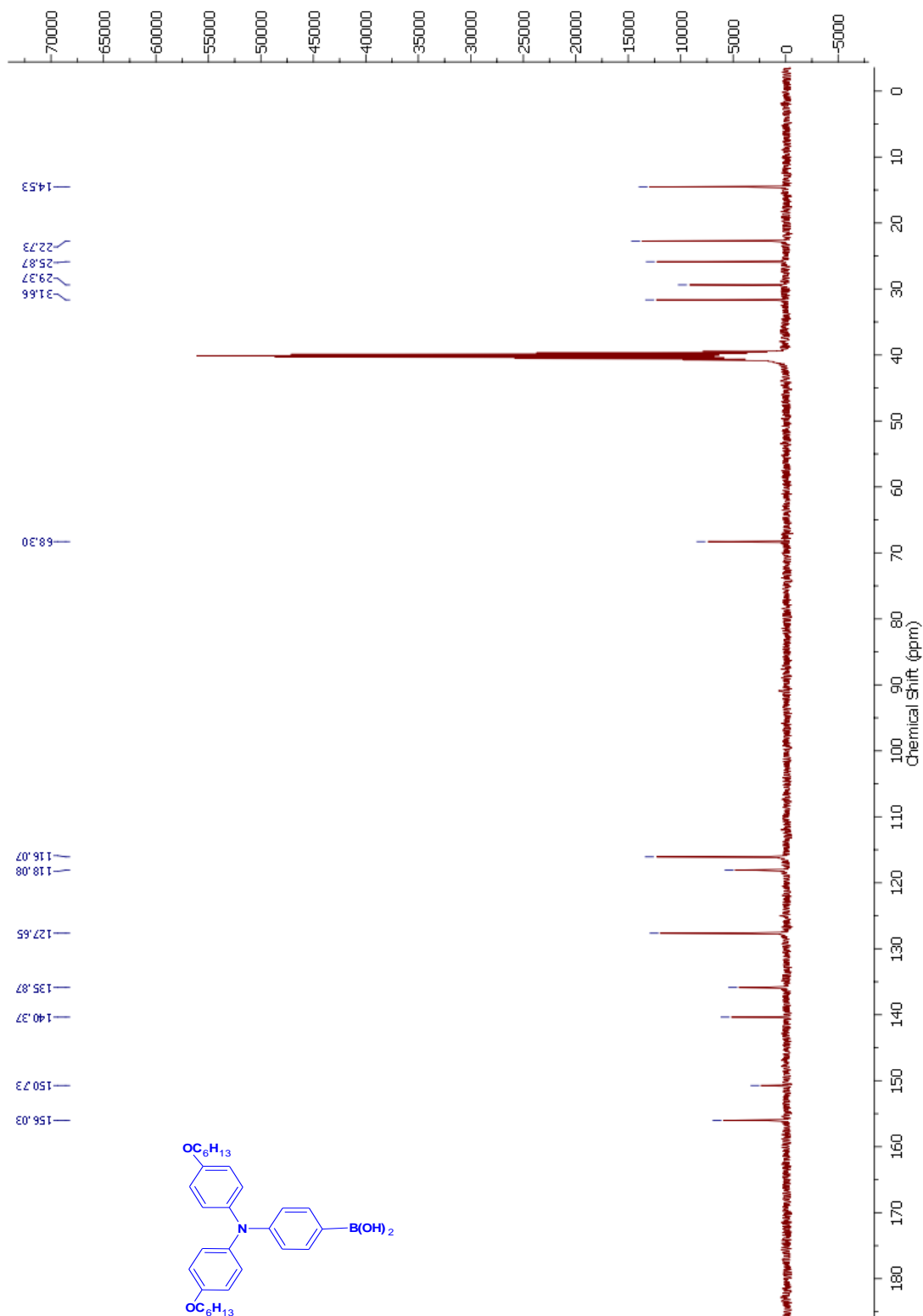


Figure 16. $^1\text{H-NMR}$ of 4-(4-{bis[4-(hexyloxy)phenyl]amino}phenyl)-7-oxo-7*H*-benzimidazo[2,1-a]benzo[de]isoquinoline-11-carboxylic acid

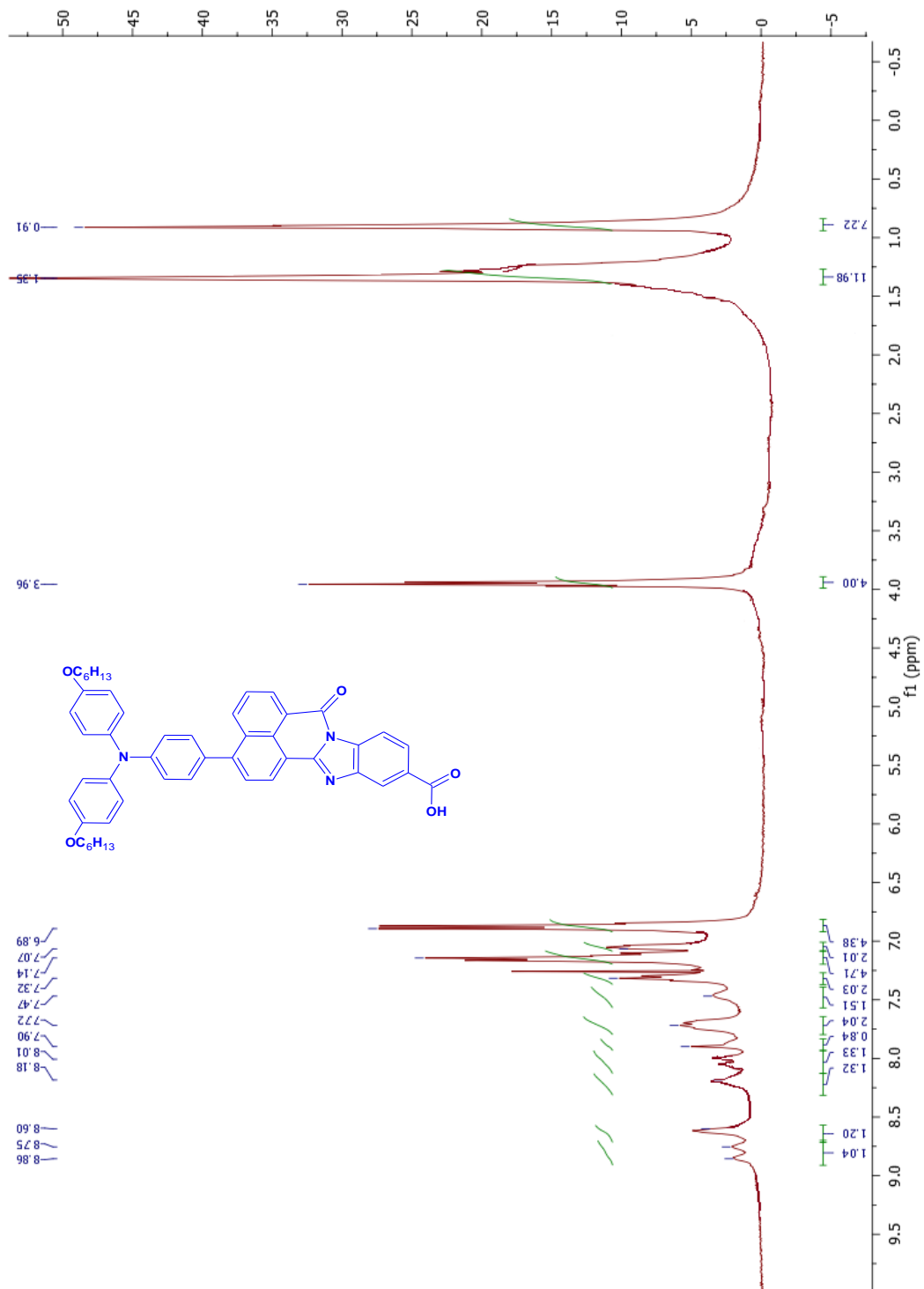


Figure 17. ^{13}C -NMR of 4-(4-{bis[4-(hexyloxy)phenyl]amino}phenyl)-7-oxo-7H-benzimidazo[2,1-a]benzo[de]isoquinoline-11-carboxylic acid

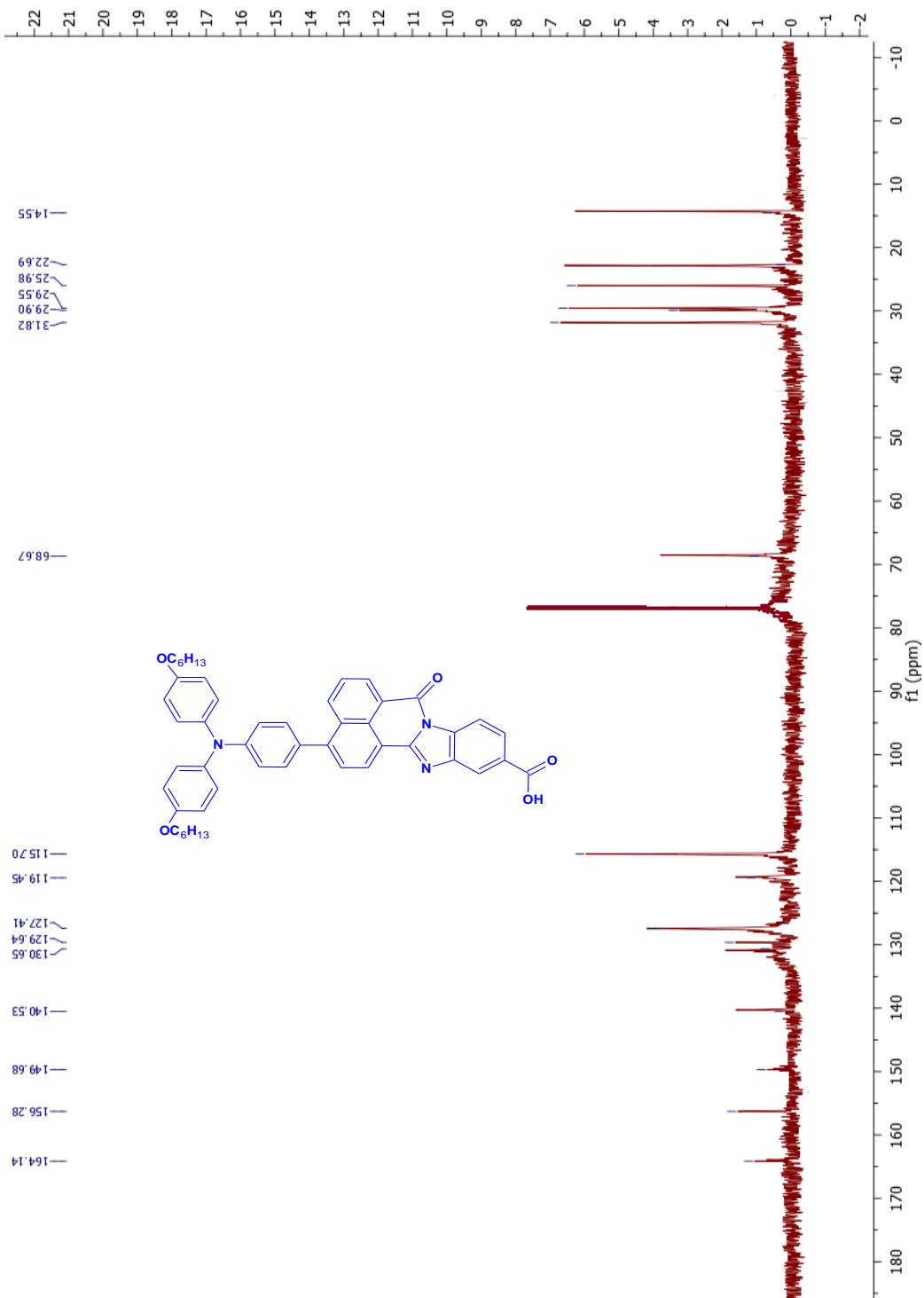


Figure 18. FT-IR spectrum of 4-(4-{bis[4-(hexyloxy)phenyl]amino}phenyl)-7-oxo-7H-benzimidazo[2,1-a]benzo[de]isoquinoline-11-carboxylic acid

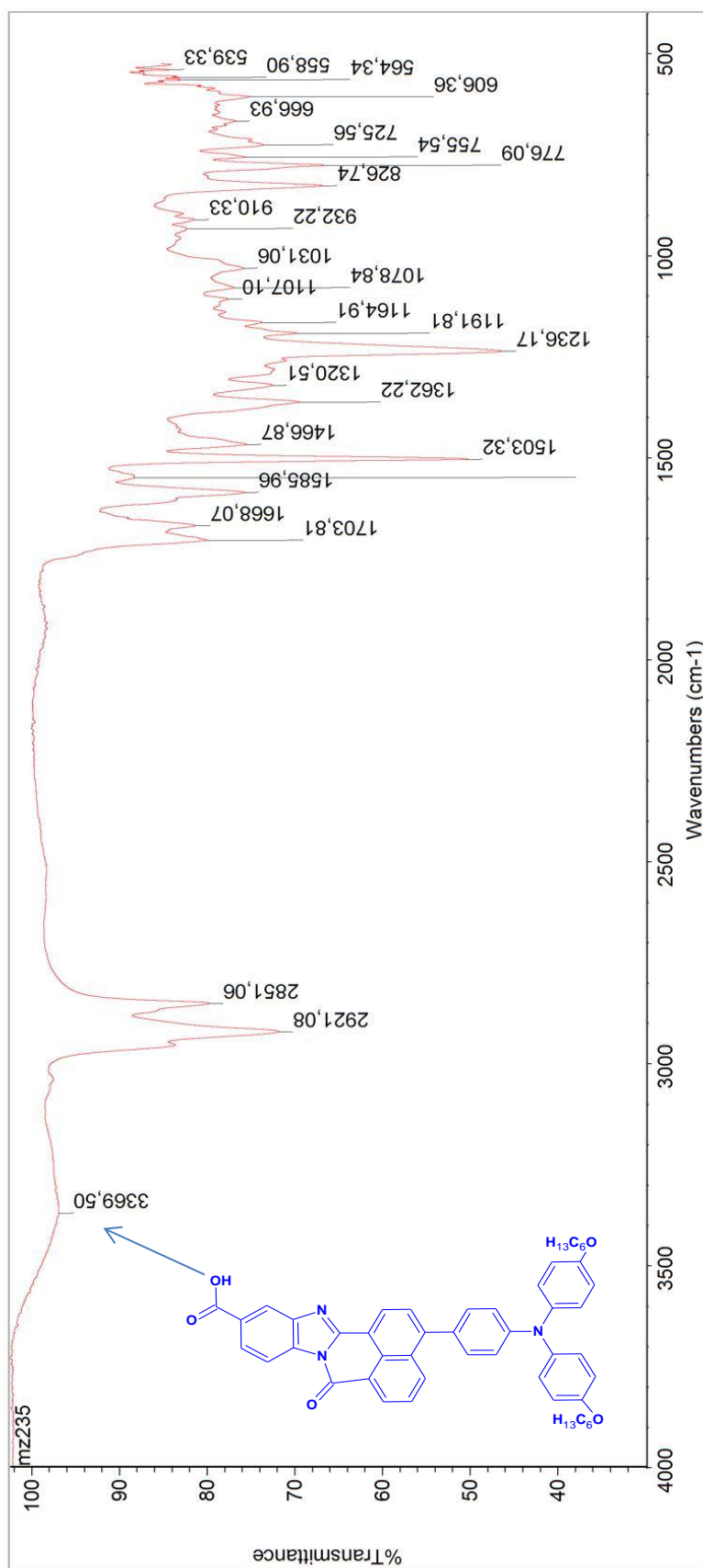


Figure 19. $^1\text{H-NMR}$ of 4-[4-(diphenylamino)phenyl]-7-oxo-7*H*-benzimidazo[2,1-*a*]benzo[*de*]isoquinoline-11-carboxylic acid

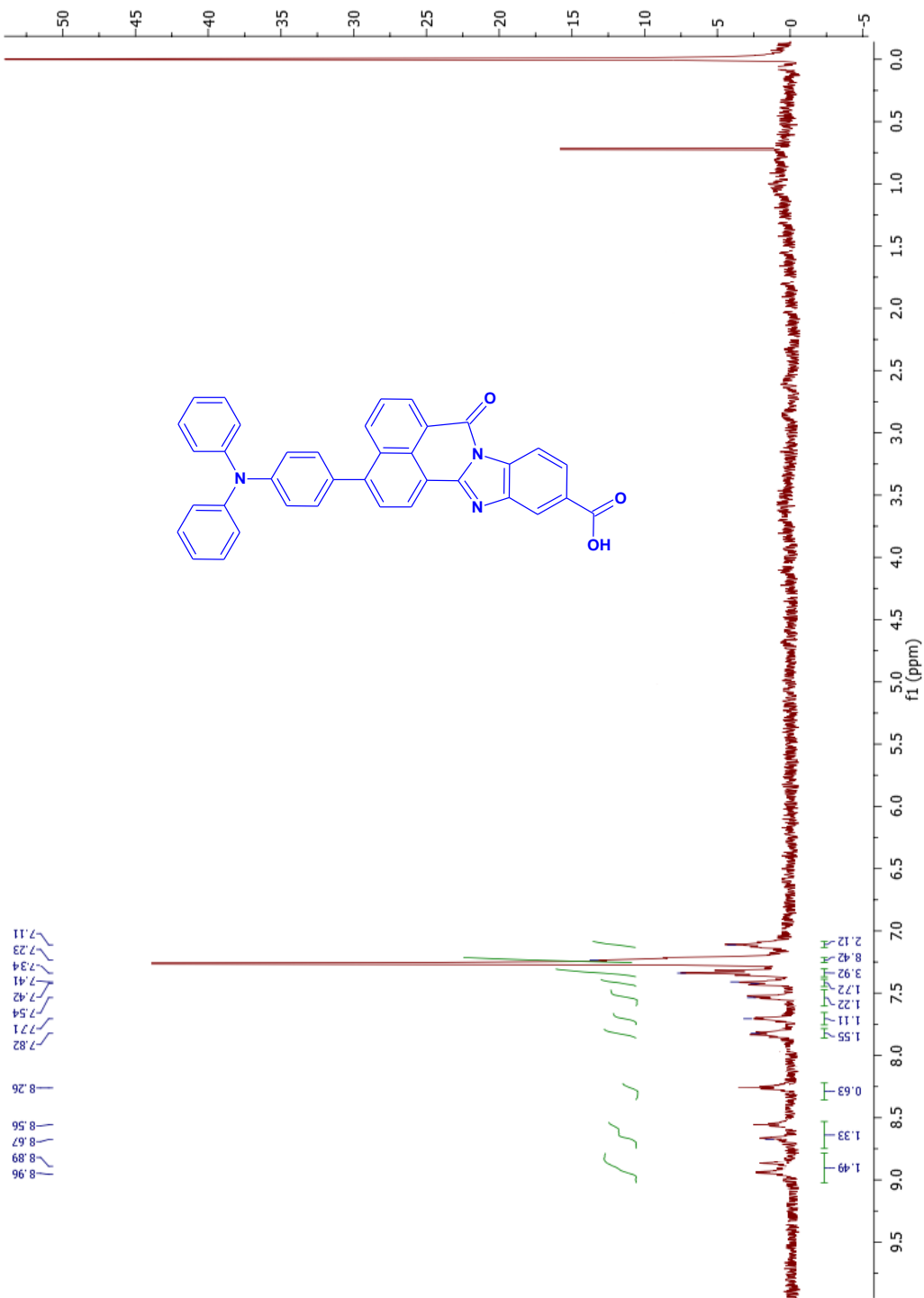


Figure 20. ^{13}C -NMR of 4-[4-(diphenylamino)phenyl]-7-oxo-7H-benzimidazo[2,1-a]benzo[de]isoquinoline-11-carboxylic acid

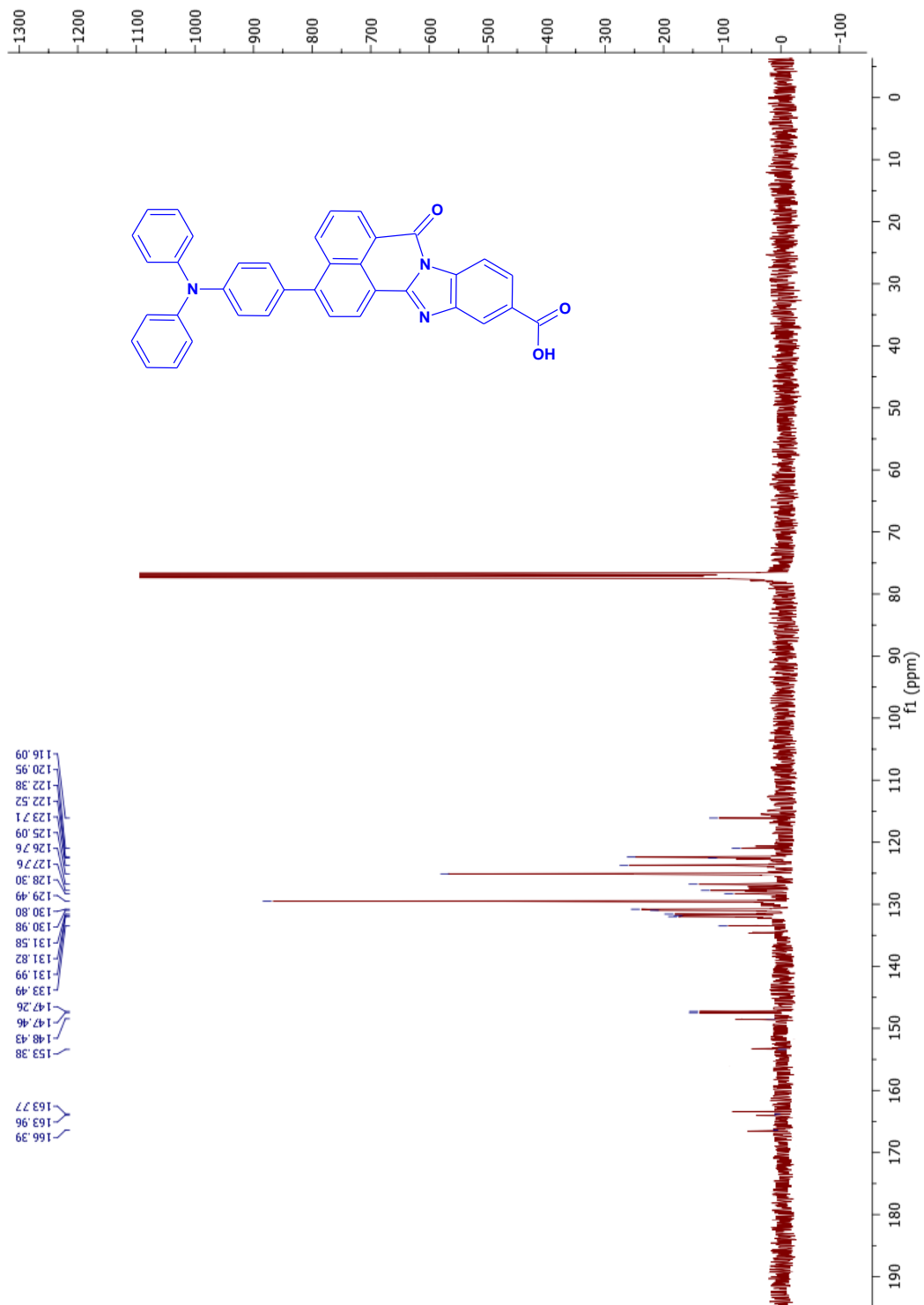
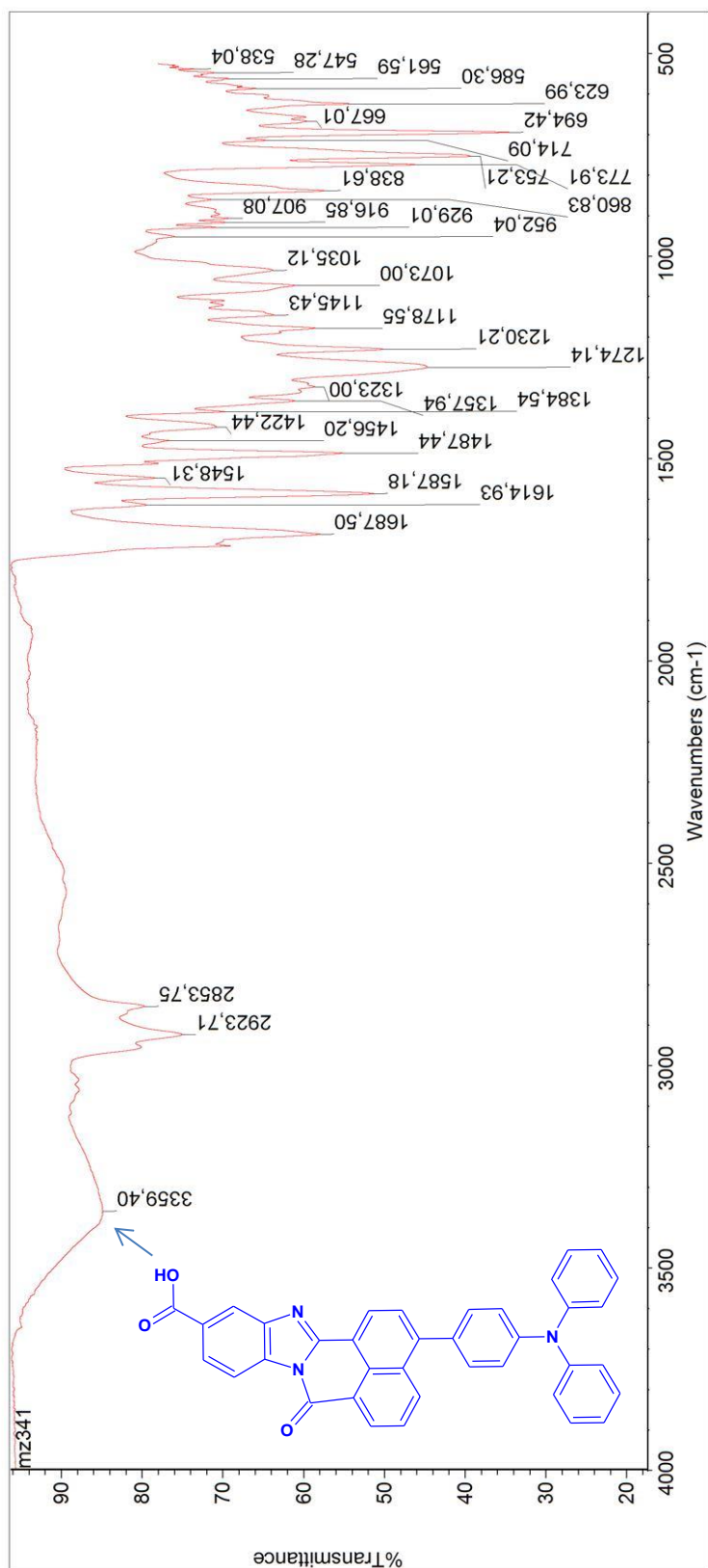


Figure 21. FT-IR spectrum of 4-[4-(diphenylamino)phenyl]-7-oxo-7H-benzimidazo[2,1-a]benzo[*de*]isoquinoline-11-carboxylic acid



CURRICULUM VITAE



Name Surname : Mesude Zeliha ARKAN

Place and Date of Birth : İzmir 24.01.1988

E-Mail : yigitmz@gmail.com

EDUCATION :

- **B.Sc.** : 2011, Ege University, Faculty of Science, Chemistry Department
- **M.Sc.** : 2013, Ege University, Institute of Science, Solar Energy Department

PUBLICATIONS, PRESENTATIONS AND PATENTS ON THE THESIS :

An. Margalias, K. Seintis, **M.Z. Yigit**, M. Can, D. Sygkridou, V. Giannetas, M. Fakis, E. Stathatos, The effect of additional electron donating group on the photophysics and photovoltaic performance of two new metal free D- π -A sensitizers, *Dyes and Pigments*, Volume 121, 2015, pp. 316-327

OTHER PUBLICATIONS, PRESENTATIONS AND PATENTS:

1. M. Can, **M. Z. Yigit**, K. Seintis, D. Karageorgopoulos, S. Demic, S. Icli, V. Giannetas, M. Fakis and E. Stathatos, Synthesis of two tri-arylamine derivatives as sensitizers in dye-sensitized solar cells. Electron injection studies and photovoltaic characterization, *Synthetic Metals*, 188 (2014) 77-85
2. Faruk Ozel, Mahmut Kus, Adem Yar, Emre Arkan, **M.Zeliha Yigit**, Abdalaziz Aljabour, Sümeýra Büyükcelebi, Cem Tozlu, Mustafa Ersoz, Electrospinning of Cu₂ZnSnSe_{4-x}S_x nanofibers by using PAN as template, *Materials Letters*, 140(2015) 23–26

3. **Mesude Zeliha Yigit**, Hakan Bilgili, Emre Sefer, Serafettin Demic, Ceylan Zafer, Mustafa Can, Sermet Koyuncu, Effect of a pi-bridging unit in triphenylamine-benzothiadiazole based donor acceptor chromophores for dye-sensitized solar cells, *Electrochimica Acta*, Volume 147, 2014, pp. 617-625
4. M. Can, A. K. Havare, **M. Z. Yiğit**, Ş. Demiç, S. Okur, S. İçli, Kendiliğinden Organize Tek Katman Olarak Oluşturulabilen Triarilaminlerin Sentezi, 25. *National Chemistry Congress*, 27 Haziran-02 Temmuz 2011, Erzurum, Turkey.
5. M. Can, **M. Z. Yiğit**, K. Demirak, B. Gültekin, Ş. Demiç, C. Zafer, S. İçli, Synthesis and Photovoltaic Applications of Two Novel Dyes Based On Triarylamine, *Solar TR-2; Solar Electricity Conference & Exhibition*. 7-9 Kasım 2012, Antalya, Turkey.
6. C. Zafer, K. Demirak, **M.Z. Yiğit**, M. Can, D.A. Ergün, Ş. Demiç, Photovoltaic Performance Improvement of Triarylamine Substituted Quinoxaline Push-Pull Dyes for DSSCs, *Solar TR-2; Solar Electricity Conference & Exhibition*. 7-9 Kasım 2012, Antalya, Turkey.
7. D.A. Ergün, **M.Z. Yiğit**, K. Demirak, M. Can, Ş. Demiç, C. Zafer, Molecular Engineering of New Quinoxaline Based Acceptors to Improve Charge Generation in Organic Photovoltaics, *Solar TR-2; Solar Electricity Conference & Exhibition*. 7-9 Kasım 2012, Antalya, Turkey.
8. **M. Z. Yigit**, H. Bilgili, S. Demic, C. Zafer, S. Koyuncu, M. Can, Effect of pi Bridge Unit for Triphenylamine-Benzothiadiazole Based Donor Acceptor Dye, *ICWEE-2013; The Second International Conference on Water, Energy and the Environment*, 21-24 Eylül 2013, Kuşadası, Turkey.
9. **M. Z. Yigit**, M. Can, A. N. Ozcivan, E. S. Cakmak, H. Bilgili, S. Koyuncu, S. Demic, O. Mermer, Photovoltaic Characterization and Electrical Modeling of Dye-Sensitized solar cells using novel synthesized organic dyes, *ICWEE-*

2013; *The Second International Conference on Water, Energy and the Environment*, 21-24 Eylül 2013, Kuşadası, Turkey.

10. Koray Kara, **M.Zeliha Yiğit**, Hakan Bilgili, Mahmut Kuş, Mustafa Can, Optimizing The Organic Solar Cell Efficiency Using Novel Small Molecule As Dopant, *IWOBOE-2014; International Workshop on Flexible Bio- and Organic Printed Electronics*, 1-3 Mayıs 2014, Konya, Turkey

